REPORT 233

ADVISORY GROUP FOR AERONAUTICAL
RESEARCH AND DEVELOPMENT

REPORT 233

DEVELOPMENT OF THE SPARK-HEATED, HYPERVELOCITY, BLOWDOWN TUNNEL-HOTSHOT

by
R. W. PERRY and W. N. MACDERMOTT

JUNE 1958

NORTH ATLANTIC TREATY ORGANIZATION
PALAIS DE CHAILLOT, PARIS 16

REPORT 233

NORTH ATLANTIC TREATY ORGANIZATION

ADVISORY GROUP FOR AERONAUTICAL RESEARCH AND DEVELOPMENT

DEVELOPMENT OF THE SPARK-HEATED, HYPERVELOCITY, BLOWDOWN TUNNEL-HOTSHOT

by

R.W. Perry and W.N. MacDermott

Prepared for the Wind Tunnel and Model Testing Panel of AGARD, June 1958

SUMMARY

A new type of wind tunnel (called "Hotshot") capable of producing the true relative velocities of hypersonic flight ~~has been~~ was developed. The required high stagnation enthalpies are obtained by heating a confined mass of air with a powerful electrical discharge from a large condenser bank. The resulting hot air is expanded in a Laval nozzle and produces hypersonic flow for a period of up to 50 ~~milliseconds~~ msec.

Operation of the original 16 in. Hotshot tunnel with reservoir temperatures of 4000°K to 8000°K (7200°R to 14,400°R) and reservoir pressures of 15,000 lb/in.^{2} to 20,000 lb/in.^{2} has been reduced to routine practice. Also a family of instrumentation techniques has been developed which permits conventional pressure, heat transfer, and force tests to be made in the tunnel. Development-type tests of components of a number of missiles ~~have been~~ were conducted in the Mach number range of 11 to 20 and at equivalent density altitudes of 140,000 ft to 200,000 ft.

~~This report presents~~ The history, description, performance, and typical test data for the first Hotshot type wind tunnel are presented. In addition, a brief account of advanced developments based on the electric-discharge method of heating gases is given.

533.6.071

3b8c2f
3b8c2g

SOMMAIRE

Une soufflerie de type nouveau (désigné Hotshot) capable de réaliser les vraies vitesses relatives du vol hypersonique a été mise au point. Les enthalpies élevées d'arrêt nécessaires s'obtiennent par échauffement d'une masse enfermée d'air à l'aide d'une décharge électrique puissante située dans un grand magasin à condensateurs. L'air ainsi échauffé se dilate dans une tuyère Laval pour réaliser un écoulement hypersonique dont la durée maximum est de 50 millisecondes.

La soufflerie Hotshot originale de 16 pouces de diamètre, qui dispose de températures d'arrêt de 4 000 à 8 000°K (7 200 à 14 400°R) et de pressions d'arrêt de 15 000 à 20 000 lb/in.^{2} est utilisée pour des essais réguliers. En plus, il a été réalisé une famille de techniques de mesure permettant d'effectuer dans la soufflerie les mesures classiques de pressions, du transfert de chaleur, et de forces aérodynamiques. Des essais de mise au point sur des éléments d'un certain nombre d'engins guidés ont été effectués à des nombres de Mach allant de M = 11 à M = 20 et à des altitudes équivalentes de densité comprises entre 140 000 et 200 000 pieds.

La communication présente l'historique, la description et les performances de la première soufflerie du type Hotshot, ainsi que quelques résultats types d'essai. Elle se termine avec un exposé sommaire des projets d'étude en cours fondés sur la méthode qui utilise une décharge électrique pour l'échauffement des gaz.

533.6.071

3b8c2f
3b8c2g

CONTENTS

LIST OF FIGURES

NOTATION

A	cross-sectional area
c	specific heat
C	constant or coefficient
D	diameter
E	specific internal energy
h	heat conduction parameter, C/K
H	specific enthalpy
k	diffusivity, $K/(\rho c)$
K	thermal conductivity
M	Mach number
Nu	Nusselt number
P	pressure
Q	heat flux
r	radius
R	gas constant
Re	Reynolds number
s	coordinate measured along surface of body from stagnation point
S	specific entropy
t	time
T	absolute temperature
U	velocity
x	distance from leading edge of flat plate
ρ	density
τ	relaxation time
γ	ratio of specific heats

α	angle of attack
δ	shock detachment distance
θ	cone half-angle

Subscripts

D	drag
i	initial
L	lift
M	melting
n	nose
p	pressure
w	wall
aw	adiabatic wall
o	isentropic stagnation
1	condition upstream of normal shock
2	condition downstream of normal shock
∞	ambient test-section condition
geom	geometrical
stag	stagnation
x	distance along surface of flat plate

Superscript

*	critical or sonic conditions

Functions

erfc	complementary error function

DEVELOPMENT OF THE SPARK-HEATED, HYPERVELOCITY, BLOWDOWN TUNNEL-HOTSHOT

R.W. Perry and W.N. MacDermott*

1. INTRODUCTION

When the design of the present Gas Dynamics Facility (GDF) at the Arnold Engineering Development Center (AEDC) was initiated in 1950, it was already realized that a conventional hypersonic tunnel would not reach a sufficiently high speed for forthcoming missile developments, and a 'Tunnel F' was added to the proposed GDF test sections. Preliminary attempts to define this tunnel in 1951 led to the requirement for reproduction of the relative velocities of hypersonic flight in the test section and focused attention on shock-tube techniques as the most promising method of obtaining the required high stagnation temperatures. At that time there were no facilities for experimental investigations at the A.E.D.C., and activity on the problem was therefore confined to encouraging and sponsoring research by Cornell University at Ithaca and Cornell Aeronautical Laboratory at Buffalo in applying combustion-driven shock tubes to this requirement.

By the end of 1952, sufficient laboratory facilities had become available at the A.E.D.C. to permit the initiation of an experimental project to assist the Cornell Groups. The AEDC work concentrated upon improvement of the driver component of the shock tube to increase the air density at which a given shock velocity could be achieved. Construction of two distinct types of shock-tube drivers was undertaken. One was to use adiabatic compression of helium to design conditions of 60,000 lb/in.^{2} and 4600^{0}F, while the other was to be a high density Fowler-type[1] electrical driver. The adiabatic compressor (Fig.1) actually achieved conditions above 30,000 lb/in.^{2} and 1700^{0}F, but was so plagued with mechanical difficulties that it was abandoned at the end of 1953, and all further efforts at the A.E.D.C. were confined to various electrical techniques of heating air or other gases.

Already, in late 1952, unsteady expansion of spark-heated air from a Fowler-type driver tube had been used to supply a hypersonic nozzle without an intermediate shock-heating stage. An extremely brief period of low density hypersonic flow was apparently achieved, but no instrumentation was available. However, in a presentation before the AGARD Wind Tunnel Panel at A.E.D.C. during May 1953, this method of operation was rejected in the belief that the arc-heating necessarily yielded a contaminated and highly turbulent flow. The moving shock wave was still regarded as an essential intermediate in securing a clean and uniform flow, although it was recognized that direct arc-heating of the air could produce the required stagnation enthalpy more simply and more efficiently.

By May 1953 preliminary experimental studies of the efficiency of transfer of electrical energy to air and to helium in constant-volume spark-heating and of the magnitude of the resulting rate of heat transfer to the chamber walls were well under way, using

---

*Gas Dynamics Facility, Arnold Engineering Development Center, Air Research and Development Command, United States Air Force

less than 1000 joules of capacitor storage. This initial work has been reported in Reference 2.* Limited studies of the feasibility of extracting the required power from rotating machinery or the main TVA lines had also been made, and capacitor storage was regarded merely as a convenient expedient for the small-scale work. However, a somewhat larger bank of photoflash capacitors rated at 8000 joules was rapidly assembled to make possible extension of the experimental work to larger volumes and increased air densities and temperatures.

It has been recognized that electrical methods of generating strong shocks would require no diaphragm, an important advantage in large installations. However, it was apparent that the Fowler or spark-type electrical driver had the basic disadvantage that the ratio of shock tube length to driver chamber length could not be large, and hence the electrical discharge had to be initiated across the quite long driver through a gas at relatively high density. Much effort was lavished upon this electrical breakdown problem, but in the meantime an alternative, sustained discharge type of operation was demonstrated to be very promising. No appreciable length of driver chamber was required for such a shock tube. The discharge merely occurred across the tube, followed by continuing electrical power input to control the pressure at that station and thus send overtaking expansion or compression waves after the shock. Considerable ability to modify the shock history and to control its natural attenuation was experimentally demonstrated.

At about the same time, the Buffalo group had unexpectedly discovered a new technique for operation of combustion-driven shock tubes[3]. Merely by using thinner diaphragms than usual, they produced stronger shocks. Presumably, such diaphragms burst before combustion was complete, and energy release continued much as in the sustained electrical discharge already discussed. However, since energy release rate during combustion cannot be nearly so well controlled as in electrical discharges, it was to be expected that rapid pressure rises at the origin or behind the interface would occur and cause such strong compression waves that secondary shocks would form before reaching the principal shock. Such secondary shocks have now been unmistakably observed, and the 'constant pressure' combustion system has largely been abandoned because the resulting entropy variations throughout the shock-heated air are highly detrimental to aerodynamic tests[4].

By December 1953, though, this difficulty was not yet apparent and in a presentation before the GDF Working Panel it was recommended that a prototype shock-tube tunnel of one square foot test section and capabilities up to Mach 20 be constructed at the A.E.D.C. with the shock tube suitable for either electric or combustion drive. By July 1954 such a project was approved and a one-million-joule, one-eighth-farad, 4000-volt capacitor bank was ordered, since capacitors had already proven so convenient in the earlier work. However, delivery of even the first few capacitors was so severely delayed that the experimental chamber and shock tube studies necessarily remained on the previous small scale well into 1955. During this period the acceleration of $\frac{1}{16}$ in. nylon pellets to 9800 ft/sec was demonstrated, with arc-heated helium used as the propellant in an otherwise conventional gun. The closely associated study of jets issuing from such small chambers also finally aroused new interest in the direct expansion of

*See also Col. J.A. Dodge, 'Ultra-High Temperature Aerodynamic Testing Facilities', Arnold Engineering Development Center TN-54-61, October 1954

arc-heated air to achieve hypervelocity flows. There were still many doubts as to the quality of such flows, but it was gradually recognized that the extreme temperatures and relatively high densities would themselves tend to promote equilibrium in the chamber and the initial part of the expansion. It was also realized that shock-heating offered no significant advantage over arc-heating with respect to formation of nitric oxide and that the very large hypersonic expansion ratios would produce a strong damping of any possible additional turbulence in arc-heated reservoirs.

As a result of such considerations, the 16 in. diameter 'Hotshot I', which had been designed as an electrically driven, shock-tube tunnel, was rapidly converted during assembly into a spark-heated hypersonic blowdown tunnel and fired for the first time on December 28, 1955. Some of the work contributing to this decision was reported in Reference 5. Many advantages of this simple, direct approach quickly became obvious, particularly the 20 to 30 millisecond duration of hypersonic flow shown by Fastax movies.

By April 1956, a project was approved for construction of a 50 in. diameter Hotshot II to exploit apparent advantages of increased size in this type of tunnel. On October 22, 1956, this tunnel was fired for the first time, with a temporary power supply. After more than one hundred low-power runs, it has now been provided with a 10-megajoule inductive-type power supply and larger arc chamber. Details of this second tunnel will be reported after the completion of initial development and calibration.

In the meantime, the original 16 in. tunnel has successfully come into routine operation, has been used in the development of basic instrumentation for this type of tunnel, and since February 1957 has been used in developmental testing for the aircraft and missile industry.

2. DESCRIPTION OF HOTSHOT I

2.1 Operation

This installation (Figs. 2, 3, 4, 5) consists essentially of a capacitor electrical energy storage system, a spark-heated reservoir, a simple con-di-type nozzle, and a 16 in. diameter cylindrical test section discharging into a conical Laval 24 in diameter vacuum tank. It bears a striking resemblance to a coupling into a sonic blowdown wind tunnel, with the spark-heated high-pressure reservoir corresponding to the stilling chamber of a conventional tunnel. In operation, conventional super- of highly heated air from the reservoir occurs through the nozzle, a quasi-steady expansion speeds in the test section. When the pressure ratio across the nozzle to produce hypersonic critical value, the flow breaks down to a turbulent subsonic stream. The nozzle decays to some

This tunnel differs from the conventional wind tunnel in two important respects: much shorter run times and constant volume, electrical supply air. Air is initially confined in the reservoir at moderate pressures and at room temperature by a thin, plastic diaphragm located just upstream of the throat of the tunnel. Electrical energy is conveniently stored in a large capacitor bank and remotely discharged in a powerful spark through the pressurized air within the reservoir, greatly increasing the temperature and pressure.

The
can
fr
m the spark channel to the remainder of the confined air is accomplished by a
combination of shock-wave heating, convection, and radiation. Pressures exceeding
20,000 lb/in.^{2} have been recorded in the reservoir, and from these peak pressures,
peak temperatures exceeding 8000°K have been computed, using the air properties of
Reference 6.

capacitor discharge, during which peak currents exceeding one million amperes
occur, is completed in less than one millisecond. The transfer of the energy

At these extreme conditions the diaphragm vaporizes and after the usual starting shock process, the quasi-steady expansion through the nozzle occurs. The flow into the vacuum tank, however, is unsteady and flow breakdown occurs in the test section when the initial shock wave returns after reflecting from the end of the vacuum tank. Depending upon the specific initial conditions, the run times vary from 25 to 50 milliseconds. Though short, these run times are an order of magnitude longer than the test times in a shock tube tunnel. During the duration of the supersonic flow there is, of course, a steady decay in the reservoir conditions due to the mass flow through the nozzle and the heat transfer to the walls of the arc chamber. This decay amounts to about 10% of the reservoir pressure in seven or eight milliseconds for typical present operating conditions.

2.2 Wind Tunnel

The test section (Fig.3(a)) is 16 in. in diameter and 30 in. long, internally chrome-plated, with a pair of 12 in. circular window openings centered at one-third of the length. The entire cylindrical section may be turned end for end so that either the upstream or the downstream portions of the test section may be viewed as desired. Glass windows may be mounted tangent to the circular cross section, or they may be replaced with flush steel inserts when external optical instrumentation is not required. Normally, models are mounted on a 1 in. diameter sting which is externally and independently supported. Angles of attack are achieved through use of either a double-knickle sting or a sector. A vertical sting holder enters the tunnel through a flexible, bellows-type vacuum seal in a short spool-piece between the test section and the vacuum tank. Instrumentation leads emerge through sealed terminals in the same spool-piece.

The vacuum chamber is a 24 in. diameter tank, 12 ft long, capable of being evacuated to below one micron Hg. It is equipped with a hinged end flange to permit convenient access to the tank and test section. The upstream entrance is an abrupt expansion from the 16 in. diameter of the test section and instrumentation insert to the 24 in. diameter of the tank. A 6 in. oil booster pump and 130 ft^3/min mechanical pump rapidly evacuate the tank, test section, and nozzle to the one-micron level.

The nozzle is a conical, convergent-divergent design with no attempt to refine the contour. The 5° half-angle divergent portion is internally chrome-plated and relatively permanent because of its size. The convergent portion and throat region, however, are readily replaced (Fig.3(b)). In general, the approach to the throat has consisted of a smooth converging curve followed by a 15° half-angle cone. A plastic (Mylar) diaphragm a few thousandths of an inch thick and about ¼ in. in diameter, analogous to the quick-opening valve of other blowdown tunnels, is installed at a suitable joint in the conical approach region. The throat diameter has been varied from about 0.06 in. to nearly 0.2 in. Refractory materials with good mechanical

properties are required for the throat and approach to it because of the intense local heat transfer and shear loads. Tungsten has so far proven acceptable for this rigorous service, but is difficult to machine. Generally, ultrasonic machining techniques have been satisfactory, although still tedious.

2.3 Arc Chamber

Whereas the sub-assemblies just described have few unconventional features, the arc chamber (spark-heated reservoir) (Figs. 3(b) and 4) bears only a functional resemblance to the analogous component of other blowdown tunnels. Essentially, this is a cylindrical vessel designed to contain transient pressures up tc 60,000 lb/in.^{2} and is provided with openings for pressure transducers and suitable electrodes for spark-heating of the air. The chamber has approximately a 2.5 in. internal diameter and a volume of about 20 cubic inches and is lined with electrically insulating material. It contains a pair of massive, insulated, electrode assemblies with tungsten tips, and a smaller trigger electrode to ionize the gap between the main electrodes when it is desired to initiate the capacitor bank discharge. Besides suitable openings for several stagnation pressure transducers, means are also provided for initially pressurizing the chamber to vary the confined air mass and, hence, the stagnation temperature attained after arcing. Simple rubber O-ring seals at each joint have proven adequate even for the extreme conditions to which the chamber is subjected.

2.4 Power Supply

The capacitor bank (Figs. 3(c) and 5) merits some attention in its own right because it is probably among the larger installations of energy storage capacitors in actual operation. Design rating is one-eighth of a farad at 4000 volts, which permits storage of up to one million joules (watt-seconds). The bank is divided for safety and flexibility into ten independent racks, each containing 100 individual 125-microfarad photoflash-type capacitors connected in parallel. A 5 kW rectifier taper-charges the entire bank to rated voltage in less than two minutes. The operation of the bank is remotely controlled by relay switches to protect personnel from the occasional explosion of a weak capacitor, a hazard deliberately accepted in designing the installation for minimum overall cost. Since the bank can deliver an initial current of at least two million amperes, coaxial bus fabricated from standard copper pipes was installed throughout in order to use the material most effectively in pure tension and compression. Additional advantages deriving from the coaxial bus are the relatively low inductance and the reduced radiation during discharge resulting from confinement of the electro-magnetic field largely within the bus.

3. INSTRUMENTATION

3.1 Pressure Measurements

Initial attempts to instrument this tunnel were based on proven shock-tube techniques, even though Hotshot test times were demonstrably longer than those in shock tubes. It was felt that instrumentation capable of microsecond time response would be even easier to apply to millisecond phenomena. It was soon determined, however, that there were numerous problems peculiar to this type of tunnel which did not exist in shock-

tube operation, and most of these early techniques were abandoned. The pressure rise in the arc chamber is measured with either a strain-gage or variable-capacitance, high pressure transducer, of which there are numerous types available today. Piezoelectric crystal pressure transducers were given extensive study for the purpose of measuring test section and model pressures, as described in Reference 7, but it proved impossible to raise the signal output level of these high-impedance pickups above the noise level created by the intense source of electromagnetic radiation at the arc chamber. Eventually, a standard variable-reluctance pressure transducer of low impedance was adopted and proved capable of measuring all pressures in the tunnel test section from 100 microns Hg to 5 lb/in.^{2}. The only shortcoming of the gage was its physical size, about 1 in. long and $\frac{5}{8}$ in. diameter. These dimensions limited the number of instrumentation channels that could be installed in a small model. The correspondingly large internal volume also required large orifices in the model to obtain satisfactorily short response times.

Figure 6 shows the comparative sizes of a miniaturized, variable-reluctance pressure transducer designed at A.E.D.C. and the commercial gage initially used. Figure 7 shows a hemisphere-cylinder model for either pressure or heat transfer investigations. The ¼ in. openings accept either ¼ in. diameter heat transfer gages or plugs containing the pressure orifices.

Figure 8 shows a typical installation of the now standard, miniaturized pressure transducers in the 4 in. hemisphere-cylinder model. Also shown is the reference manifold supplying the known pressure to the back chamber of all gages and the miniaturized coaxial output cable bundle. The internal volume of these gages, 0.005 cubic inches, has been sufficiently reduced so that adequate response is obtained with model orifices as small as 1/32 in. diameter during tunnel run times from 20 to 50 milliseconds. A commercial 20 kc/s carrier amplifier is used and the gage outputs are recorded in analog form on a commercial recording oscillograph. Figure 9 is a typical oscillograph record of the pressures obtained on this hemisphere-cylinder at a reservoir pressure of 14,500 lb/in.^{2} absolute, a reservoir temperature of 4000°K, and a Mach number of 16. The starting transients occur during the first two or three milliseconds of the run; then there follows a slow decay in all the pressures caused by the drop in reservoir conditions as the air flows from the closed reservoir; and finally, there is a breakdown to turbulent subsonic flow after a run of about 33 milliseconds.

3.2 Heat Transfer Measurements

Heat transfer measurements were initially attempted with the thin-film resistance thermometers which have been put to remarkably good use in shock-tube work. However, it was soon learned that, near stagnation regions, at least, the increased length of run time in Hotshot resulted in destruction of the thin films. Other difficulties were experienced with these gages, but attempts are still being made to apply them to heat transfer rate measurements at model locations where the heat rates are not so high.

Since the key to the basic worth of Hotshot as a new research tool was judged to be in the ability to measure the extreme rates of heat transfer at the stagnation regions of models, a correspondingly large effort was directed towards this goal. The result of this effort was the conception and design of an entirely new and unconventional type of heat-transfer gage based on the variable-reluctance principle (Fig. 10).

The heat-sensitive element is a 0.010 in. thick copper ring, 3/16 in. outside diameter and 1/16 in. inside diameter, contoured to the surface of the model. The inner coils are excited with a 20 kc/s carrier wave, and the copper ring is thus inductively coupled to the inner coil. As the resistance of the upper ring is increased by the temperature rise, a signal proportional to the total heat added to the copper is produced and is amplified and recorded with the same equipment as used for measuring of pressures (Fig.12). Although this new gage has introduced new problems, mainly of calibration, it has been demonstrated that heat-transfer measurements with this gage are possible with a resonable degree of accuracy and with millisecond time resolution. A number of these small, variable-reluctance calorimeters are shown installed in the hemisphere-cylinder model in Figure 11.

3.3 Force Measurements

These two measuring techniques have been offered to Hotshot users as the standard quantitative techniques for the past year. At the same time, a considerable amount of experimental work has been directed toward the goal,of a force-measuring capability for the Hotshot tunnels. A single component, internal strain-gage balance was successfully developed and was used to measure the drag on several shapes (Fig.13). To achieve the required frequency response of 1 to 2 kc/s, it was necessary to use a model of very low mass with a balance and model support of very high stiffness. The same amplifying and recording equipment was used as for the pressure and heat transfer systems.

Further encouraging progress has been made in the extension of this design philosophy to a three-component balance to measure lift, drag, and pitching moment. The first version of this three-component balance (Fig.14) has been found to be inadequately damped in the two normal force components (Fig.15), and a second design has been built and will soon be evaluated. Nevertheless, a limited amount of interesting data has been obtained with the first balance on the AGARD fiberglass-filled plastic model (Fig.14)

3.4 Optical Techniques

There are also available the usual optical techniques which are completely external to the test section. A schlieren system has been developed with which such things as shock shape and detachment distance can be obtained (Fig.16). In addition, much qualitative information can be obtained from Fastax movies exposed by the air's own luminosity, with results similar to the single exposure shown in Figure 16.

4. TUNNEL CALIBRATION

4.1 General

The production of useful aerodynamic test data in any wind tunnel is based on two fundamental operations, a measurement of the effect of the tunnel airstream on a model and a determination of the conditions of the airflow itself. The first of these operations has already been described. The second is commonly referred to as the tunnel calibration which, in a conventional wind tunnel, consists mainly of determining the effect of the boundary layer and contour imperfections on the velocity or Mach number pattern in the tunnel test section for a fairly limited number of tunnel reservoir

conditions. It is possible to minimize the number of reservoir conditions in the calibration of a conventional tunnel simply because the temperature is usually in the range where the specific heat ratio is constant, which leads to explicit expressions for the non-dimensional flow parameters in terms of only one independent variable, such as the Mach number or area ratio. The effect of reservoir conditions on the calibration of a conventional tunnel is the relatively minor effect of the tunnel Reynolds number on the 'effective area ratio' produced by variations in the boundary layer displacement thickness.

The calibration of a Hotshot tunnel is much more complicated because of three factors which are not present in a conventional wind tunnel calibration:-

(a) *Real gas effects* are introduced by the high temperatures used in the reservoir. It is not simply a matter of expansion at a different value of γ for each reservoir condition; it is the more general case of expansion with a continuously varying γ. Even when the flow parameters are non-dimensionalized there exists a different relation between them for each specific reservoir condition and generalized tabulations of isentropic flow parameters are not possible.

(b) *Lack of repeatability* in producing specific reservoir conditions results from the inability to duplicate exactly the amount of energy added to the air from shot to shot. The scatter is usually no more than ±10%, but there are significant differences in the isentropic flow relations for changes of reservoir conditions of this order, thus requiring a separate isentropic expansion calculation for nearly every run.

(c) *The timewise decay of reservoir conditions* results from the mass flow from the closed reservoir and energy lost to the walls of the reservoir by radiation and convection. The rate of this decay in comparison with the transit time through the nozzle is small enough so that a quasi-steady expansion process may be assumed with good accuracy. However, the changes in reservoir conditions with time are large enough in general to require a separate isentropic expansion calculation for each instant at which data are recorded.

In addition to these special complications, the Hotshot calibration must still account for the usual boundary layer displacement effect on area ratio, and a typical calibration consists of the following steps:-

(i) Determination of initial reservoir conditions before any mass flows.

(ii) Determination of reservoir conditions as a function of time after beginning of mass flow.

(iii) Determination of the relation between flow parameters in an isentropic expansion from the instantaneous reservoir conditions.

(iv) Determination of conditions behind a normal shock wave at any point of the isentropic expansion.

(v) Determination of the degree of expansion or 'effective area ratio' at a specific point or points in the nozzle by an experimental measurement of some parameter of the flow at that point or points.

4.2 Initial Reservoir Condition before Mass Flow

The thermodynamic state of the air in the reservoir after the electrical energy has been added and before the tunnel flow begins is determined by the values of the two state variables ρ_{oi} and P_{oi}, the initial density and pressure, respectively.

The initial density is computed from the measured pressure and temperature of the charge in the reservoir prior to the arc discharge. The initial pressure is measured at the peak of the oscillograph trace of the reservoir pressure versus time (Fig. 9). These two parameters define the thermodynamic state, and the other parameters of interest—enthalpy, internal energy, entropy, and temperature—are then obtained by interpolation from the tables of air properties at high temperature[6].

4.3 Reservoir Conditions a Function of Time

The instantaneous reservoir conditions vary because of the combined effect of mass transfer and energy transfer from the chamber, as already mentioned. At the extremely high temperatures which exist in the arc chamber, the only thermodynamic variable which can be conveniently and accurately measured as a function of time is the pressure P_o (Fig. 9). Thus, the thermodynamic state in the reservoir cannot be completely determined by measured values of the primary thermodynamic variables. However, the instantaneous density ρ_o can be obtained by an integration of the mass flow through the nozzle, which is a calculable function of the instantaneous reservoir conditions and the throat size A^*:-

$$\rho_o = \rho_{oi} - \int_0^t (\rho^* U^* A^*)dt/(\text{reservoir volume}) \qquad (1)$$

The product $\rho^* U^*$ results from isentropic expansion calculations as described in the next section. It is a function of ρ_o and P_o and the integration must be performed by a step-by-step summation with $\rho^* U^*$ adjusted for each step of the summation. Once the state is defined as a function of time by $\rho_o(t)$ and $P_o(t)$, the other thermodynamic variables are obtained by interpolations in the air tables.

It is noted that although the change in state in the reservoir is partially due to the energy transfer to the walls of the chamber, it is not necessary to calculate this energy loss to define the changes in state. This overall heat loss to the walls, however, can be obtained as a by-product of the reservoir condition calculation. By definition, if the change of state with time is known, $E_o(t)$ and $H_o(t)$ are known and the condition of conservation of energy for the reservoir can be written as

$$\text{rate of energy loss in reservoir} = \text{rate of loss by mass flow through throat} + \text{rate of loss by heat transfer to walls} \qquad (2)$$

or

$$\text{reservoir volume} \times \rho_o\left(\frac{dE_o}{dt} + E_o \frac{d\rho_o}{dt}\right) = \rho^* A^* U^* H_o + \text{heat transfer to walls} \qquad (3)$$

Arc chamber heat transfer rates have been computed with this relation and were found to lie in the range of 10^3 to 10^4 Btu/ft^2 sec (Figure 4 of Reference 8).

4.4 Isentropic Expansion

The isentropic expansion from a specific thermodynamic state in the reservoir consists of a series of successive thermodynamic states at constant entropy S_o, as shown on a Mollier diagram in Figure 17. With one of the state variables defined by the entropy, each of the succeeding states is defined by only one other parameter. Usually the density ρ_1 is used as this single independent variable. Thus,

$$P_1 = P_1(\rho_1, S_o) \tag{4}$$

$$T_1 = T_1(\rho_1, S_o) \tag{5}$$

$$H_1 = H_1(\rho_1, S_o) \tag{6}$$

The velocity at any point in the expansion is derived from the energy equation

$$\tfrac{1}{2}U^2 + H = \text{constant} \tag{7}$$

or

$$U_1 = \sqrt{[2(H_o - H_1)]} = U_1(\rho_1, S_o) \tag{8}$$

The flow Mach number M_1 is usually of interest only in the vicinity of the test section, where the static temperature is low enough to neglect any real gas effects on the speed of sound. Thus,

$$M_1 = \frac{U_1}{\sqrt{(\gamma R T_1)}} \tag{9}$$

where

$$\gamma = 1.4 \tag{10}$$

By a consideration of the conservation of mass between the throat and any location in the nozzle, the familiar area ratio is formed:-

$$\frac{A_1}{A^*} = \frac{\rho^* U^*}{\rho_1 U_1} \tag{11}$$

The product $\rho^* U^*$ is usually obtained by graphically finding the maximum value of the density-velocity product (maximum mass flow per unit area) for the particular isentropic expansion in question.

4.5 Normal Shock Calculations

At any specific point (1) beyond the sonic point (*) in an isentropic expansion (Fig. 17) a normal shock wave calculation can be made by simultaneously imposing the three laws of conservation of mass, momentum, and energy. The resulting flow parameters, P_2, ρ_2, T_2, H_2, S_2, and U_2, define the state point (2) downstream of a normal

shock, where S_2 is usually much larger than S_0. Then by following an isentropic compression along S_2 to the required enthalpy at a stagnation point H_0, the various parameters at a stagnation point behind a normal shock wave may be determined, P_{02}, ρ_{02}, T_{02}, $H_{02} = H_0$, and $S_{02} = S_2$.

4.6 Determination of Effective Area Ratio

The results of the calculations described in the two preceding sections give tunnel performance curves in terms of the area ratio parameter, and are shown for several reservoir conditions in Figure 18*. As in low temperature tunnels, the tunnel calibration given by the geometric area ratio is only a first approximation to the actual calibration. In fact, it is a much poorer approximation in Hotshot because of the proportionately thicker boundary layers at the high hypersonic Mach numbers and low Reynolds numbers. To determine the actual calibration, the 'effective area ratio' concept is used, wherein one or more parameters are measured experimentally and the effective area ratio is then determined from the calculated curves of these parameters (Fig. 18). Values of all the other parameters at this effective area ratio then form the tunnel calibration at the point of measurement and for the specific instantaneous reservoir conditions. Although a nozzle static pressure is sometimes used to determine the effective area ratio, the parameter most frequently used is the total head ratio P_{02}/P_0, with P_{02} determined either by a pitot probe or by a stagnation point orifice on a model. Typical calibration data for the Hotshot tunnel are given in Figure 19, in the form of effective area ratio plotted against geometric area ratio.

4.7 Approximations Involved

There are several simplifying assumptions implicit in the foregoing discussion of the calibration procedure for this tunnel. The first of these assumptions is that the expansion process from the reservoir to the test section proceeds at thermodynamic equilibrium. As discussed in a subsequent section, calculations have indicated that small departures from equilibrium do occur for the operating conditions currently in use. Further, experimental evidence indicates that departures of the 4000°K expansion from equilibrium are smaller than the present measuring accuracy. This is based upon the apparent equality of the tunnel calibration given separately by pitot pressure measurements and static pressure measurements for this expansion. Preliminary experimental evidence indicates, though, that relaxation effects will be measurable for the 6000°K expansion.

The second assumption is that the gas which flows from the arc chamber is actually pure air. It is inherent in the arc-heating technique that a certain amount of contamination of the air must occur because of the vaporization of electrode material. Measurements have demonstrated an erosion of tungstem electrode tips averaging 1.3 grams per shot, about four per cent of the total mass of heated air. It is expected that these metallic vapors oxidize and condense during expansion of the air, with their principal effect being only a mild sand-blasting of the model.

A more significant type of contamination results from pyrolysis of the plastic diaphragm and arc chamber lining, followed by oxidation of the products of pyrolysis.

---

*In this and the following figures density is given in terms of atm equal to the standard density at a pressure of 1 atm and a temperature of 273°K (0.0804 lb/ft^3).

Significant amounts of oxygen are consumed and replaced by various gaseous contaminants such as carbon dioxide, hydrogen, water vapor, and nitrogen oxides. Recently the nylon arc chamber liner has been replaced by a steel liner to minimize this type of contamination. Eventually it is proposed that an oxide liner of some sort will be used. Also, as larger chambers become available and larger air masses are heated, the relative proportion of any contaminants arising from surface reactions is expected to decrease.

Still a third approximation is involved in the use of the National Bureau of Standards air tables, which include no Van der Waals' effects, at reservoir densities as high as 70 atm. Thus, the enthalpy and entropy corresponding to the experimentally determined reservoir pressure and density may be in error. The effect of errors in reservoir entropy or enthalpy upon the test section density and upon the stagnation pressure and density behind a normal shock in the test section is expected to be small; however, the static pressure is much more sensitive, particularly to errors in entropy.

Another assumption is that the throat size A* remains constant during the tunnel run. Early calculations[8] indicated that the tungsten throat inserts reached melting temperatures in about one millisecond. These calculations have since been found to be overly conservative, as discussed in a subsequent section, and it appears that a substantial portion of each test run is over before any throat melting occurs. The increase in throat area actually measured before and after a large number of runs has been observed to vary from three per cent for large throat diameters to nine per cent for small throat diameters, although much, or even most, of this growth probably occurred during the subsonic flow after breakdown. In most cases the variation is neglected by assuming a constant throat area equal to the initial throat area. In a few instances a crude attempt has been made to account for this area change by assuming a linear variation of throat size with time during the run.

5. TYPICAL TEST DATA

5.1 Pressure Data

A fairly extensive set of test data* has been obtained on the 4 in. hemisphere-cylinder model shown in Figures 7 and 11, partly as an internally sponsored test of the A.E.D.C. and partly under the sponsorship of the Ramo-Wooldridge Company. Figure 20 shows a typical pressure distribution on this model at a reservoir temperature of 4000°K and two slightly different Mach numbers. The measured pressures are non-dimensionalized by the stagnation point pressure and appear to follows the $(\cos)^2$ variation of the modified Newtonian theory from the stagnation point up to and slightly beyond the sonic point, a result which has been observed in numerous conventional wind tunnels at lower Mach numbers and temperatures. An interesting result is the fact that the pressure at the intersection of the hemisphere and the cylinder is closely approximated by matching to the Newtonian theory a Prandtl-Meyer expansion** computed with $\gamma = 1.40$ rather than $\gamma = 1.20$, although the latter is closer to the value for thermal

*J. Christopher Boison. *Experimental Investigation of the Hemisphere-Cylinder at Hypervelocities in Air.* AEDC-TR-58-20, November 1958. (AD-204392).

**This procedure was suggested in Reference 10 and consists of matching the two flows at the point where both the pressure ratios and their derivatives are equal.

equilibrium in that region of the flow. The pressure at this intersection which would be computed for $\gamma = 1.2$ is about 40% higher than for $\gamma = 1.4$, a difference which is considerably larger than the experimental scatter of the measured pressures. It appears that this may be explained as resulting from partially 'frozen flow' about the body. Downstream of the shoulder the pressures on the cylinder fall off slowly with distance and appear to approach the curve representing the blast wave analogy as proposed in References 9 and 10.

Figure 21 is a schlieren photograph of the flow over a flat plate with a sharp leading edge. Pressure measurements on the upper side of this plate, which was aligned with the tunnel axis, are presented in Figure 22. The Reynolds numbers based on the thickness of the leading edge are of the order of 10 to 20 for this data, and therefore the viscous leading-edge interaction would be expected to predominate over the inviscid interaction[17]. It is noted that the combination of the very high Mach numbers and the very low Reynolds numbers results in much larger values of the viscous interaction parameter, $M_\infty^3/\sqrt{(Re_x)}$, than have previously been investigated. It is obvious that there is no correlation of the data with either of the adiabatic theories or with the adiabatic data of Reference 16. The wall temperatures were not measured during the runs, but it is known from other tests that they would not rise over 10^0F or so during each run. The ratio of wall temperature to reservoir temperature for all this data has been computed to lie in the highly cooled range of 0.075 to 0.085. A comparison with the Li-Nagamatsu cooled-wall theory[18] shows the experimental data to be nearly evenly spread between the values for $T_w/T_0 = 0.10$ and $T_w/T_0 = 0$ for the lower values of the interaction parameter. At the higher values of the interaction parameter, the experimental data appears to converge on the theoretical curve for infinite cooling, $T_w/T_0 = 0$.

5.2 Heat Transfer Data

The measured heat transfer distribution for the hemisphere-cylinder at the same tunnel conditions as those for Figure 20 is given in Figure 23. The maximum scatter for these measurements is greater than for the pressure measurements and in some locations is as large as ±15%. Within this scatter, however, there is observed a reasonable agreement with the calculated heat transfer distributions over the hemispherical part of the model. The calculated curve for $\gamma = 1.40$ was based on the method of Reference 11, while the real gas variation was based on the same method with slight modification to allow for the real gas variation of parameters around the body. Downstream of the shoulder the experimental distribution is lower than both of the calculated curves by a significant amount and in a direction which is opposite in sense to the indicated correction for the real gas effects. A similar behavior has been observed on at least two other shapes. It is not known whether this is an actual flow phenomenon or whether it is simply due to an inadequate calibration of the heat transfer gages.

The data of Figure 23 represent the highest quality of heat transfer data yet obtained in the Hotshot tunnel. They were obtained using an improved gage and improved calibration techniques. Correlation of the absolute magnitudes of the heat rates for these runs has been only partially completed. Therefore Figure 24 shows, instead, a correlation of heat transfer data obtained at a two-dimensional stagnation point with the lower quality gages and techniques in use during an earlier test. It is clear that the scatter of these measurements is greater than for those with the improved gages. The average scatter is about equal to the difference between the Fay-Riddell theory[12] and the Lees

theory[11], rendering impossible any statement regarding experimental support for either theory.

5.3 Shock Detachment Data

A considerable amount of shock detachment data has been obtained for the hemisphere-cylinder over the range of reservoir temperatures from 4000°K to 8000°K and computed shock density ratios from 9 to 13 (Fig. 25). The theoretical variation is that suggested by Serbin in Reference 13. The cold-tunnel data is from References 14 and 15, except for the Naval Ordnance Laboratory data, which was taken from Reference 13. The relatively large degree of scatter in the Hotshot data results from the difficulty in obtaining distinct schlieren images in the presence of the intensely glowing air at the stagnation point and at the low density levels currently available. The reading errors are estimated to be of the order of 10% and, in view of this, there seems to be a definite systematic discrepancy between the data and the theoretical curve. In view of the previously noted possibility of an effect on the pressure distribution by a partial freezing of the internal degrees of freedom of the air downstream of the bow shock, it is further noted that the same phenomenon could explain the discrepancy in the shock detachment data, since such a partial freezing would lower the actual density ratios across the shock.

5.4 Force Data

The three-component force balance was evaluated by a series of tests of the AGARD Model B wing-body configuration fabricated of fiberglass reinforced plastic (Fig. 14). The body is cylindrical with a fineness ratio of 8.5 and a quartic nose section resembling an ogive. The wing is a 60° delta with a span four times the body diameter and a symmetrical circular arc airfoil section of 4% maximum thickness. This model is poorly shaped for the hypersonic range and was chosen for the balance evaluation mainly as a matter of convenience in fabrication. Also, for this shape a considerable amount of test data was locally available in the Mach number range from 1.5 to 5.0.

Figure 26 presents the lift curve obtained for AGARD Model B at a Mach number from 15 to 16, a Reynolds number based on model length of 200,000 and a reservoir temperature of 4000°K. The scatter in the measured lift coefficients increased as the angle of attack increased simply because the effect of the inadequate damping was proportional to the magnitude of the lift force being measured. The typical nonlinear hypersonic variation of C_L was obtained.

In comparing the Hotshot force data with that obtained in the supersonic tunnel E-1 at A.E.D.C. (Figs. 27 to 30), the order-of-magnitude difference in Reynolds number must be kept in mind as well as the large difference in the Mach number range. The effect of the Reynolds number upon the lift characteristics would be expected to be fairly small and, indeed, both the lift-curve slope and the center-of-pressure location in the Hotshot data appear to lie on a reasonable extrapolation with respect to Mach number only (Figs. 27 and 28).

With respect to the drag forces, however, a rather large effect of the order-of-magnitude reduction in Reynolds number would be expected in addition to the effect of the high Mach number, and this is exactly what was observed. The lift-drag polar is given in Fig. 29 with the experimental scatter of the Hotshot data indicated by the

size of the rectangular data points. Based on the difference in Mach number alone, the minimum drag coefficient at M = 15 would be expected to be slightly less than at M = 5.0, but because of the lower Reynolds number it was actually increased by 250%. The combined effect of the very high Mach number on the lower speed configuration and the low Reynolds number is a reduction in maximum lift/drag ratio to slightly less than one. By assuming, as a first approximation, that the difference in minimum drag is entirely a Reynolds number effect, and therefore subtracting uniformly from the polar obtained in Hotshot the difference in minimum drag coefficients between the two sets of test data, it can be shown that the AGARD B shape at M = 15 would still produce lift/drag ratios of only about two, even at Reynolds numbers of the order of three to four million.

Although it is likely that in the near future an order-of-magnitude increase in Reynolds number will be attained in the Hotshot tunnel, there will still be a sizable gap between tunnel and flight Reynolds numbers. The procedure of correcting the polar to higher Reynolds numbers may not be possible because there may be little or no data available on the proposed hypersonic shapes from other wind tunnels. The possibility of a purely analytic correction of the minimum drag coefficients depends entirely on the assumption that the variation of $C_{D_{min}}$ with Reynolds number can be completely represented by the simple variation of skin friction coefficient with Reynolds number, whereas, in actuality, it seems likely that strong secondary influences of Reynolds numbers, such as viscous interactions and variable laminar separations, would be important. This conclusion is partially supported by a comparison of the Hotshot and Tunnel E-1 minimum drag coefficients plotted against Reynolds number (Fig. 30). It is seen that the measured values from Hotshot lie 30% higher than the values computed from the low Mach number data with a reasonable allowance for the difference in Mach number, plus an allowance for the decreased Reynolds number based upon the increased skin friction only.

5.5 General Remarks on Test Data

It is realized that much room remains yet for improvement of the instrumentation and the flow quality of the Hotshot tunnels. However, the foregoing examples of the variety and the quality of the data already obtained appear very encouraging. In addition, confidence in the validity of measurements in Hotshot has been increased by the verification in flight of the pressure distribution determined for one nose cone and good agreement with the drag coefficients measured for another nose cone model in the free-flight wind tunnel at the NACA Ames Laboratory.

6. ADVANCED DEVELOPMENTS

In addition to the original 16 in. Hotshot tunnel in which the work described was accomplished, there now exist two others of 50 in. and 8 in. diameter, geometrically similar, and locally labelled 'Hotshot II' and 'Halfshot', respectively. Halfshot shares the million-joule capacitor bank and many spare parts with the original Hotshot tunnel and is primarily intended to accelerate investigation of many promising tunnel improvements, such as a second-throat diffuser, to permit their inclusion in the final design of a still larger Tunnel F, of which the Hotshots are prototypes.

The 50 in. tunnel (Fig.31) is expected to have an order-of-magnitude improvement in Reynolds number throughout its Mach number range because of its large size and higher reservoir pressure, but it differs primarily from the original Hotshot in the method of storing the electrical energy for the air-heating spark. Because of the cost and bulk of capacitors, the inductive storage system of Figure 32(a) was adopted instead to deliver the desired ten million joules into the air. The operation of such a system has already been described by Early and Walker[19]. Basically, a direct current generator which is momentarily driven by a heavy high-speed flywheel builds up a large circulating current in an air-cored reactor, thus storing large amounts of readily accessible energy in the resulting magnetic field. This energy is returned to the circuit at a greatly increased rate when an attempt is made to interrupt the current, as by opening a switch within the air-heating chamber. Power at a rate of over 10^6 kilowatts is thus delivered to heat the air, although the entire initial input to the storage system is accomplished by a 184 kW electric drive motor.

As indicated in Figures 32(a) and 32(b), the inductive power supply of the 50 in. tunnel is shared by an experimental electric gun (Fig.33) which gives promise of achieving muzzle velocities exceeding Mach 20 and which perhaps is even capable of reaching escape velocity[20]. The propellant is spark-heated hydrogen or helium. A gun barrel replaces the Laval nozzle of the Hotshot tunnels, but so many parts are interchangeable and the operation is otherwise so similar that this gun has been named Potshot. In parallel with development of this new type of gun, an attempt is under way to produce a small, rugged, multichannel telemeter to radio back from the moving projectile detailed quantitative information of the type usually obtained in a wind tunnel. To date, a 20 Mc/s oscillator has functioned satisfactorily in flight after a peak acceleration of 200,000 times gravity[20]. Attempts to ruggedize the necessary transducers are also in progress.

7. FLIGHT SIMULATION AND LIMITATIONS OF HOTSHOT TYPE TUNNELS

Because of the high degree of flexibility of the electric power supply, the Hotshot tunnels may be operated over an exceptionally wide range of density, velocity, and Mach number. However, if it is desired to completely simulate flight, certain definite relations between the reservoir conditions and nozzle expansion ratio must be imposed to insure that the test section density and temperature are related as in the earth's atmosphere.

7.1 Reservoir Conditions and Area Ratio for Flight Simulation

The reservoir conditions required for complete simulation of flight velocity and ambient atmospheric conditions correspond to the isentropic stagnation state in flight and are indicated in Figure 34, as computed on the basis of References 6 and 21. The corresponding effective* area ratio A/A^* is shown in Figure 35 and was calculated from the following empirical relation, which is valid for reservoir densities from 10 to 100 atm and reservoir temperatures between 2000°K and 9000°K:-

*The actual geometric area ratio required would be somewhat larger (Fig. 19).

$$\log_{10}(\rho^*U^*) = 0.486\log_{10}P_o + 0.516\log_{10}\rho_o + 2.792 - \frac{0.0005(\log_{10}P_o - 0.96\log_{10}\rho_o - 1.63)}{0.0008 + (\log_{10}P_o - 0.96\log_{10}\rho_o - 1.63)} \quad (12)$$

7.2 Performance Limitations of Flight-Simulating Tunnels

One limitation to the possible performance of Hotshot-type tunnels operating with flight simulation is immediately apparent from Figure 34. The mechanical strength of the reservoir will permit duplication of only those altitude-airspeed combinations which are above and to the left of the corresponding constant reservoir pressure line. A number of other limitations are now discussed, in relation to Hotshot tunnels having *effective* test section diameters of 16, 50, and 100 in. and utilizing conical nozzles of 10^o total expansion angle. In several cases the effect of the reduction of nozzle expansion angle of 5^o is indicated.

One performance limitation is imposed by the design of the throat and diaphragm assembly. Because of the difficulty in machining the materials used for the throat region, there will generally be a minimum throat diameter that can be used on any given tunnel. The initial pressures which the diaphragms must hold are determined by the reservoir densities shown in Figure 34.

The volume of the reservoir is another potential limitation to the tunnel performance. If it is too small, the reservoir conditions decay so rapidly that the flow becomes unsteady. To insure quasi-steady flow, it is arbitrarily assumed that the fractional efflux should be less than one percent during the transit time of a particle through the nozzle. The particle transit time is chosen in preference to the signal transit time, not only because it is more conservative but also because this presumably insures quasi-steady entropy in addition to quasi-steady pressures. Using approximate transit times for conical nozzles based upon infinitely small throats and constant velocities equal to the test section velocities, the reservoir volumes necessary to satisfy the foregoing criterion were calculated and are given in Figure 36.

Of course, another possible limitation is the energy required to heat this mass of air to the desired temperature. Figure 36 also shows the energy requirements for the volumes given, assuming 100% efficiency of transfer to the air.

The combined effects of these mechanical and electrical limitations upon the flight-simulation type of performance of Hotshot tunnels are shown in Figures 37(a) and 37(b). Quasi-steady flight duplication in the 16 in. tunnel (Fig.37(a)), is presently limited by the minimum throat size, 0.05 in. diameter; by the reservoir pressure, 1000 atmospheres, which can be routinely contained; and by the reservoir size, 20 cubic inches, which is conveniently available. Improvements which seem to be entirely feasible would increase the reservoir pressure limit to 2000 atmospheres and the chamber volume to 60 cubic inches, with the resulting performance improvements shown. The million-joule energy supply seems more than adequate even for the higher performance operation.

In the case of the 50 in. tunnel (Fig.37(b)), quasi-steady flight duplication is temporarily limited by the presently attainable reservoir pressure, 2000 atmospheres,

and the existing 60 cubic inch pressure vessel. A 250 cubic inch chamber which is currently being fabricated will improve the performance as shown. The existing energy supply and throat sizes do not seem to be important limitations in this installation at present.

7.3 Throat Heat Transfer in Temperature-Simulating Tunnels

In addition to the mechanical and electrical limitations, nearly all methods of achieving hypervelocity airflows are subject to restrictions imposed by the intense rate of heat transfer to the walls of the nozzle at the minimum cross section of the flow. This was pointed out in Reference 22 and, although the throat heating was over-estimated because of the assumption of a constant heat flux into the wall even up to the melting temperature, the general nature of the problem is as described. If, instead of being constant, the heat flux is assumed equal to $C(T_{aw} - T_w)$, where C and T_{aw} are constants, then the wall temperature is given as a function of time by Reference 23:-

$$T_w = T_i + (T_{aw} - T_i)[1 - e^{h^2 kt}\operatorname{erfc}\sqrt{(h^2 kt)}] \qquad (13)$$

This same formula, Equation (13), also relates the melting temperature and the time when the surface begins to melt. It is compared with the more conservative estimate of Reference 22 in Figure 40. Clearly, the simpler relation only holds in the limit when the melting temperature is small compared to the recovery temperature.

In order to get an absolute value for the melting time, the constant C and T_{aw} must be evaluated in terms of the flow parameters. Assuming a recovery factor of 0.9 and a Stanton number of 0.0014, the latter as suggested in Reference 22, the heat flux to the throat wall per unit area equals $0.0014\ \rho^*U^*\ (0.9H_o - H_w)$, where ρ^*U^* is the sonic mass flow per unit area, H_o is the stagnation enthalpy, and H_w is the enthalpy of the air at the wall temperature. This can only be reduced to the form $C(T_{aw} - T_w)$ if a constant specific heat can be assumed. Since the time to melt is influenced most significantly by values of H_w near the melting condition, it seems a good approximation to define $c_p = H_M/T_M$, where T_M is the melting temperature of the wall and H_M is the corresponding enthalpy of the air, and then to take the flux to the wall as $0.0014\rho^*U^* c_p(0.9H_o/c_p - T_w)$. Thus the ratio of H_w to T_w has also been taken equal to c_p or H_M/T_M. With this assumption, the constant $C = 0.0014\rho^*U^*c_p$, while the constant $T_{aw} = 0.9H_o/c_p$. In computing the time to melt a tungsten throat for a flight-simulating tunnel (Fig. 39) c_p was specifically taken equal to 0.3 Btu/lb^{0}F.

After melting beings, it very rapidly settles down to a rate determined by the latent heat of fusion of the wall material if vaporization does not occur and if the viscosity of the melt is sufficiently low and the strength of the unmelted material sufficiently high compared to the shear stresses at the surface[24]. The corresponding rate of erosion of a tungsten throat and the rate of heat transfer after melting does begin are plotted in Figures 40 and 41, respectively. The fractional change in area of a tungsten throat per unit time after erosion begins is shown in Fig. 42 for 16, 50, and 100 in. effective test section diameters.

It is noted that this entire discussion of the throat heat transfer and throat melting is based upon the idealized assumption of a one-dimensional heat conduction in a semi-infinite slab. However, since the depth of diffusion of heat during the usual duration of hypersonic flow is generally small compared to the throat diameter, further refinement of the analysis appears unnecessary.

7.4 Relaxation in the Nozzle Expansion

Another, and perhaps the most basic, performance limitation results from relaxation effects during the rapid expansion of the high temperature air. The finite rate of de-excitation of the internal degrees of freedom of the air leads to departures from thermodynamic equilibrium. Since the seriousness of relaxation effects is indicated by the product of $d(\log_e T)/dt$ and τ, the relaxation time[25], it is clear that for the same operating conditions a larger tunnel with its longer transit time should encounter less severe relaxation. For a given reservoir temperature and expansion geometry, relaxation effects must increase as the simulated altitude increases, since relaxation time increases as the general density level decreases or the molecular collision frequency decreases. Thus the occurrence of unacceptably large departure from equilibrium will determine an upper altitude limit which can be accurately simulated at any given airspeed, just as the reservoir strength and throat heat transfer set a lower altitude limit. A detailed investigation is certainly called for to insure that there actually is a useful area of flight simulation and that these upper and lower limits do not indeed overlap. Preliminary studies have indicated that lag in nitric oxide decomposition at the lower simulated airspeeds of the range considered here ($\simeq$ 10,000 ft/sec), lag in de-excitation of nitrogen vibration at the middle speed range ($\simeq$ 14,000 ft/sec), and lag in atomic oxygen recombination at the higher speeds ($\simeq$ 18,000 ft/sec) are the principal effects to be considered. As presently operated, Hotshot I is calculated to suffer only a three per cent velocity defect and corresponding effects on the other flow parameters through all but the upper portion of its velocity range as a result of such relaxation. It seems highly probable that relaxation will prove to be the most difficult hypervelocity tunnel design problem to solve, although it can be avoided for some purposes by not fully expanding the flow and thus sacrificing Mach number simulation.

7.5 Comparison of Hotshot Tunnel with other Hypervelocity Facilities

Numerous suggestions of methods to circumvent one or another of the various performance limitations have been advanced. However, the amelioration of one condition is invariably at the expense of increasing other difficulties or at the sacrifice of flow quality or of complete flight simulation. For example, the addition of heat to a supersonic stream[22], which has been proposed to avoid the performance limitations imposed by throat heat transfer, simultaneously increases the reservoir strength required for flight duplication because of the greater entropy increase resulting from heat addition to a moving stream, and probably also increases relaxation difficulties by creating a severe disturbance in the partially expanded flow where the density level is already lowered and the relaxation time is already correspondingly lengthened. The non-reflected type of shock tunnel[26] reduces somewhat the maximum wall heat transfer, since the air is already at a Mach number of 2 to 3 when beginning its expansion, but at the expense of subjecting the entire shock tube to this still quite high heating rate. The 'wave engine' or 'Gatling gun' type of shock tunnel[27] can only escape the throat heat transfer limitation for continuous running if multiple throats or a non-reflected configuration are used, both probably leading to severe periodic disturbances in the supersonic stream which would be objectionable for aerodynamic testing.

The other three types of hypervelocity tunnel facilities—the plasma-jet, the Hotshot tunnel, and the reflected shock-tube wind tunnel— differ essentially only in their run

times and in their flow quality. In the case of the latter, the purity of the airflow may, with care, be made quite high, but the run times are so short even with quite long tubes that conventional wind tunnel measurements have proven to be very difficult to make. Also, attenuation of the shock wave as it passes down the shock tube usually leads to a rapid decay of stagnation enthalpy during the short run times. The most important advantage of the shock tunnel would appear to be the purity of air flow, since this allows the powerful spectroscopic technique to be brought to bear upon the various regions of airflow over a model. In the plasmajet, in contrast, very long run times are produced, but to avoid catastrophic throat erosion the density must be kept so low that the expanding air is essentially 'frozen'. In utilizing its long run times to investigate ablation in a high-enthalpy flow, this question of the chemical dynamics of the air is probably of minor importance, particularly since no more satisfactory facility for this purpose seems presently available. If, however, the relaxation effects are not as important as they now seem, a plasmajet simulating flight on a continuous basis would require electrical power in the amounts shown in Figure 43 for two sizes of test section.

In a Hotshot tunnel the run time is only long enough to insure quasi-steady flow and to facilitate the solution of the instrumentation problems. Thus, while keeping throat erosion within tolerable limits, the density can be increased to simulate the lower altitudes and also reduce the relaxation effects. A secondary advantage of the relatively short run times is the feasibility of using electrical energy storage techniques and constant-volume heating and compression of the supply air, thus eliminating the need for a continuous source of electrical power and a separate superpressure pumping system. The principal disadvantage in comparison with the plasmajet is that the ability to study time-dependent phenomena has been sacrificed, whereas the principal disadvantage in comparison with the shock tunnel is that the airflow is inherently more contaminated due to vaporization of electrode material. This contamination apparently has no marked effect upon the flow but would probably be a serious hindrance to spectroscopic investigations of the flow.

Also, as in combustion studies, it appears impossible to scale simultaneously all of the physical and chemical reactions occurring in the highspeed, air-body interaction. The radiative and convective contributions to the stagnation point heat transfer on a blunt body, for instance, do not scale similarly. The convection decreases with the square root of the nose radius, while the radiation increases directly with the scale, since the thickness of the shock layer increases similarly. Also, the rates of the various important chemical reactions are not equally affected by changes in density. In addition to this justification for a test section large enough to make full-scale tests, deviations from equilibrium in the expansion through the nozzle would also be reduced because of the lowered cooling rate in the larger nozzle, as already discussed. Since the fractional change in area ratio per unit time would be reduced, at a first glance the throat problem would also seem to be helped by an increase in size. However, the transit time through the nozzle would also be increased, and the probably more significant fractional change in area ratio during a particle transit time would be independent of size. In spite of this, the full-scale tunnel seems to represent a very desirable goal.

8. CONCLUSIONS

(i) The Hotshot type of wind tunnel, driven by a spark-heated source of air, has been developed to provide an aerodynamic testing tool capable of producing the true stagnation enthalpy, density level, and Mach number of hypersonic flight through the earth's atmosphere. Mach numbers from 10 to 20 have been produced at density altitudes of 140,000 to 200,000 ft.

(ii) The run times in this tunnel, 20 to 50 milliseconds, require instrumentation response times of 2 to 3 milliseconds. Although many differences in detail are necessary to achieve this response time, most of the instrumentation used is fundamentally similar to that used in conventional wind tunnels.

(iii) Pressure and heat transfer rate distributions and forces have been measured on a number of different shapes in the stagnation temperature range of 4000 to 8000^{o}K.

(iv) Calibration of the test section flow is lengthy and tedious because of the real gas effects in the nozzle expansion, the decay of reservoir conditions resulting from the expansion from a closed chamber, and the inability to duplicate the reservoir conditions exactly from shot to shot.

(v) The range of operation of this tunnel, in which an exact simulation of all the ambient conditions of flight is possible, has been defined by a consideration of energy requirements, chamber volume requirements for true quasi-steady flow in the test section, throat erosion by melting, and departures from equilibrium in the expansion. Operation outside of this range is possible, but at least one of the parameters- Mach number, density, or velocity (stagnation enthalpy) - will not be correctly simulated in such operations.

REFERENCES

1. Fowler, R.G. et alii — *Luminous Fronts in Pulsed Gas Discharges.* Physical Review, Vol.82, June 1951, pp. 879-882.

2. Bloxsom, D.E. — *Production of High-Temperature, Moderate-Pressure Gases by Means of Electrical Spark Discharges.* Arnold Engineering Development Center TN-56-17, November 1956.

3. Hertzberg, A. Smith, W.E. — *A Method for Generating Strong Shock Waves.* Journal of Applied Physics, Vol.25, 1954, pp. 130-131.

4. Wittliff, C.E. Wilson, M.R. — *Shock Tube Driver Techniques and Attenuation Measurements.* Air Force Office of Scientific Research TN-57-546, August 1957.

5. Bloxsom, D.E. — *Gas Purity of High-Temperature, High-Pressure Electrical Discharges in Air.* Arnold Engineering Development Center TN-56-15, November 1956.

6. Hilsenrath, J. Beckett, C.W. — *Tables of Thermodynamic Properties of Argon-Free Air to 15,000°K.* Arnold Engineering Development Center TN-56-12, September 1956.

7. Mulkey, M.R. et alii — *Pressure Measurements in an Arc-Discharge Wind Tunnel.* Arnold Engineering Development Center TN-58-16, April 1958.

8. MacDermott, W.N. — *Preliminary Test Results With an Arc-Heated Hypersonic Wind Tunnel at Mach Numbers of 10 to 20.* Proceedings of the Fifth Midwestern Conference on Fluid Mechanics. University of Michigan, April 1-2, 1957, pp.224-237.

9. Lin, S.C. — *Cylindrical Shock Wave Produced by Instantaneous Energy Release.* Journal of Applied Physics, Vol.25, No.1, January 1954, pp. 54-57.

10. Lees, et alii — *Inviscid Hypersonic Flow Over Blunt-Nosed Slender Bodies.* Journal of the Aeronautical Sciences, Vol.24, No.3, March 1957, pp. 195-202.

11. Lees, Lester — *Laminar Heat Transfer Over Blunt-Nosed Bodies at Hypersonic Flight Speeds.* Reprinted from Jet Propulsion, Vol. 26, No. 4, April 1956, pp. 259-269.

12. Fay, J.A. Riddell, F.R. — *Theory of Stagnation Point Heat Transfer in Dissociated Air.* Journal of the Aeronautical Sciences, Vol. 25, No. 2, February 1958, pp. 73-85.

13. Serbin, Hyman — *Supersonic Flow Around Blunt Bodies.* Journal of the Aeronautical Sciences, Vol. 25, No. 1, January 1958, pp. 58-59.

14. Heberle, J.W. et alii — *Data on Shape and Location of Detached Shock Waves on Cones and Spheres.* NACA TN 2000, January 1950.

15. Oliver, Robert E. — *An Experimental Investigation of Flow Over Simple Blunt Bodies at a Nominal Mach Number of 5.8.* California Institute of Technology, GALCIT Memorandum No. 26, June 1, 1955.

16. Kendall, James M. — *An Experimental Investigation of Leading-Edge Shock-Wave Boundary-Layer Interaction at Mach 5.8.* Journal of the Aeronautical Sciences, Vol. 24, No. 1, January 1957, pp. 47-56.

17. Hammitt, A.G. Bogdonoff, S.M. — *Hypersonic Studies of the Leading Edge Effect on the Flow Over Flat Plate.* Jet Propulsion, Vol. 26, No. 4, April 1956, pp. 241-246, 250.

18. Li, Ting-Yi Nagamatsu, H.T. — *Hypersonic Viscous Flow on Noninsulated Flat Plate.* Proceedings of the Fourth Midwestern Conference on Fluid Mechanics, September 8-9, 1955, pp. 273-287.

19. Early, H.C. Walker R.C. — *The Economics of Multimillion Watt-Second Inductive Storage.* Presented as a Conference Paper, American Institute of Electrical Engineers Winter Meeting, January 30 - February 3, 1956.

20. Stollenwerk, E.J. Perry, R.W. — *Preliminary Planning for a Hypervelocity Aeroballistic Range at AEDC.* Arnold Engineering Development Center TN-58-25, June 1958.

21. Minzner, R.A. Ripley, W.S. — *The ARDC Model Atmosphere.* Air Force Cambridge Research Center TN-56-204, December 1956.

22. Smelt, R. — *Test Facilities for Ultra-High-Speed Aerodynamics.* Proceedings of the Conference on High-Speed Aeronautics, Polytechnic Institute of Brooklyn, January 20-22, pp. 311-333.

23. Churchill, R.V. — *Modern Operational Mathematics in Engineering.* McGraw-Hill, 1944, p. 216.

24. Landau, H.G. — *Heat Conduction in a Melting Solid.* Quarterly of Applied Mathematics, Vol. VIII, 1950, pp. 81-94.

25. Logan, J.G. Jr., — *Relaxation Phenomena in Hypersonic Aerodynamics.* Institute of Aeronautical Sciences Preprint No. 728, January 1957.

26. Hertzberg, A. et alii — *Modifications of the Shock Tube for the Generation of Hypersonic Flow.* Arnold Engineering Development Center TN-55-15, March 1955.

27. Hertzberg, A. Weatherston, R. — *A New Method for Providing Continuous High Temperature Airflow for Hypersonic Research.* Proceedings of the Florida Conference on High Speed Aerodynamics and Structures. Air Research and Development Command Tech. Rep. 57-46, ASTIA No. AD-113-003, 1957.

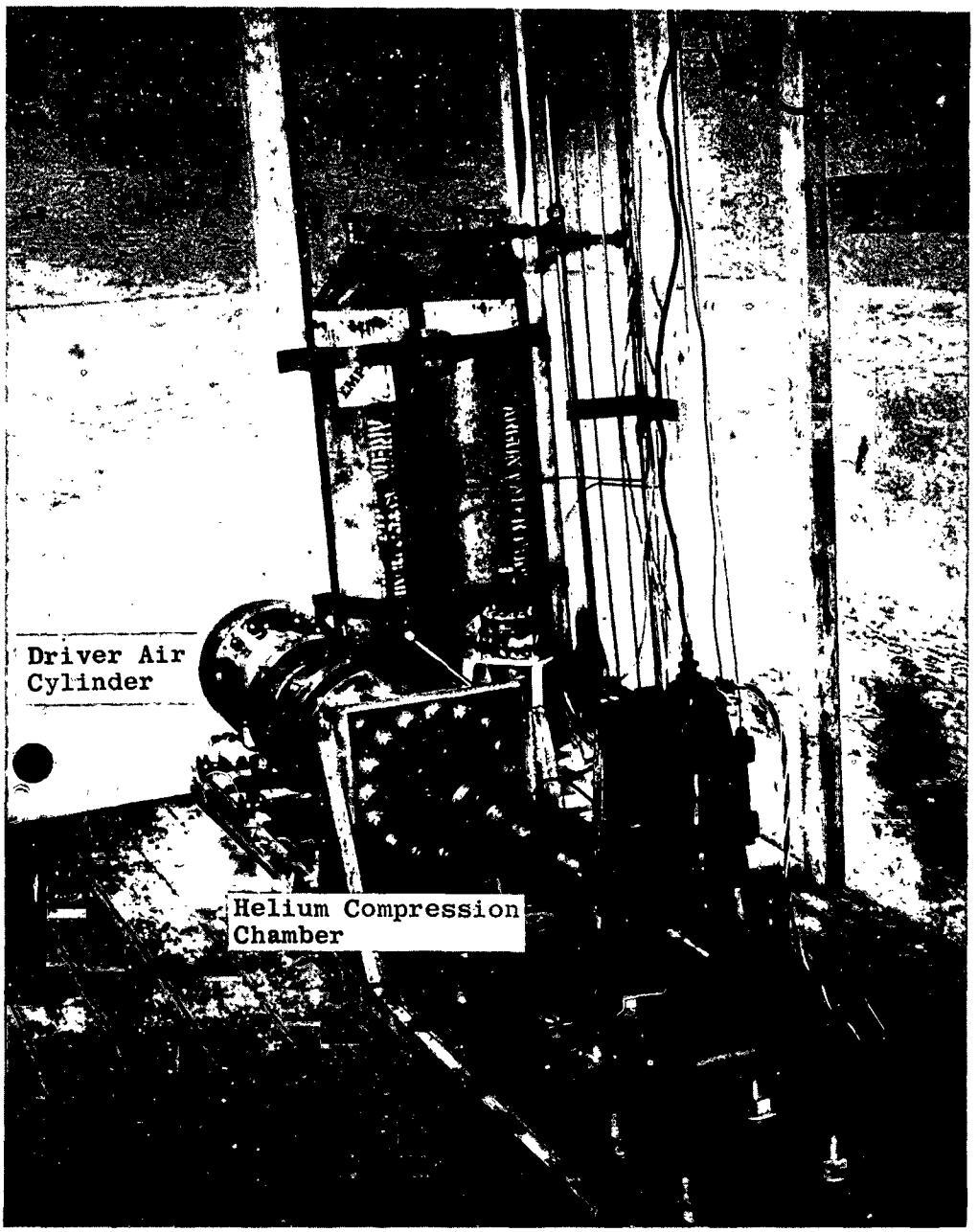

Fig.1 Adiabatic compressor

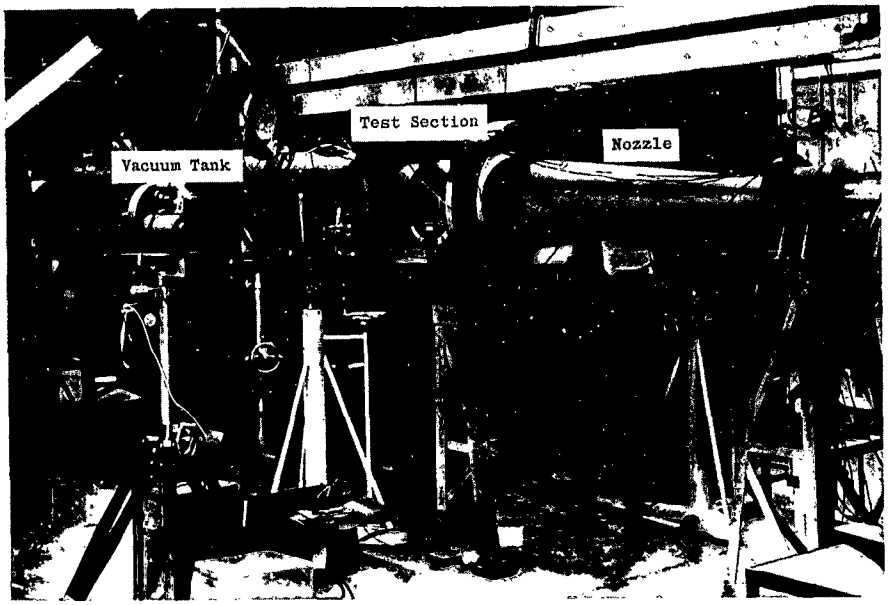

(a) Downstream view

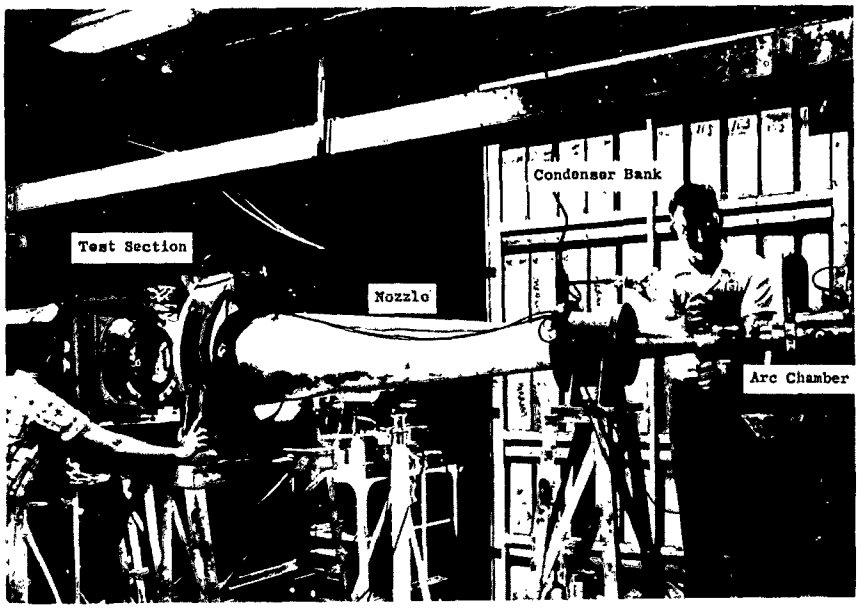

(b) Upstream view

Fig.2 Hotshot I

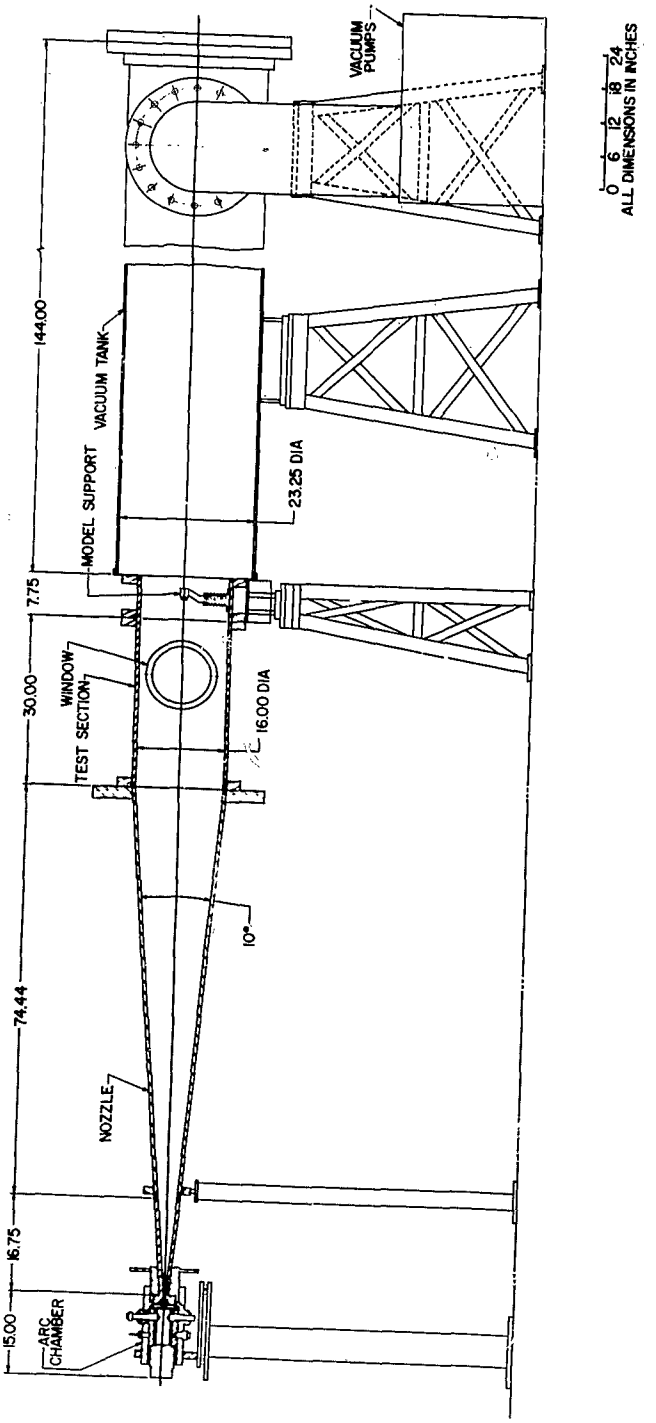

Fig. 3 Hotshot installation
(a) Tunnel assembly

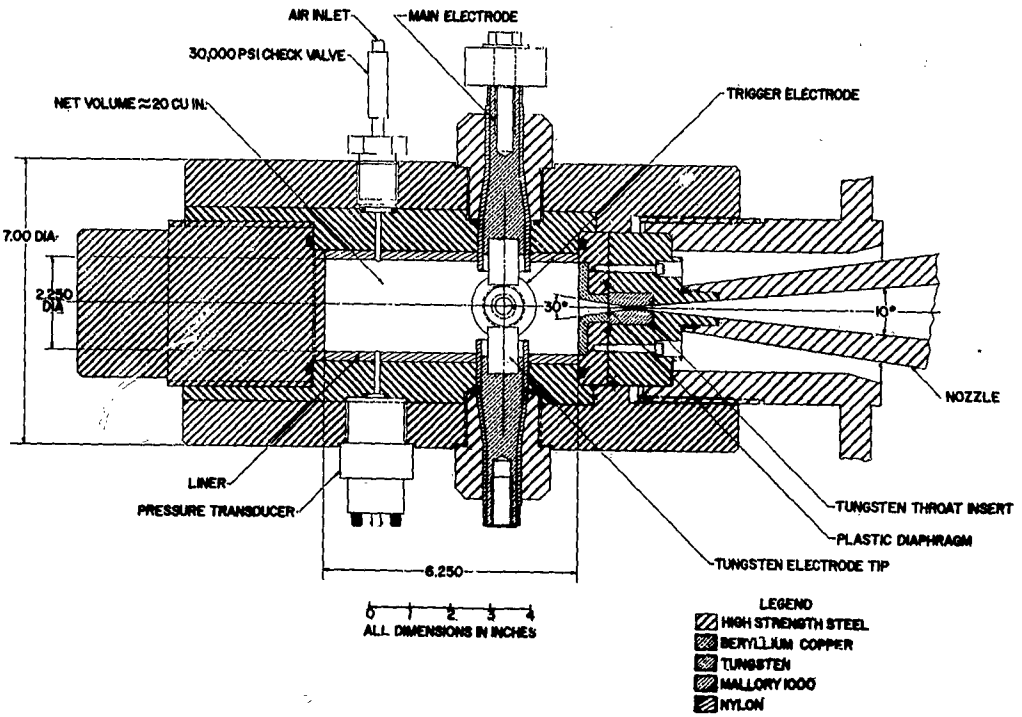

(b) Arc chamber and nozzle throat

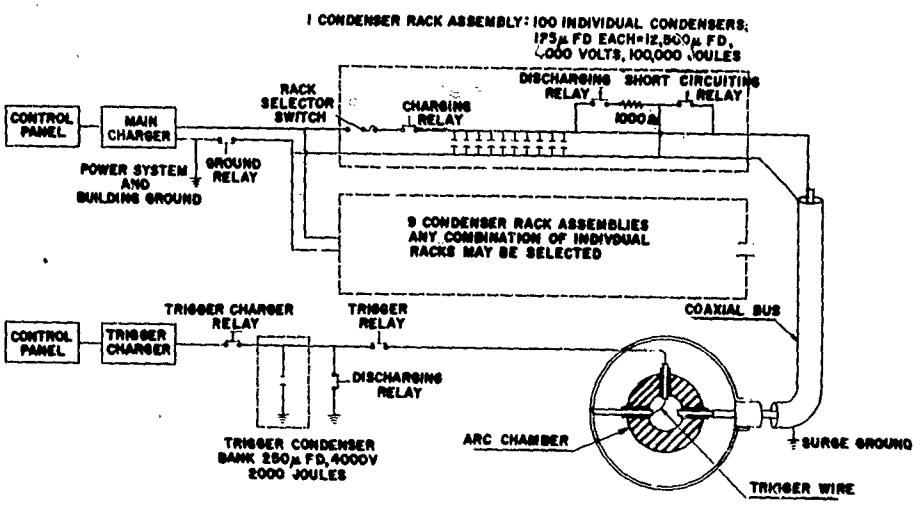

(c) Schematic layout of electrical system

Fig.3 Hotshot I installation

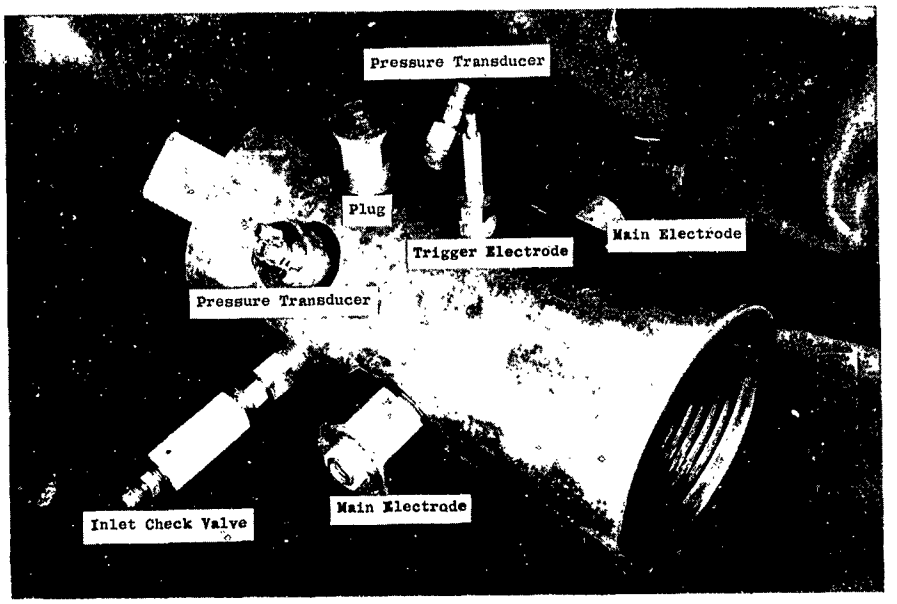

(a) Complete assembly

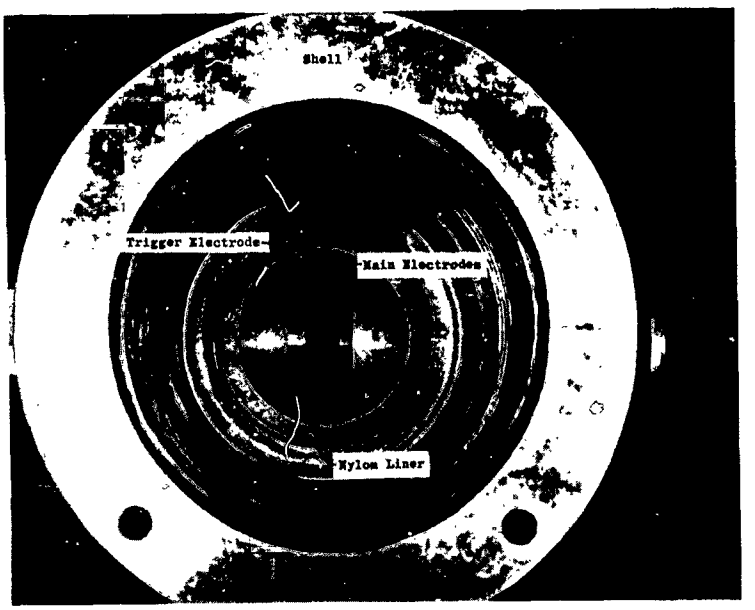

(b) Interior view of electrode assemblies

Fig. 4 Hotshot I arc chamber

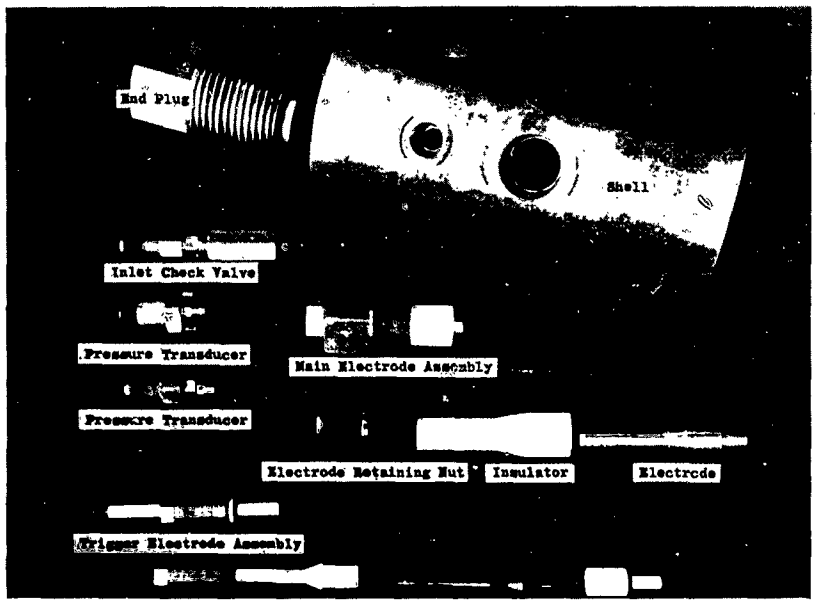

Fig.4 Hotshot I arc chamber
(c) Exploded view of individual parts

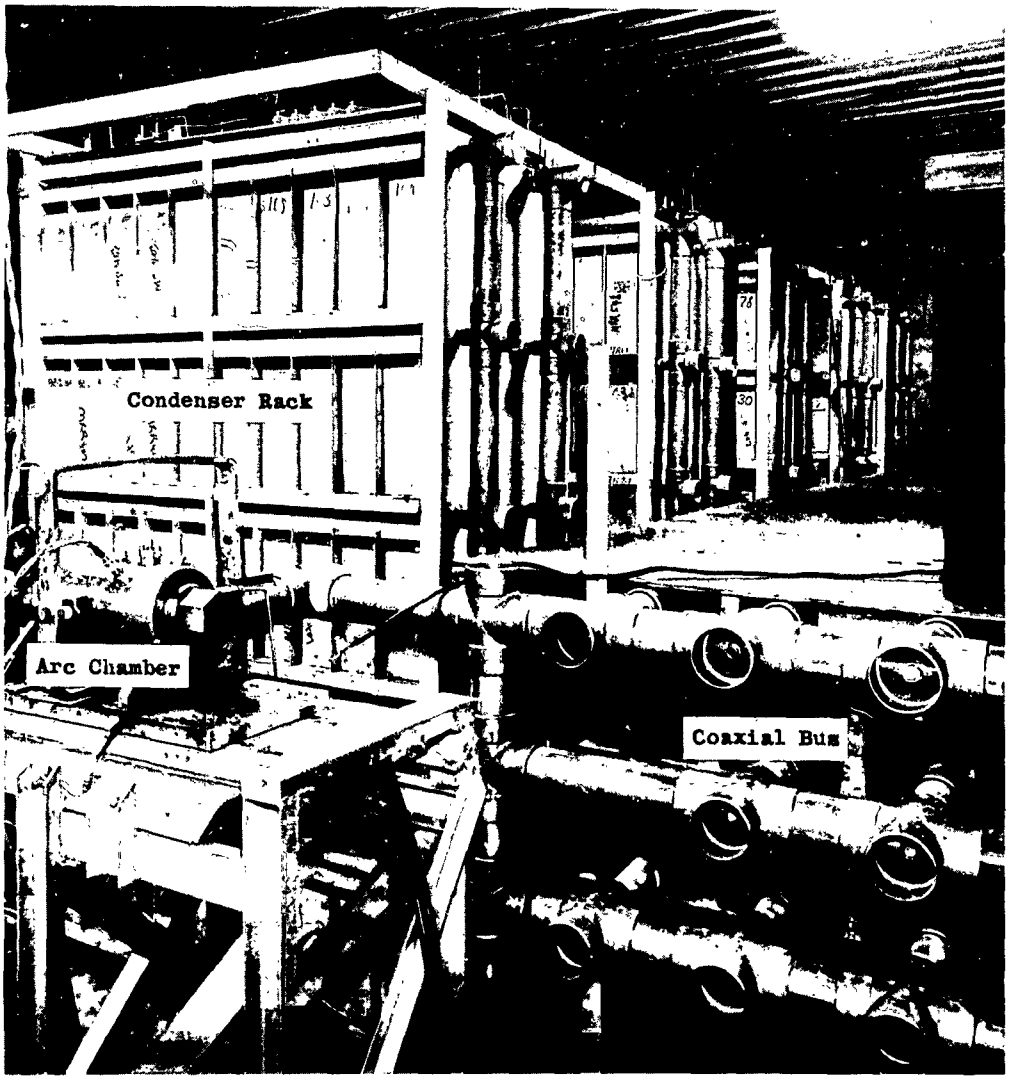

Fig.5 Million joule capacitor bank

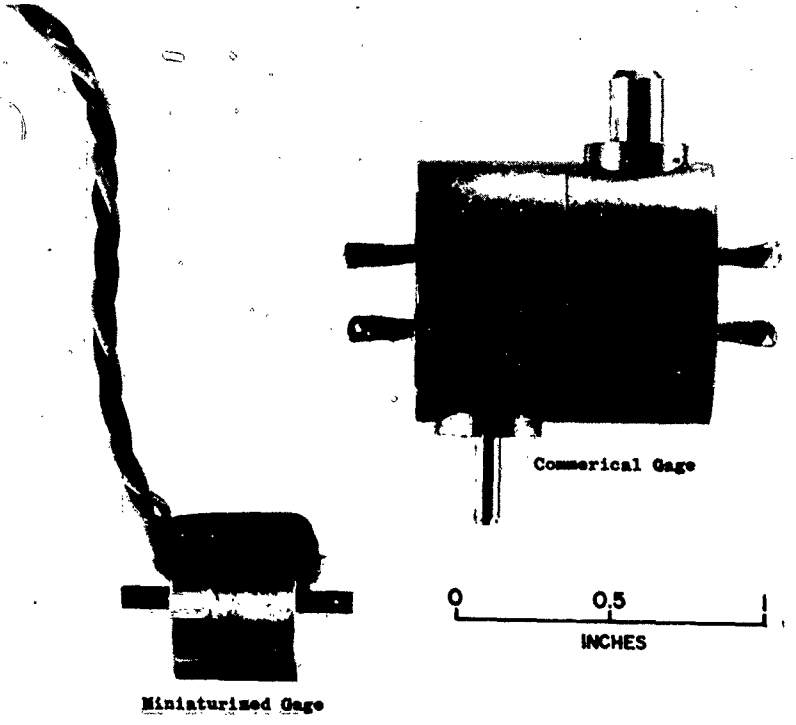

Fig.6 Comparative sizes of miniaturized and commercial pressure gages

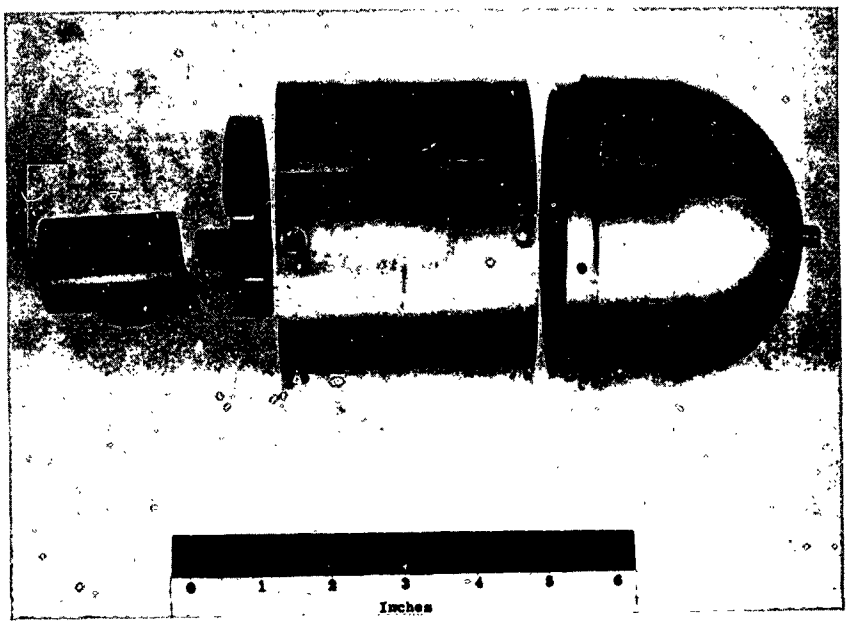

Fig.7 Typical pressure or heat transfer model

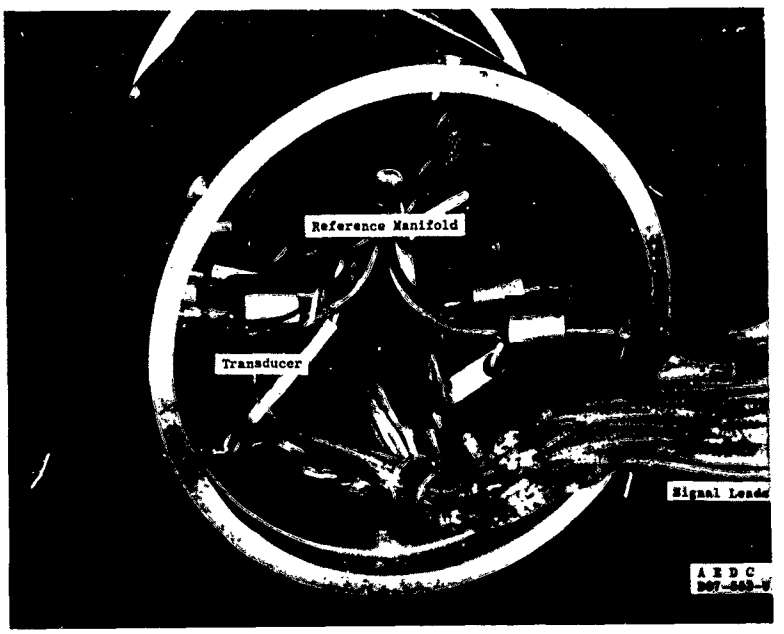

Fig.8 Typical installation of miniaturized pressure transducers

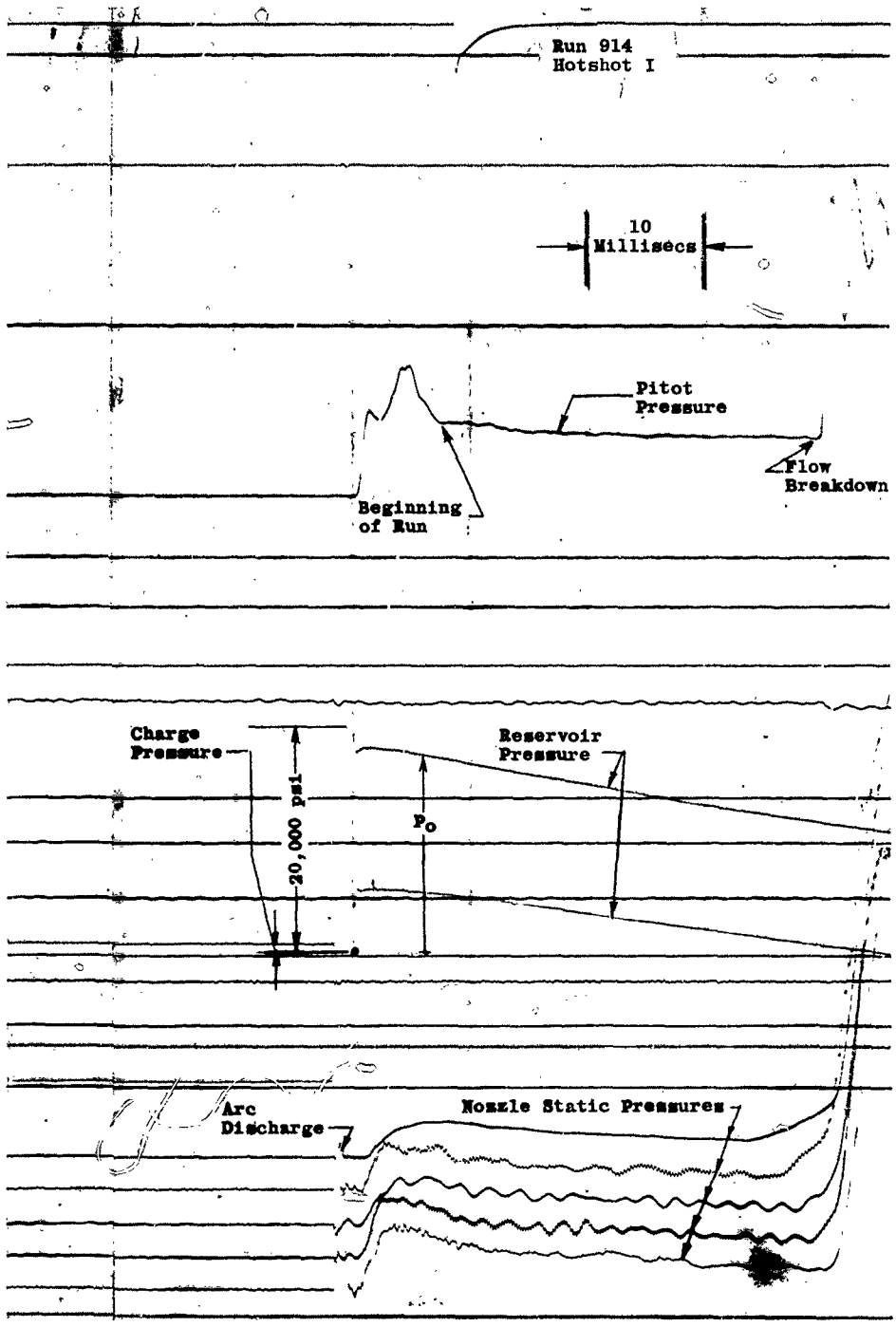

Fig.9 Typical pressure record

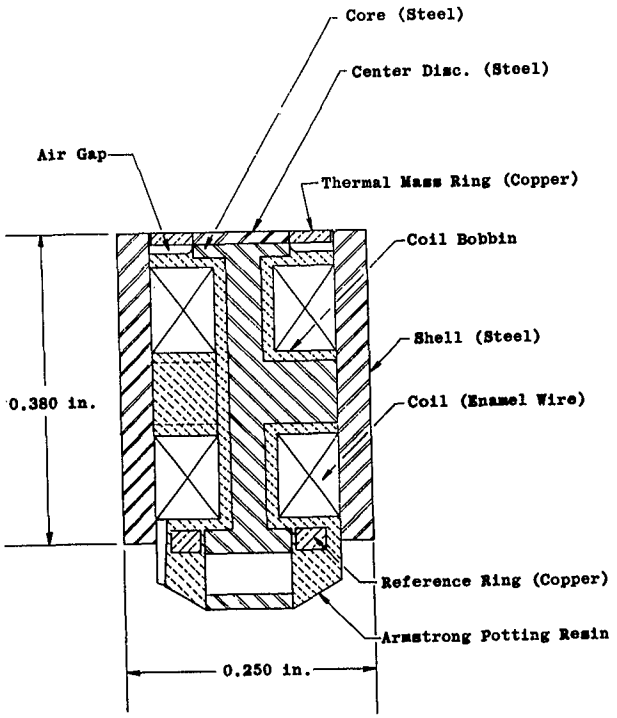

(a) Cross-sectional view

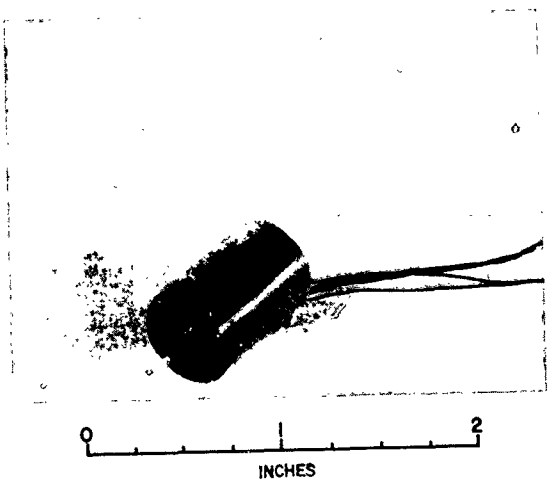

(b) Photograph of assembled gage

Fig. 10 Variable reluctance heat transfer gage

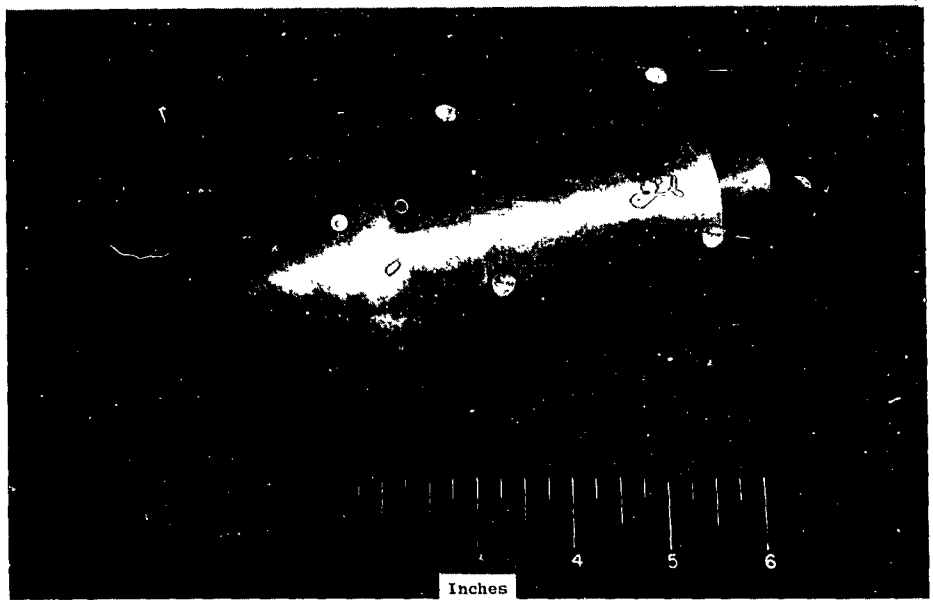

(a) Exterior view

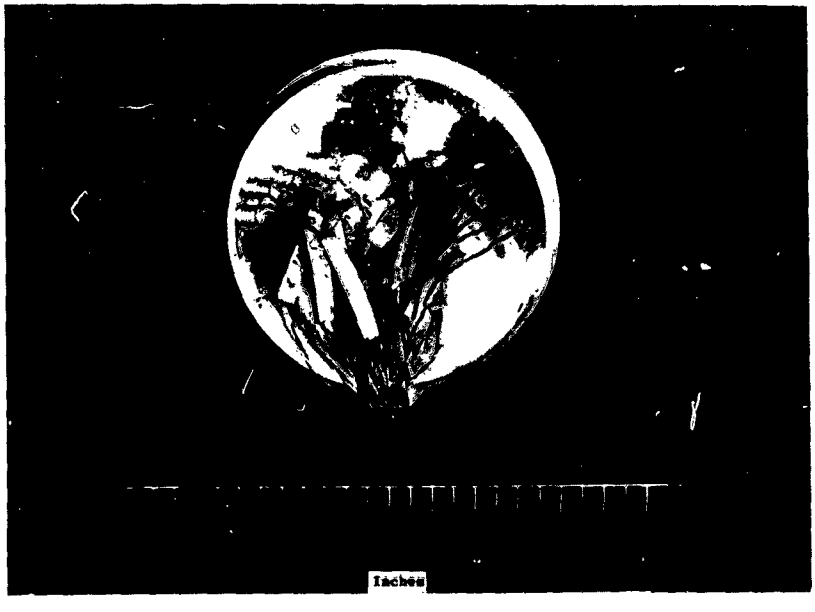

(b) Interior view

Fig. 11 Typical installation of heat transfer gages

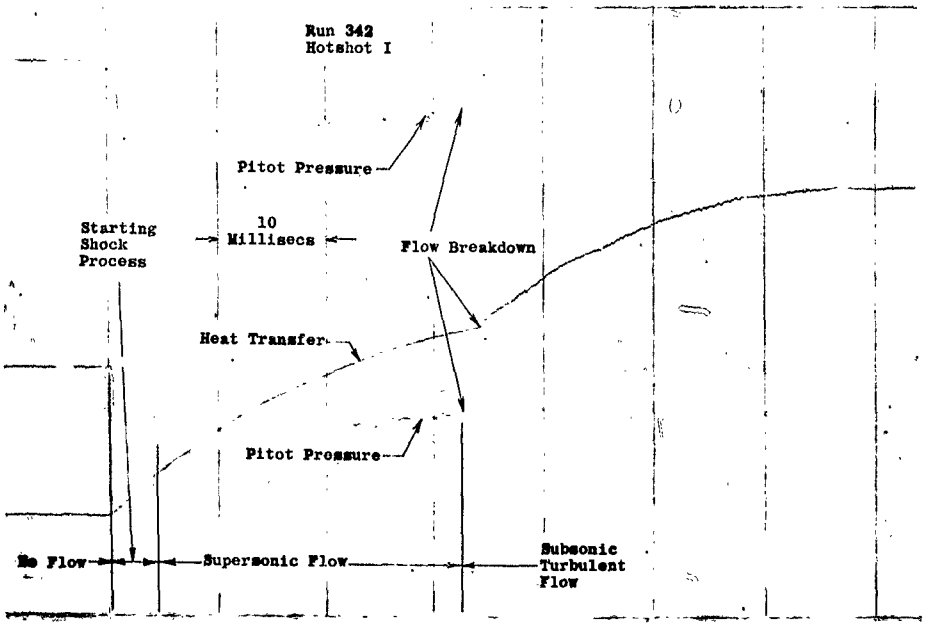

Fig. 12 Typical heat transfer record

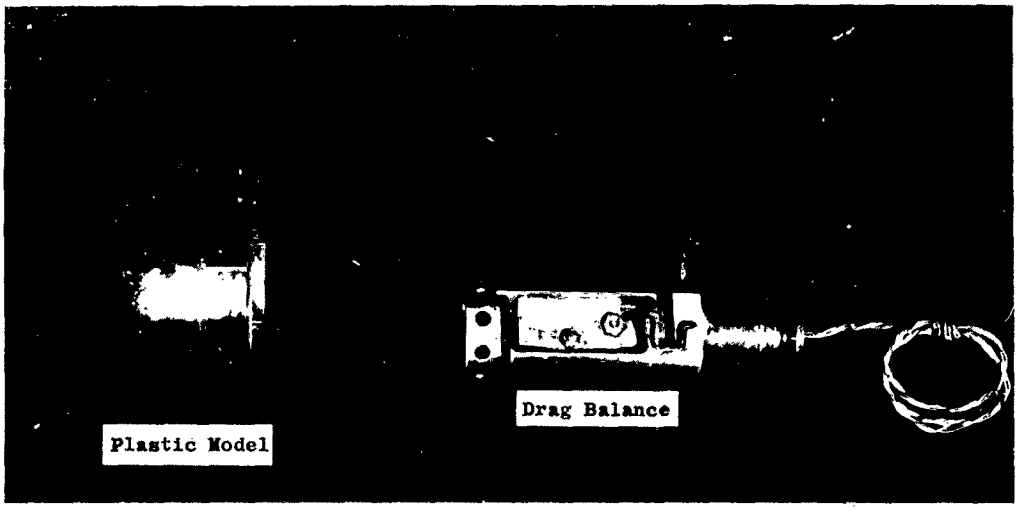

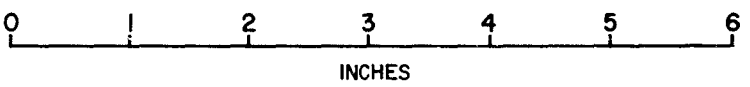

Fig. 13 Drag balance and typical drag model

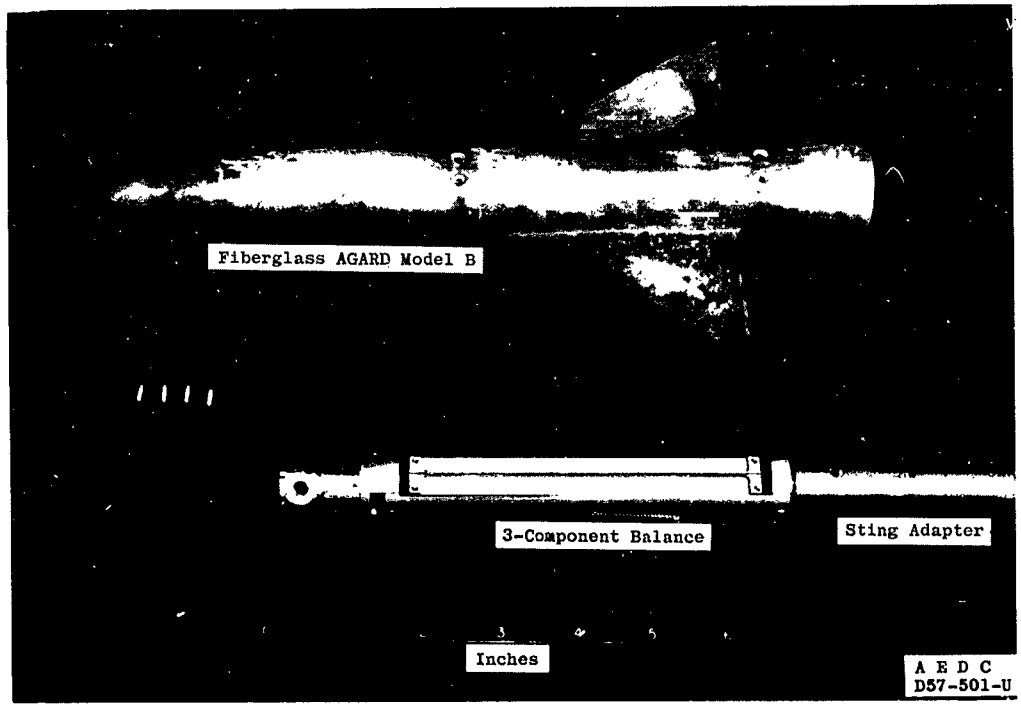

Fig.14 Three-component balance and AGARD Model B

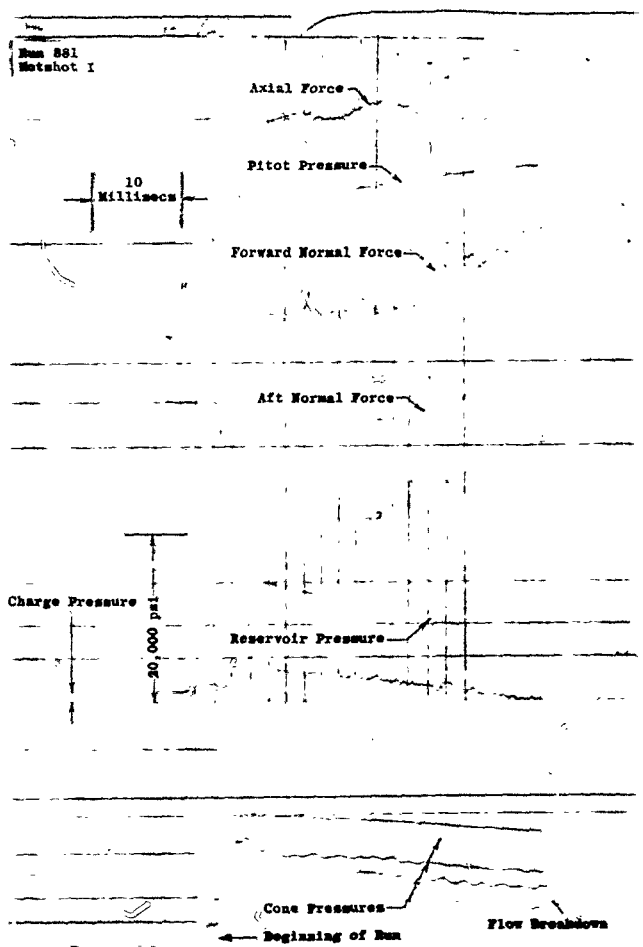

Fig.15 Typical three-component force record

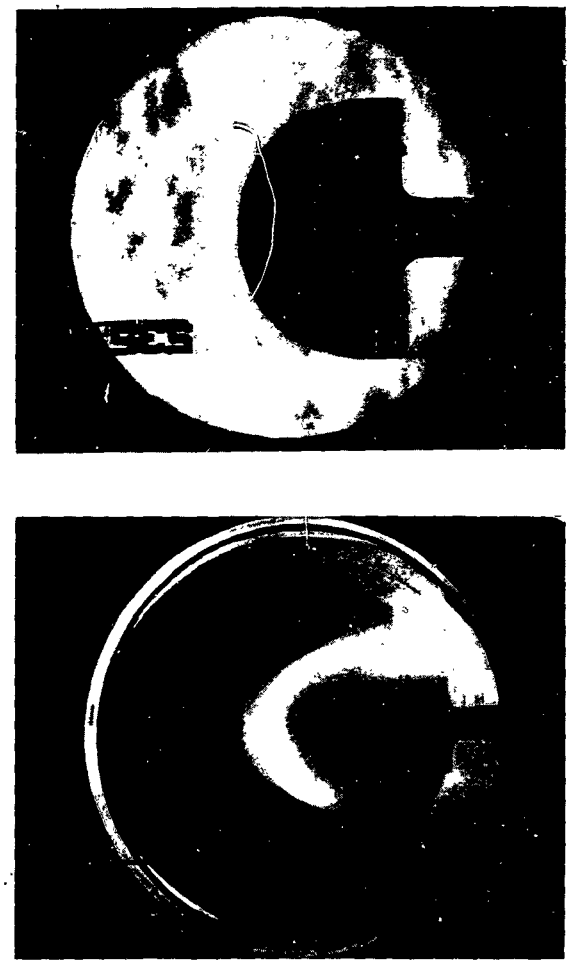

Fig.16 Typical schlieren photograph and typical self-luminosity exposure

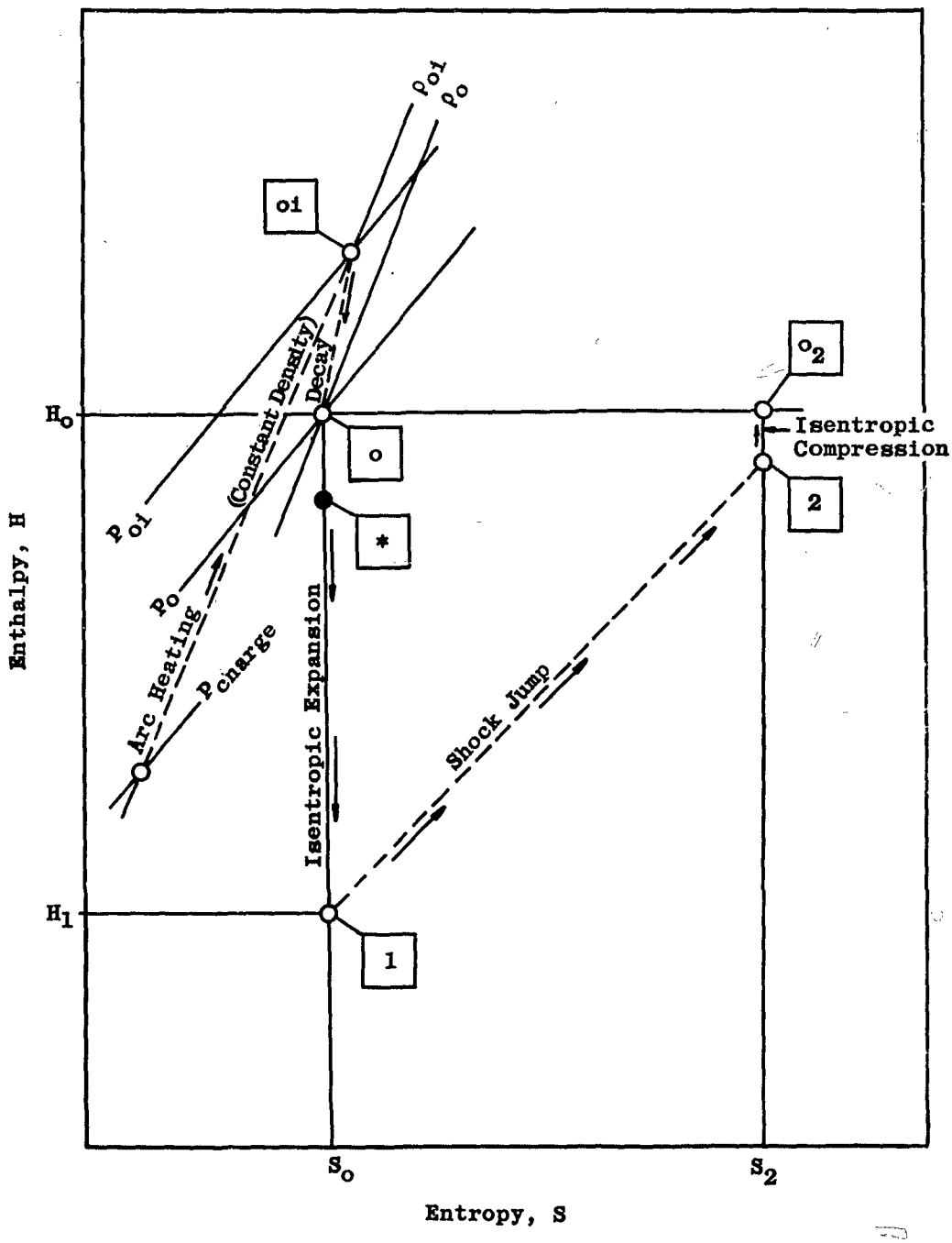

Fig.17 Tunnel Hotshot processes on a Mollier diagram

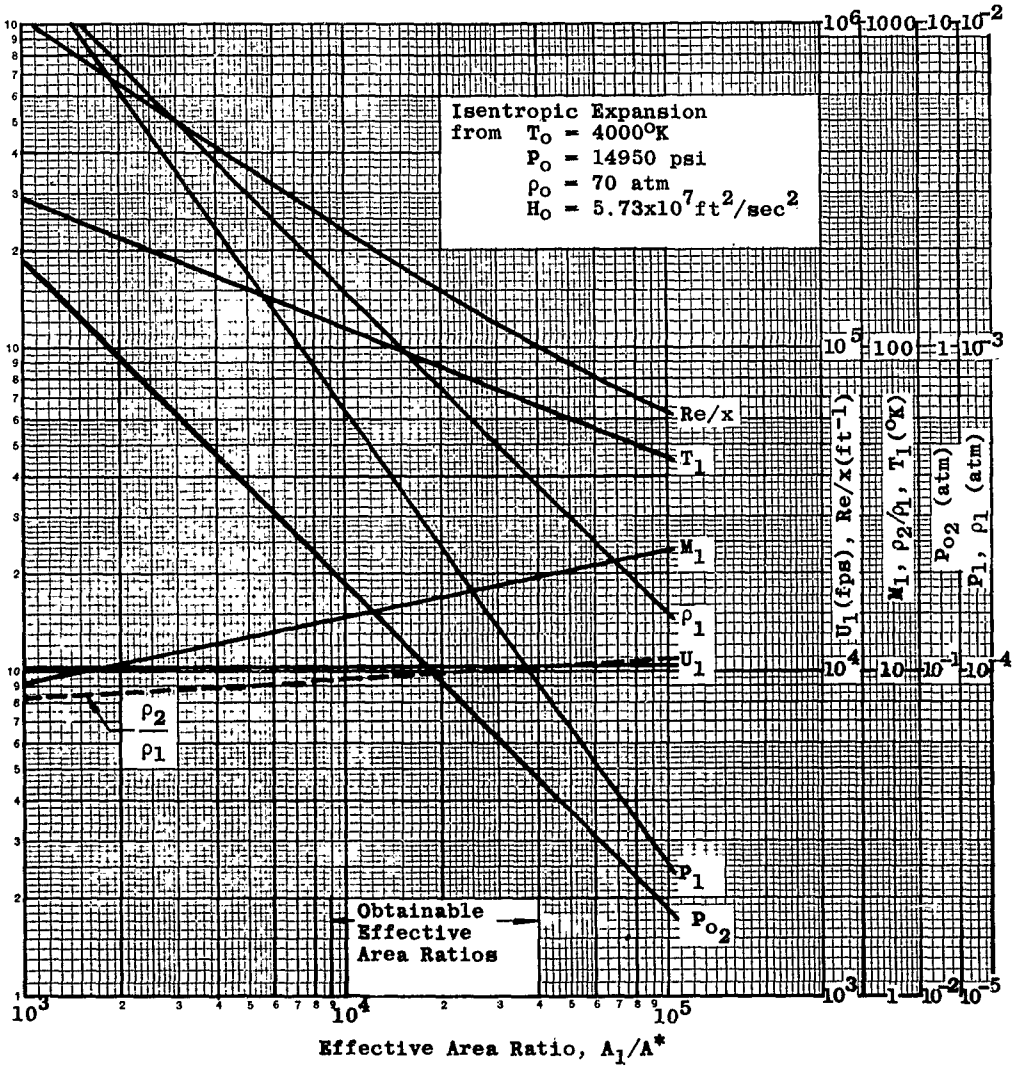

Fig.18 Tunnel performance curves

(a) T_o = 4000°K

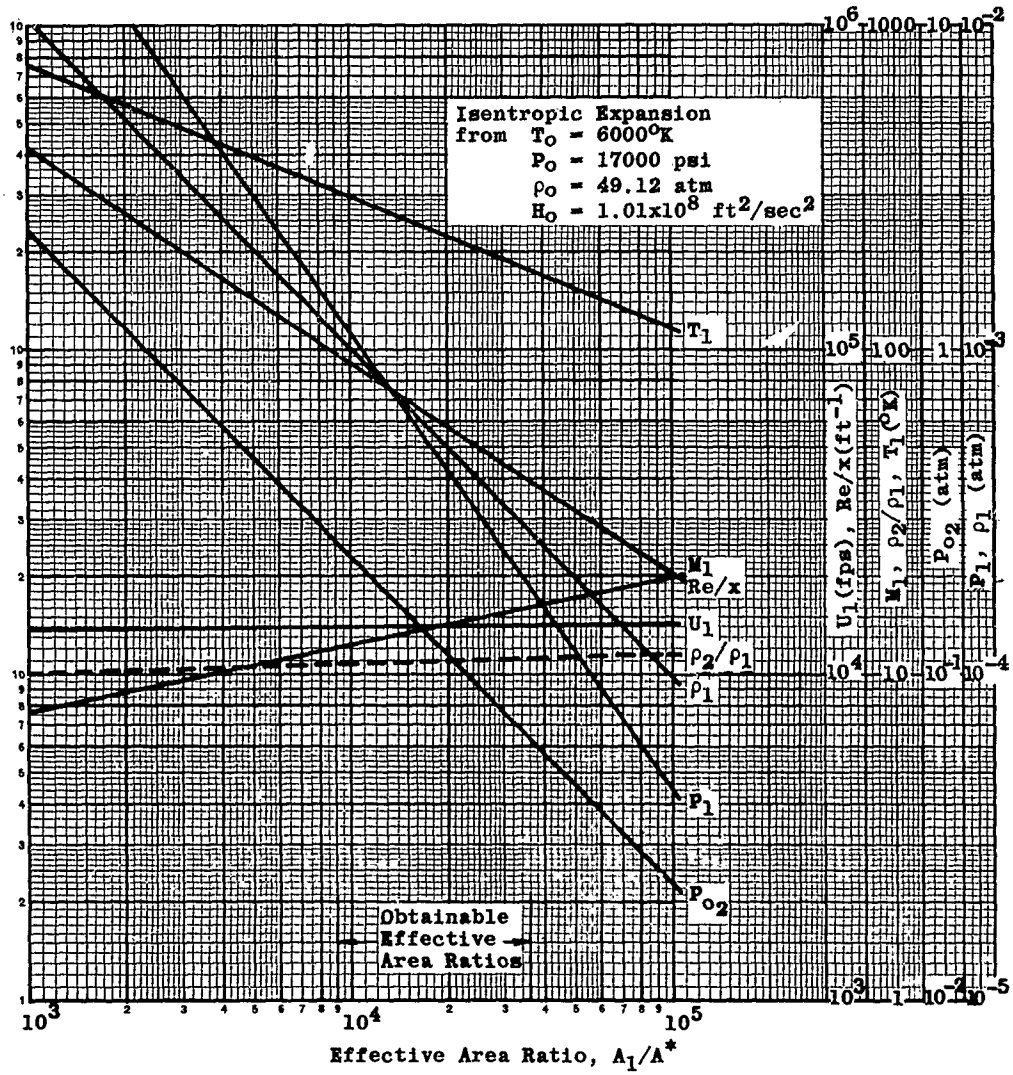

Fig. 18 Tunnel performance curves

(b) T_o = 6000°K

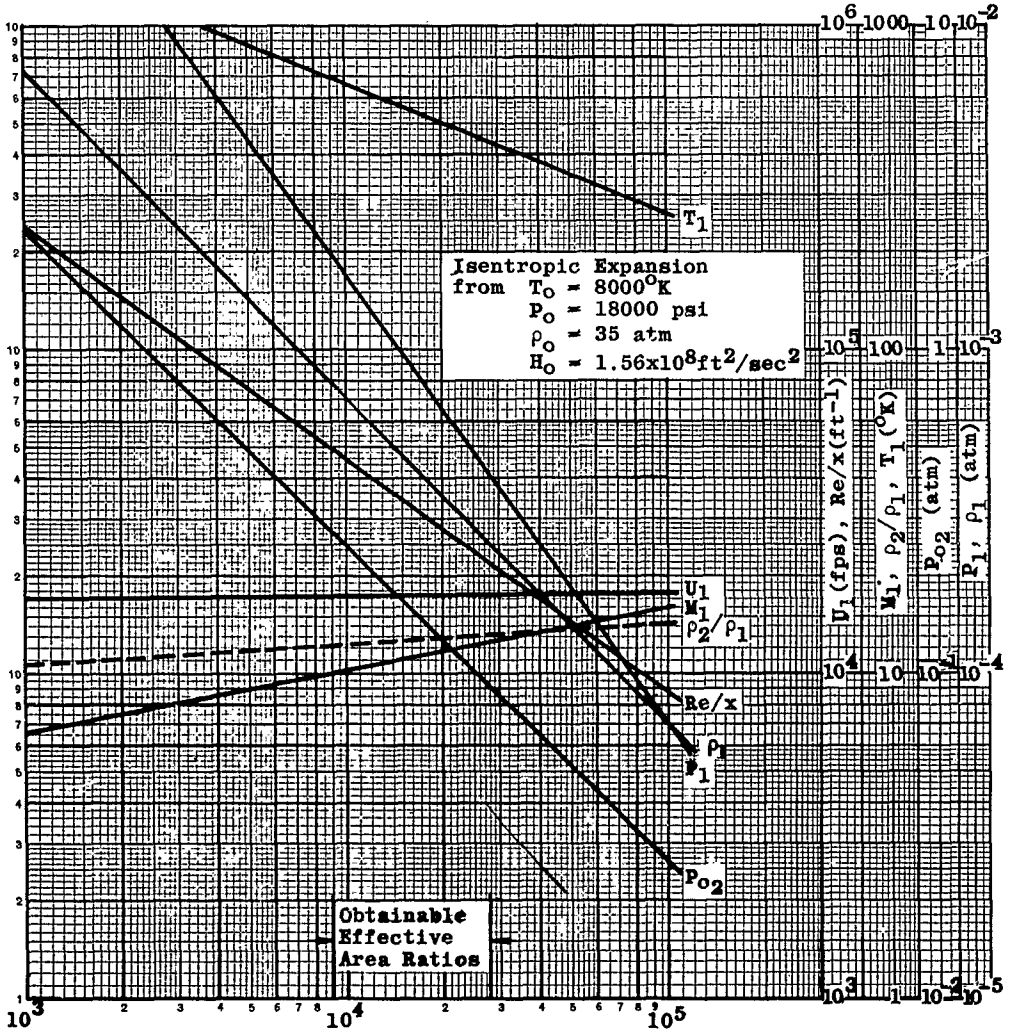

Fig.18 Tunnel performance curves

(c) T_o = 8000°K

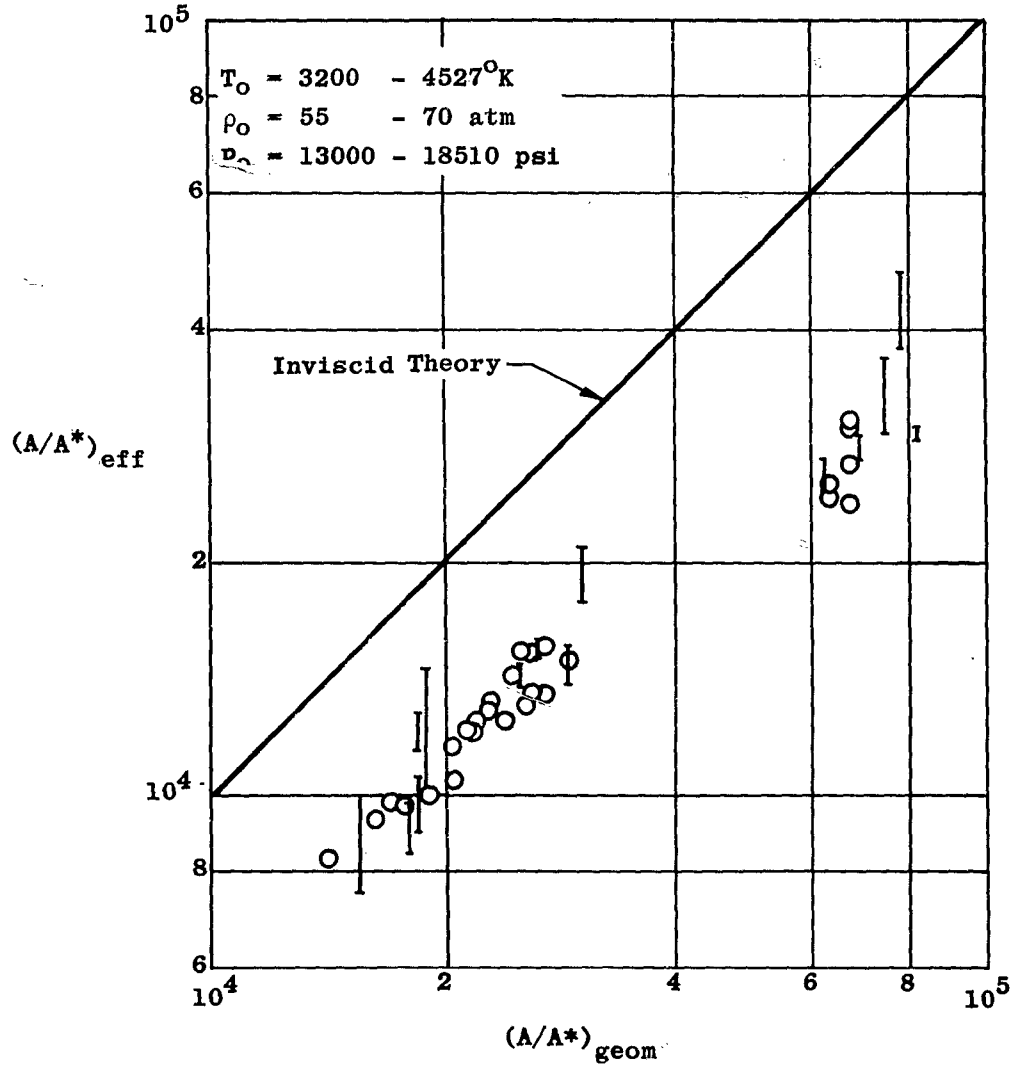

Fig. 19 Effective area ratio versus geometric area ratio

(a) $T_o = 4000°K$

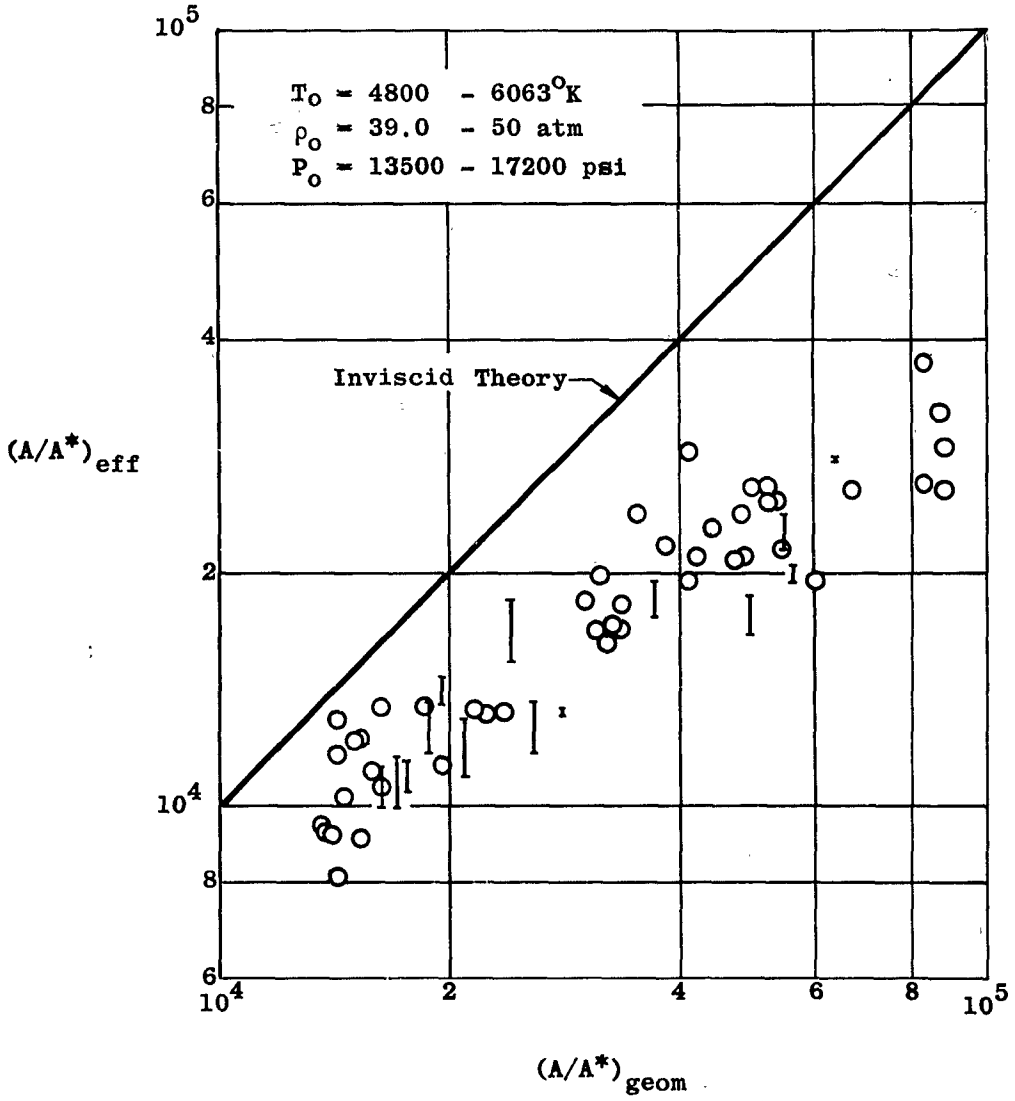

Fig.19 Effective area ratio versus geometric area ratio
(b) $T_o = 6000°K$

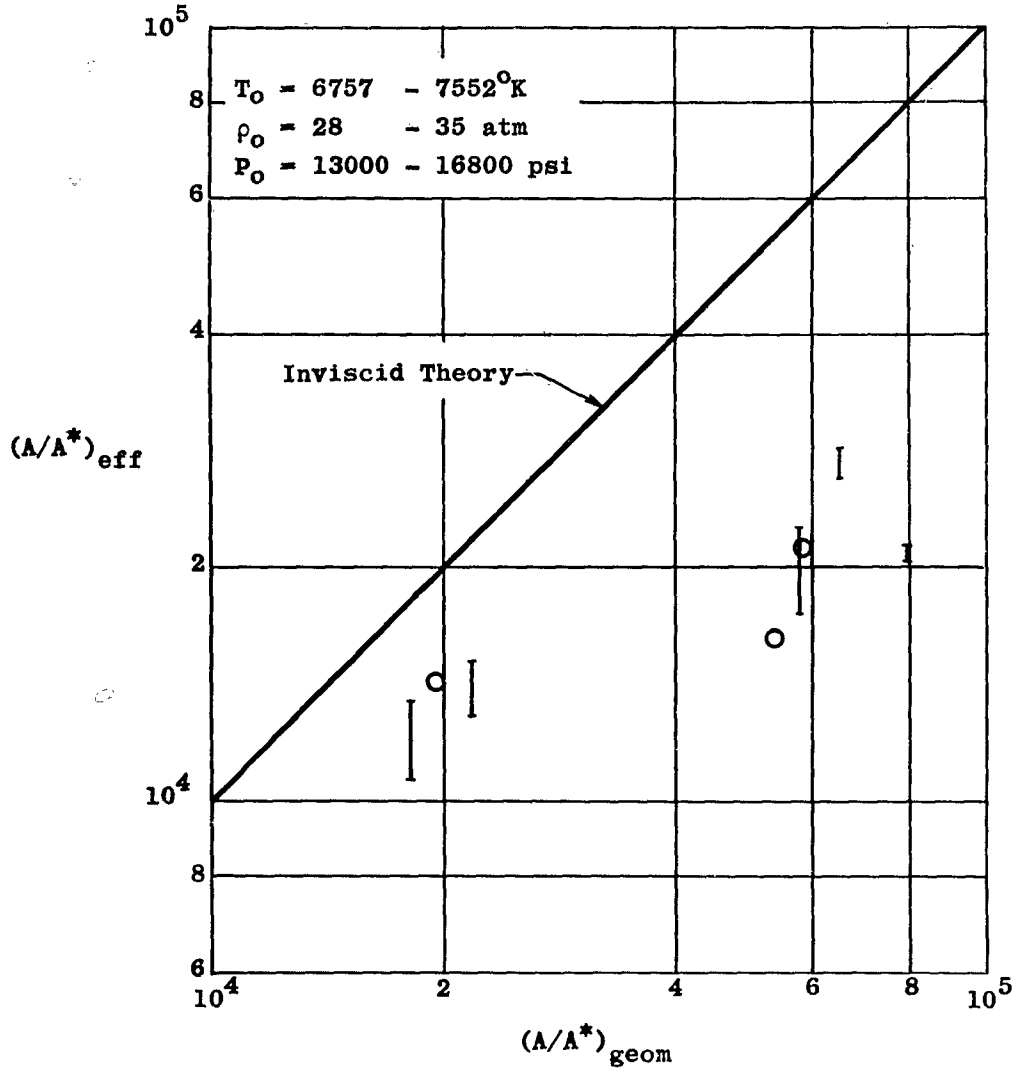

Fig.19 Effective area ratio versus geometric area ratio

(c) T_o = 8000°K

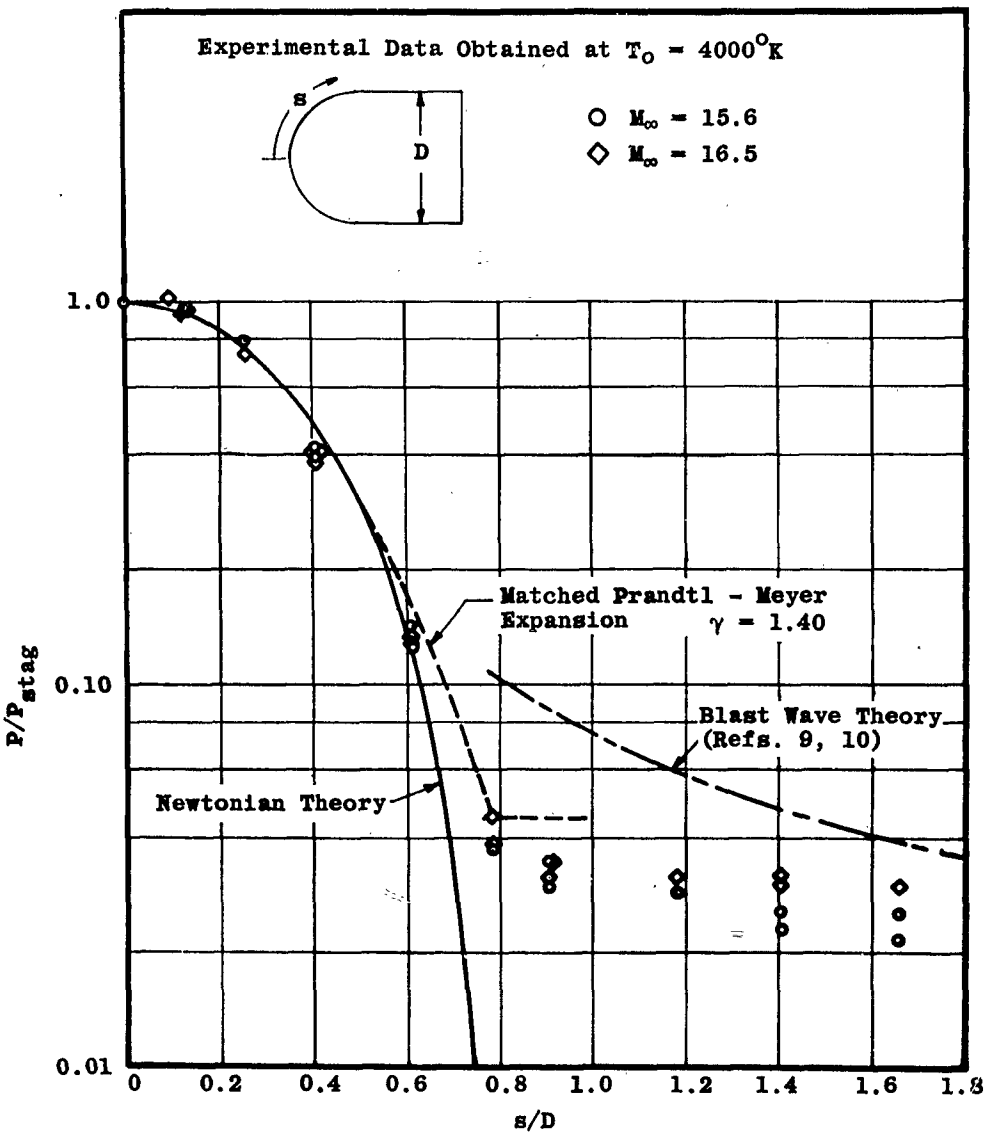

Fig.20 Pressure distribution on hemisphere-cylinder

Fig. 21 Schlieren photograph of flow over a flat plate

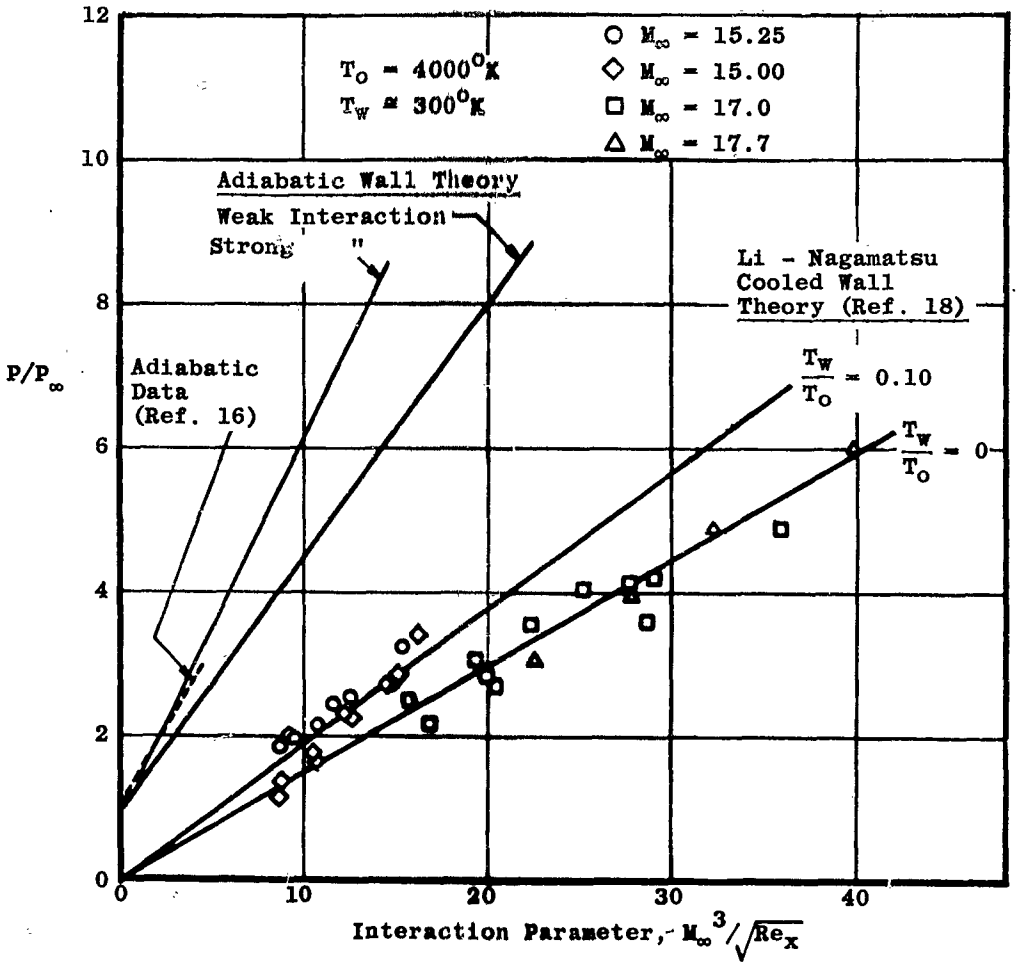

Fig. 22 Induced pressure on flat plate

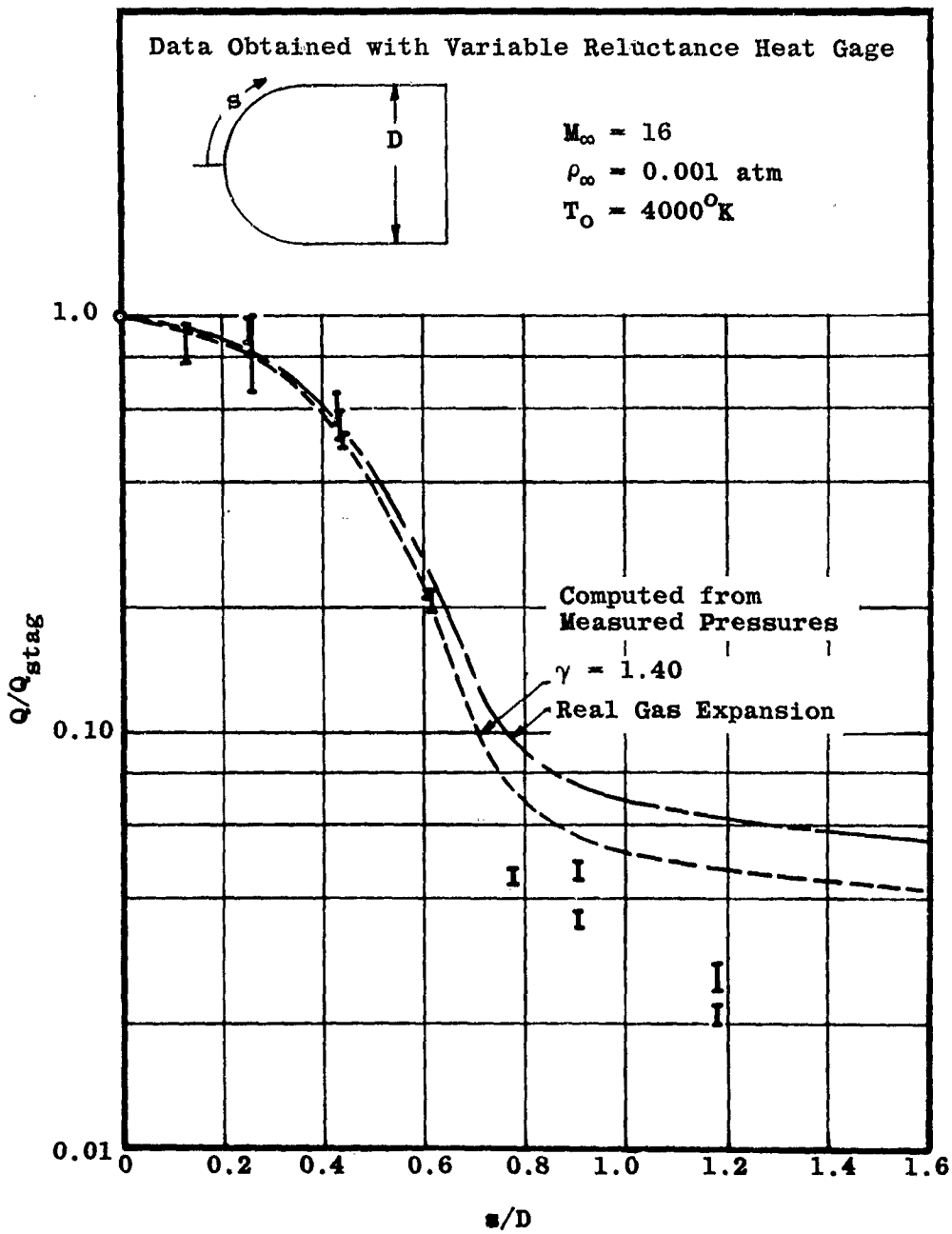

Fig. 23 Heat transfer distribution on hemisphere-cylinder

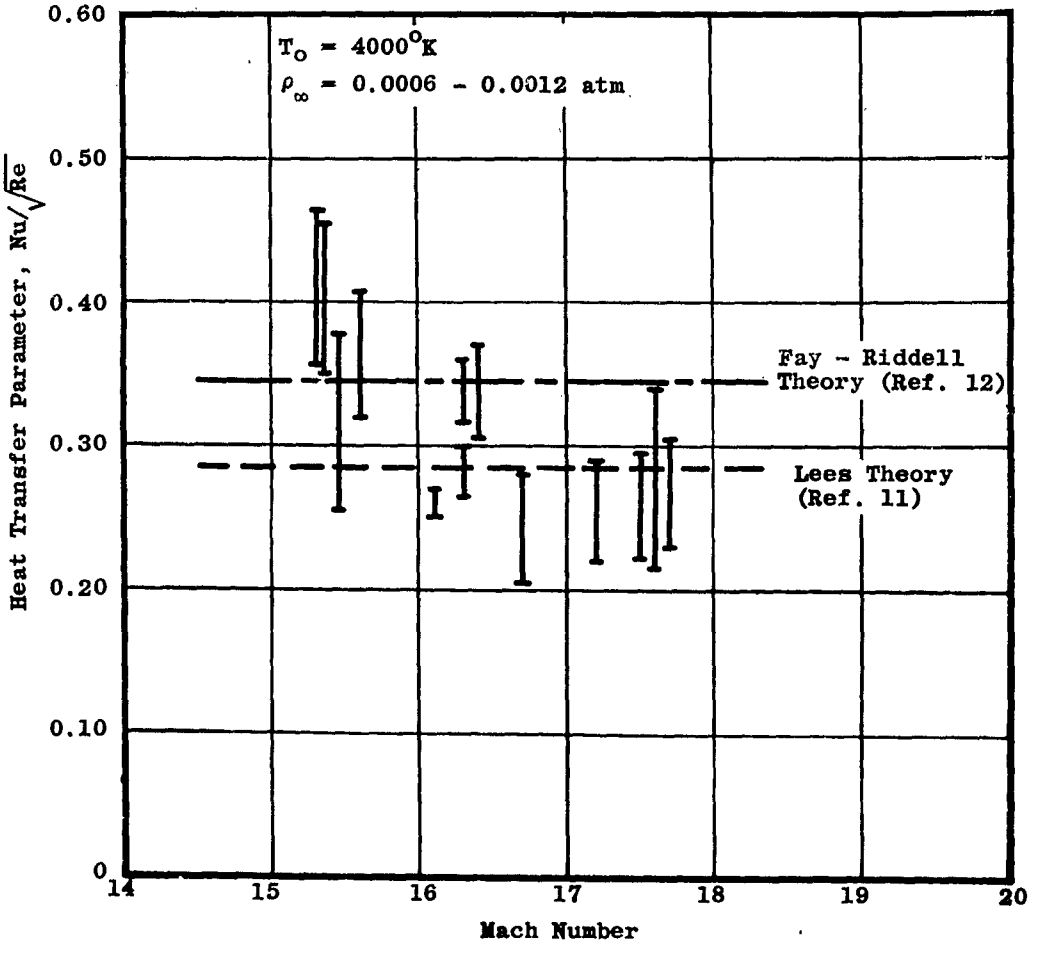

Fig. 24 Correlation of two-dimensional stagnation point heat transfer data

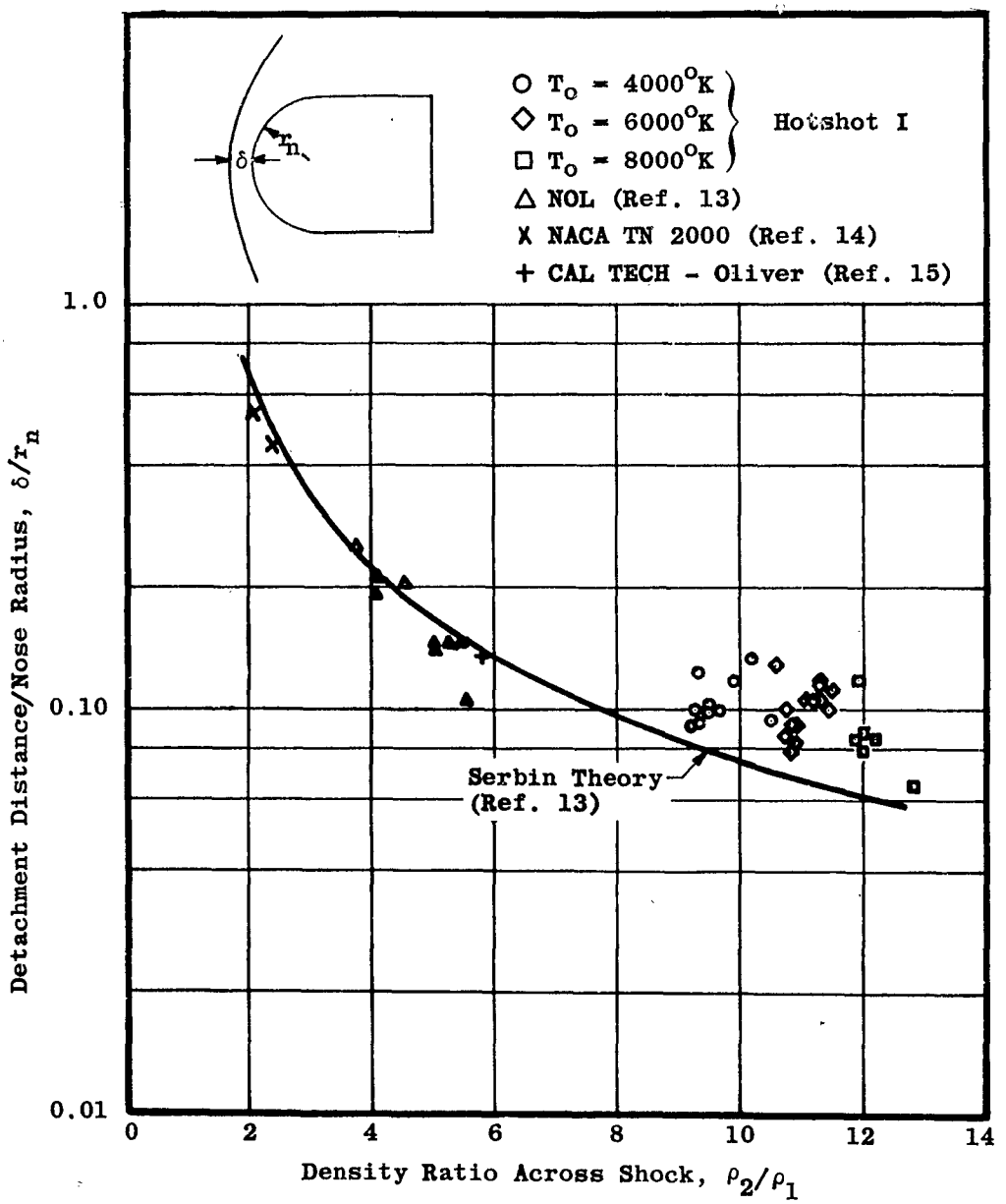

Fig. 25 Correlation of hemisphere shock detachment distance

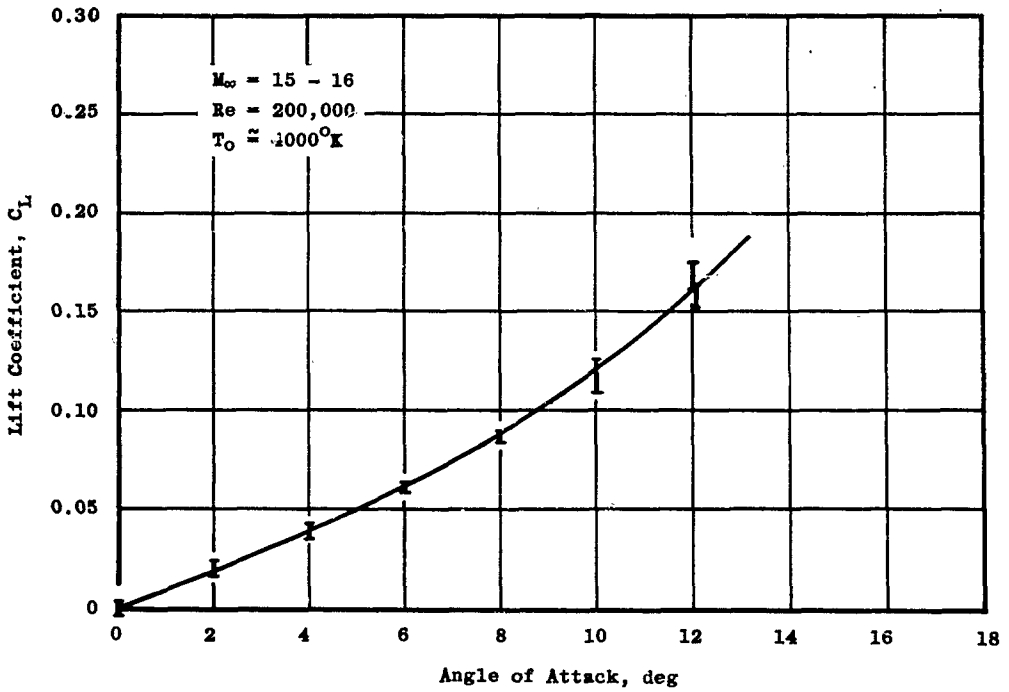

Fig. 26 Lift curve for AGARD Model B

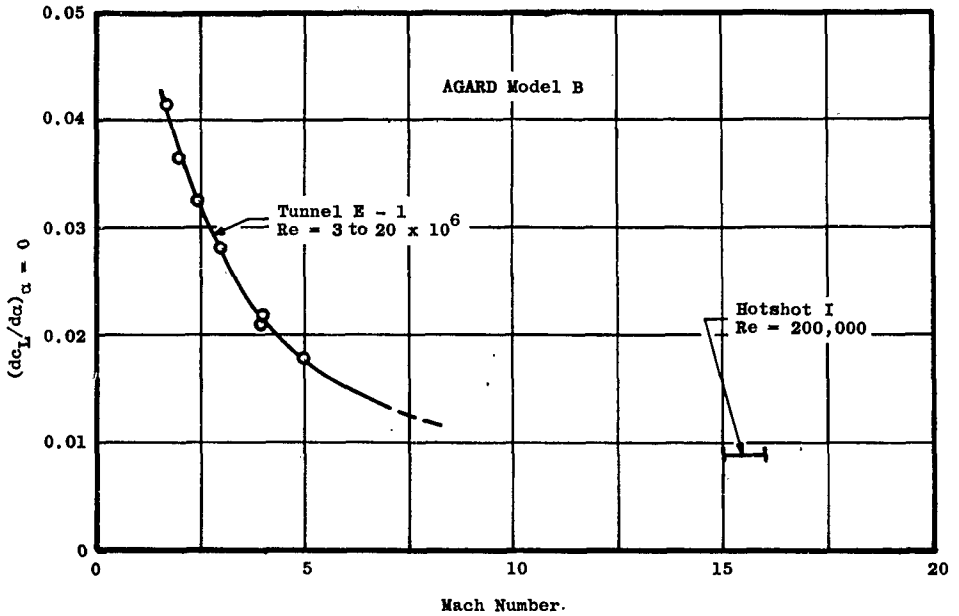

Fig. 27 Lift curve slope versus Mach number

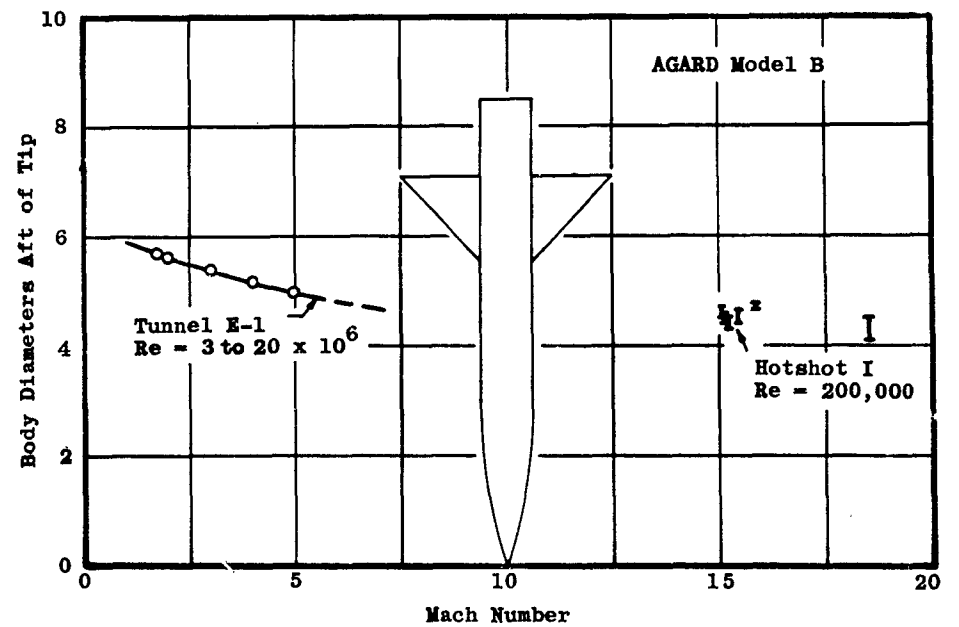

Fig. 28 Center of pressure location

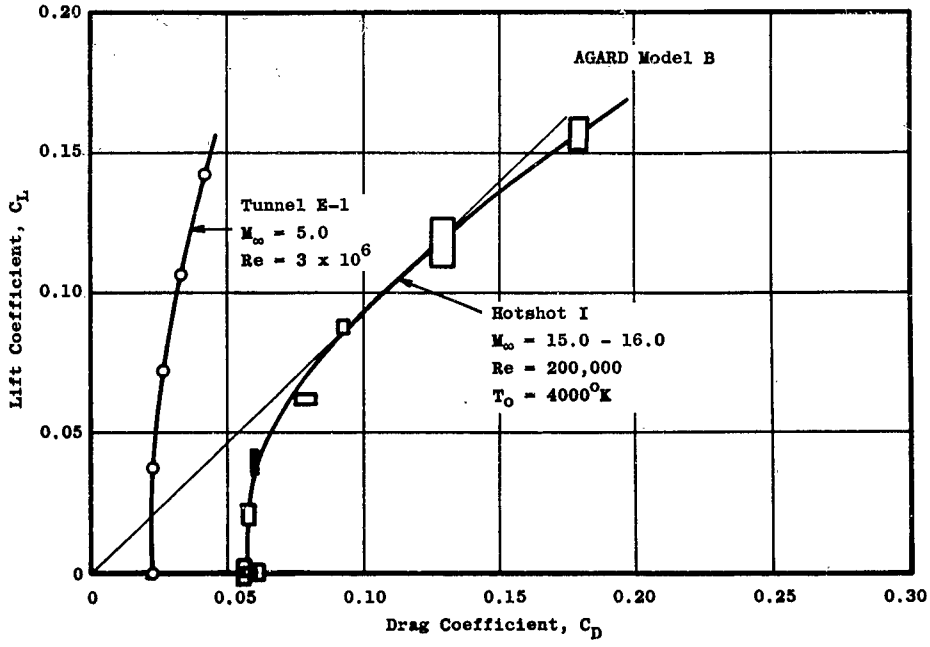

Fig.29 Lift coefficient versus drag coefficient, AGARD Model B

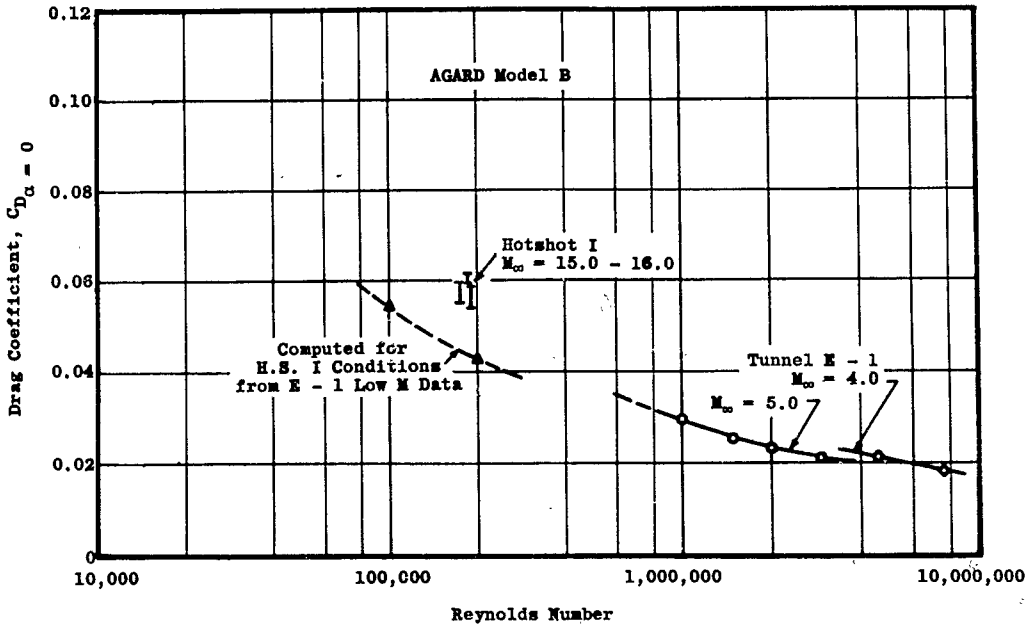

Fig.30 Forebody drag coefficient versus Reynolds number

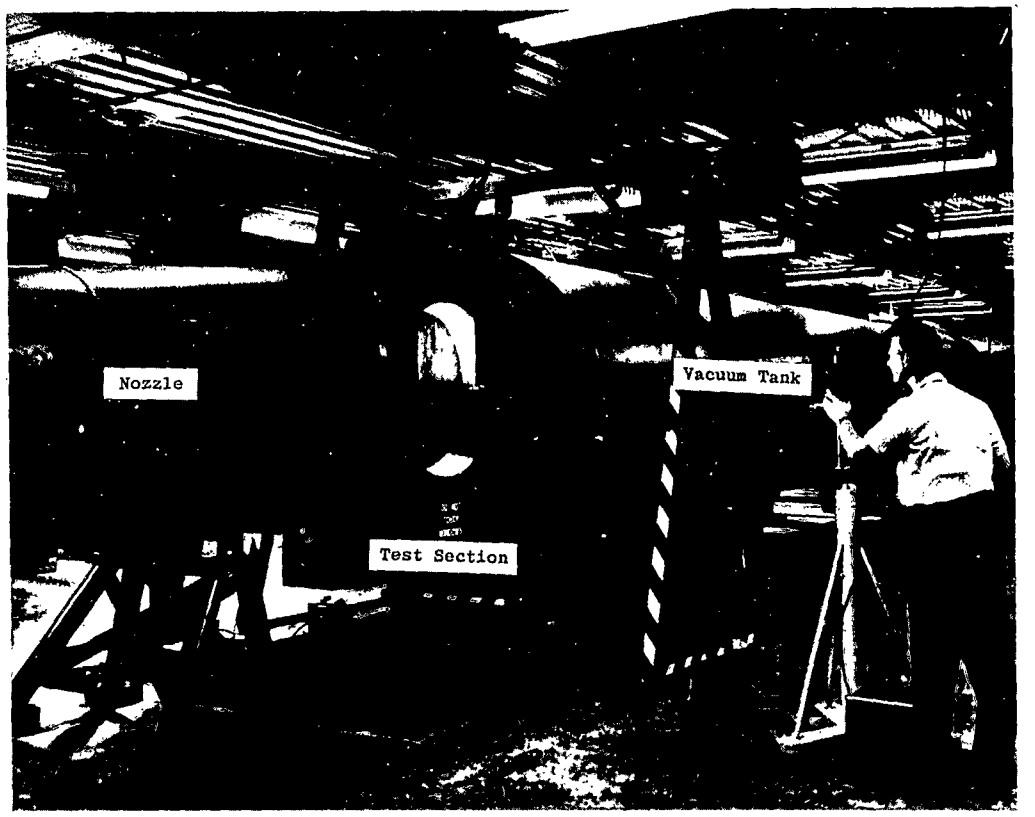

Fig.31 50 in. Hotshot tunnel

(a) General view

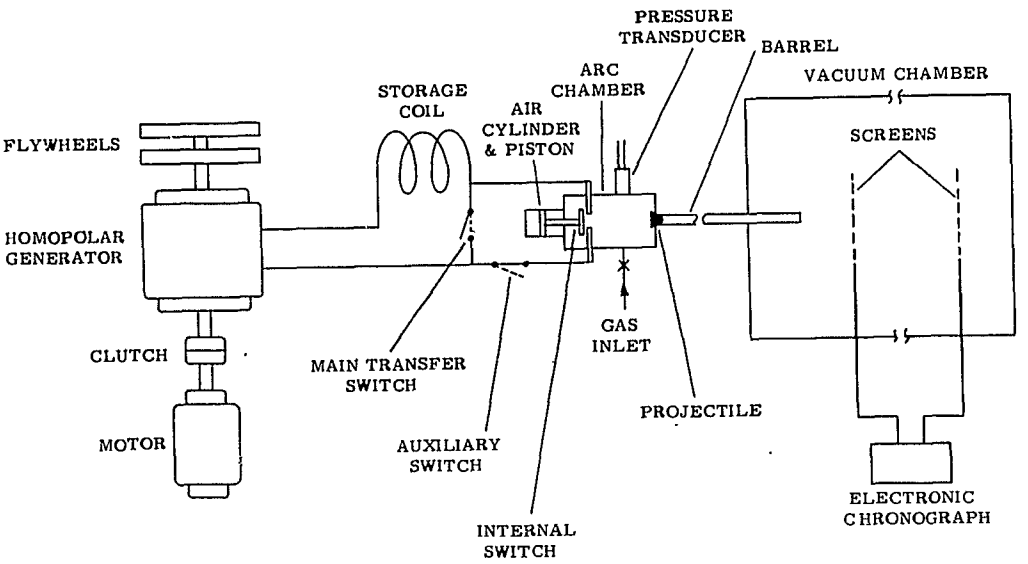

(b) Schematic layout

Fig.32 Inductive electric energy storage system

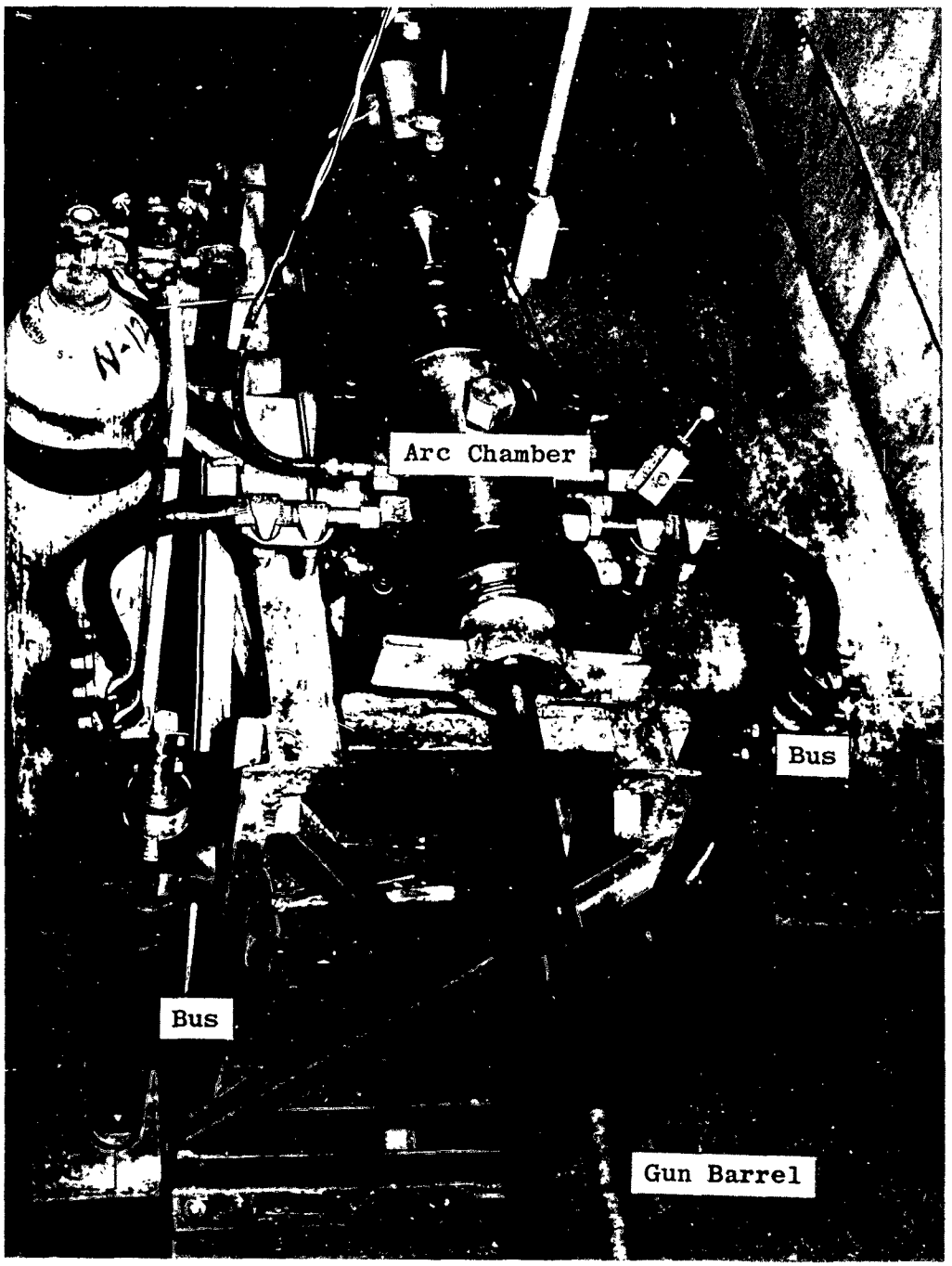

Fig.33 'Potshot' electric gun

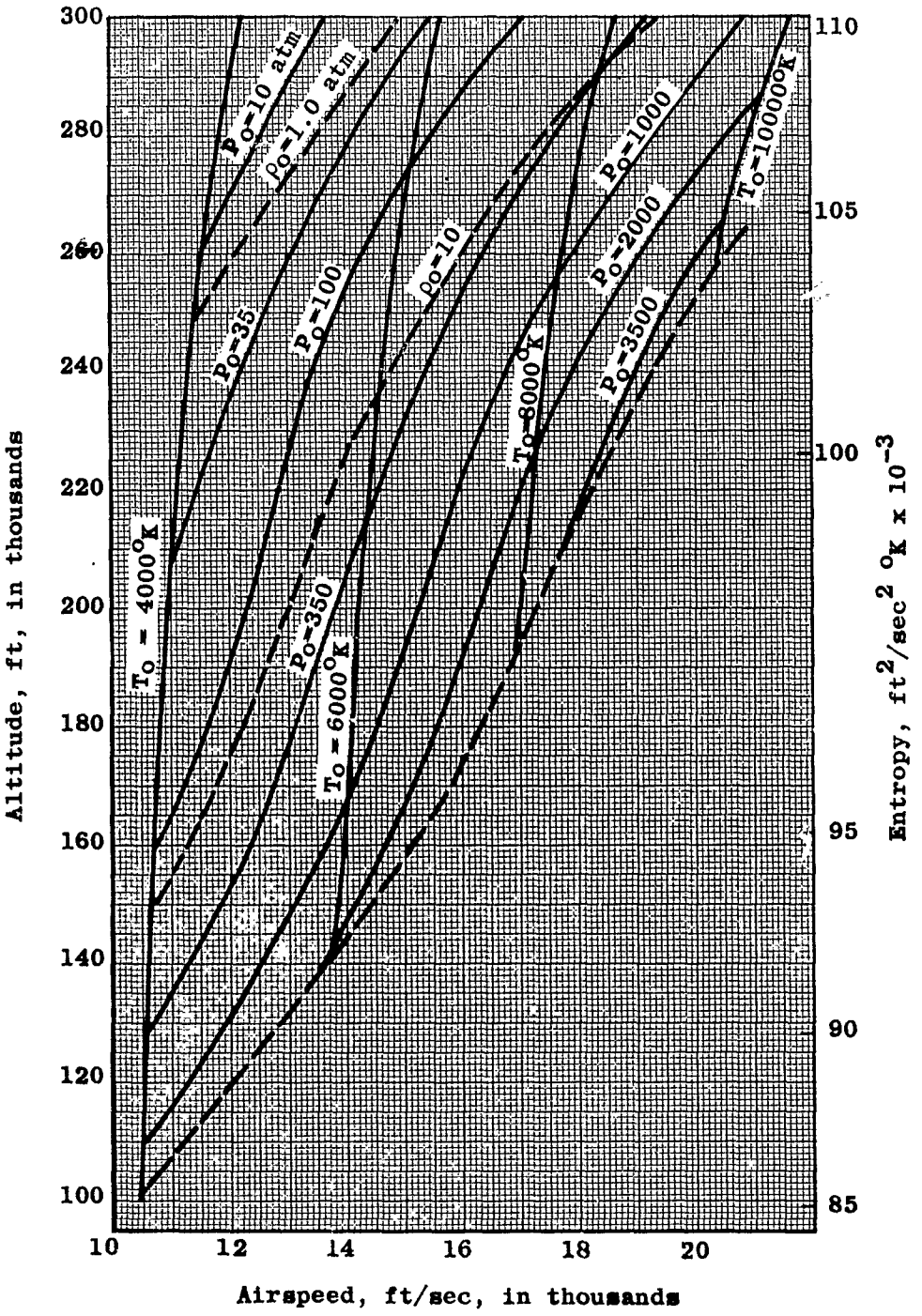

Fig.34 Required reservoir conditions for flight duplication

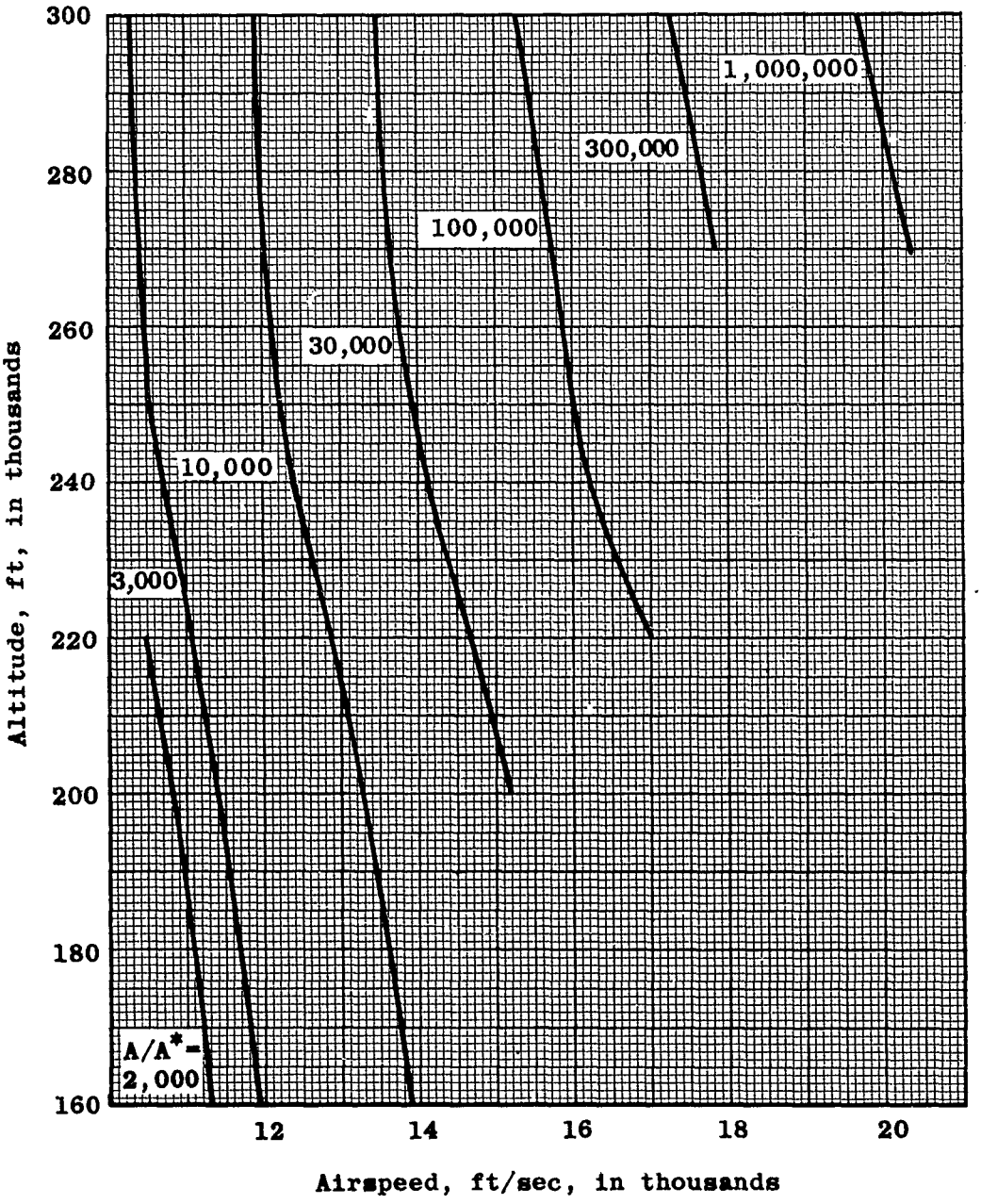

Fig.35 Required effective area ratio for flight duplication

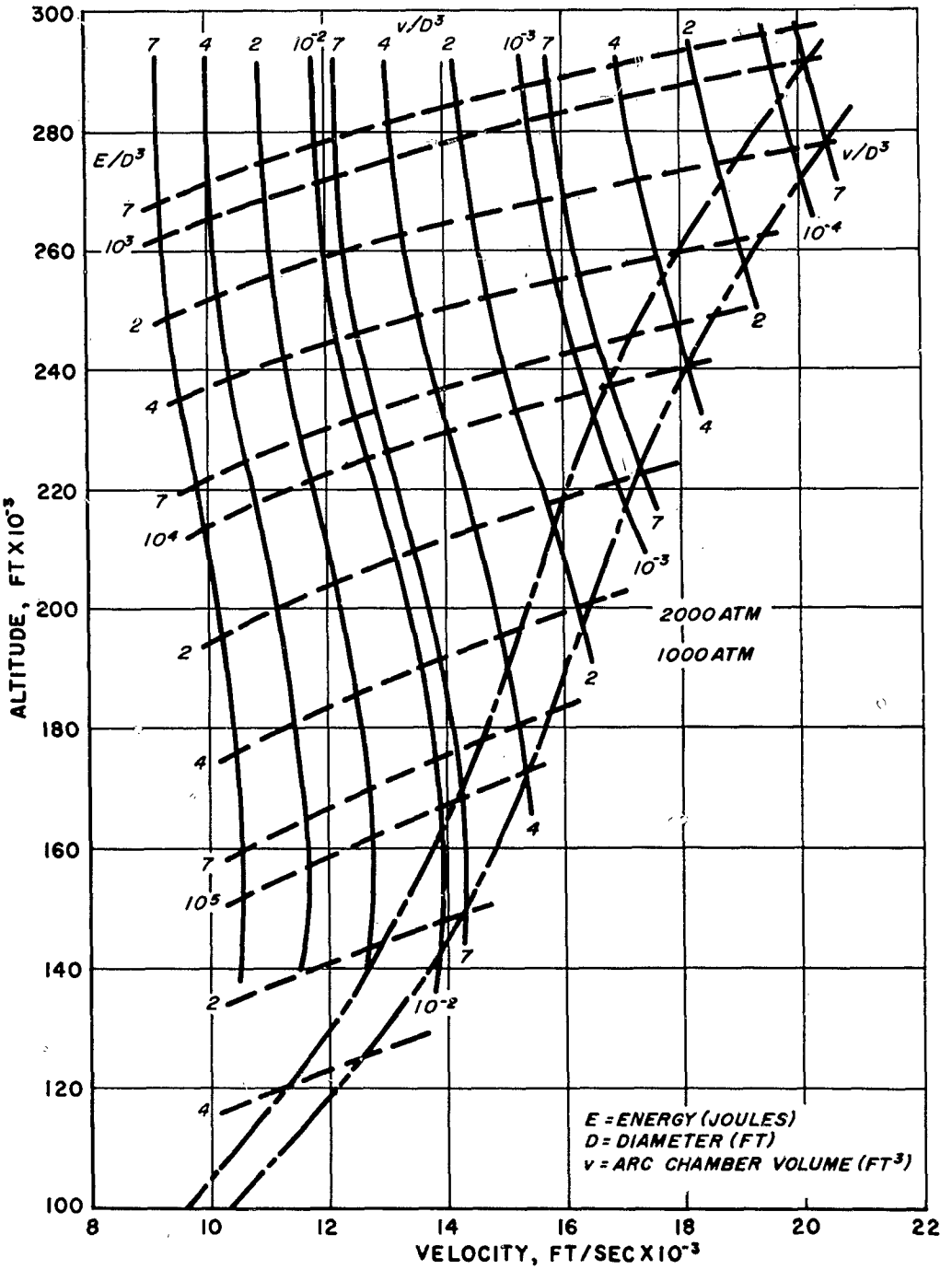

Fig. 36 Generalized performance of Hotshot tunnels for flight duplication

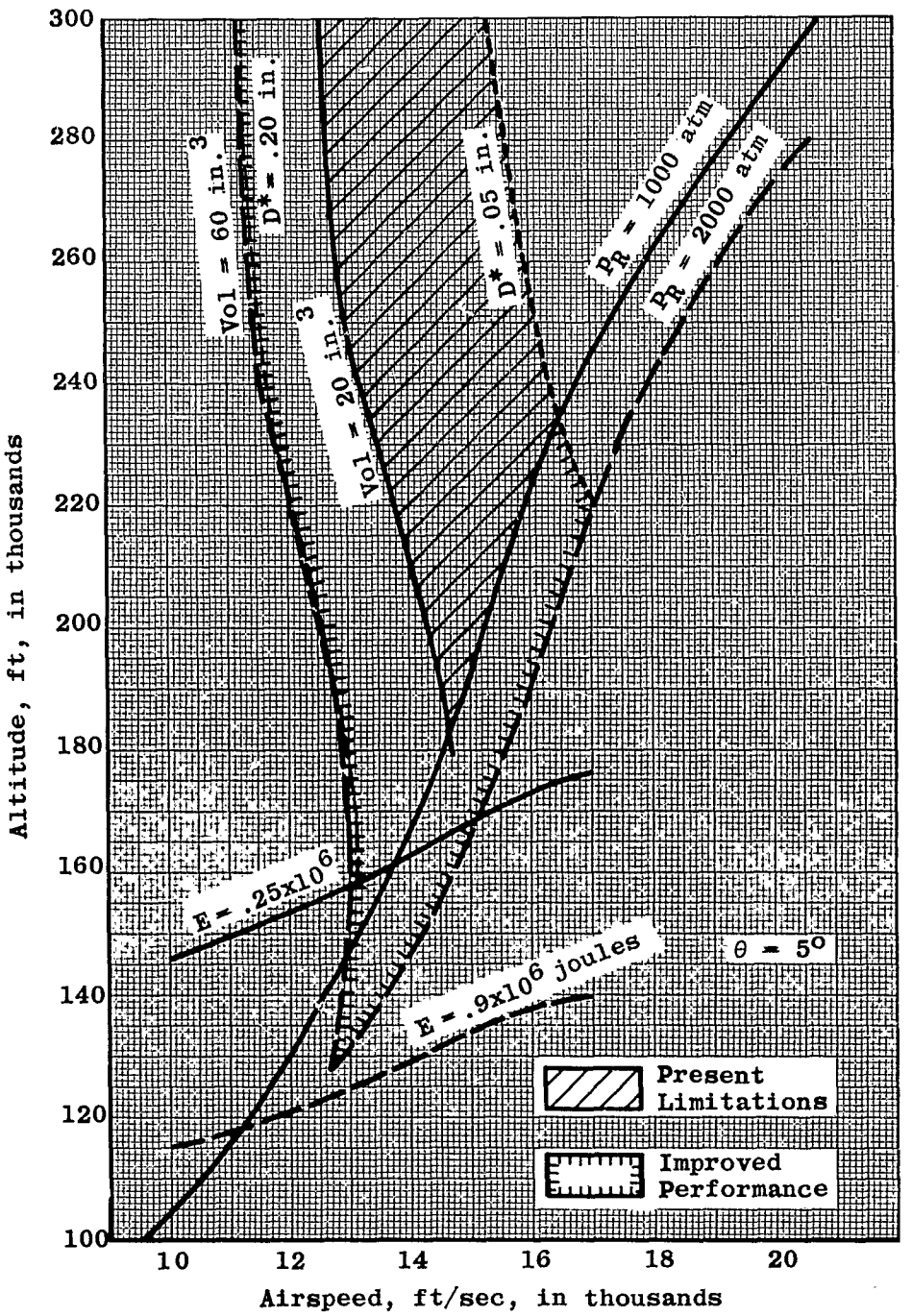

Fig.37 Mechanical and electrical performance limitations for flight duplication

(a) Effective test section diameter 16 in.

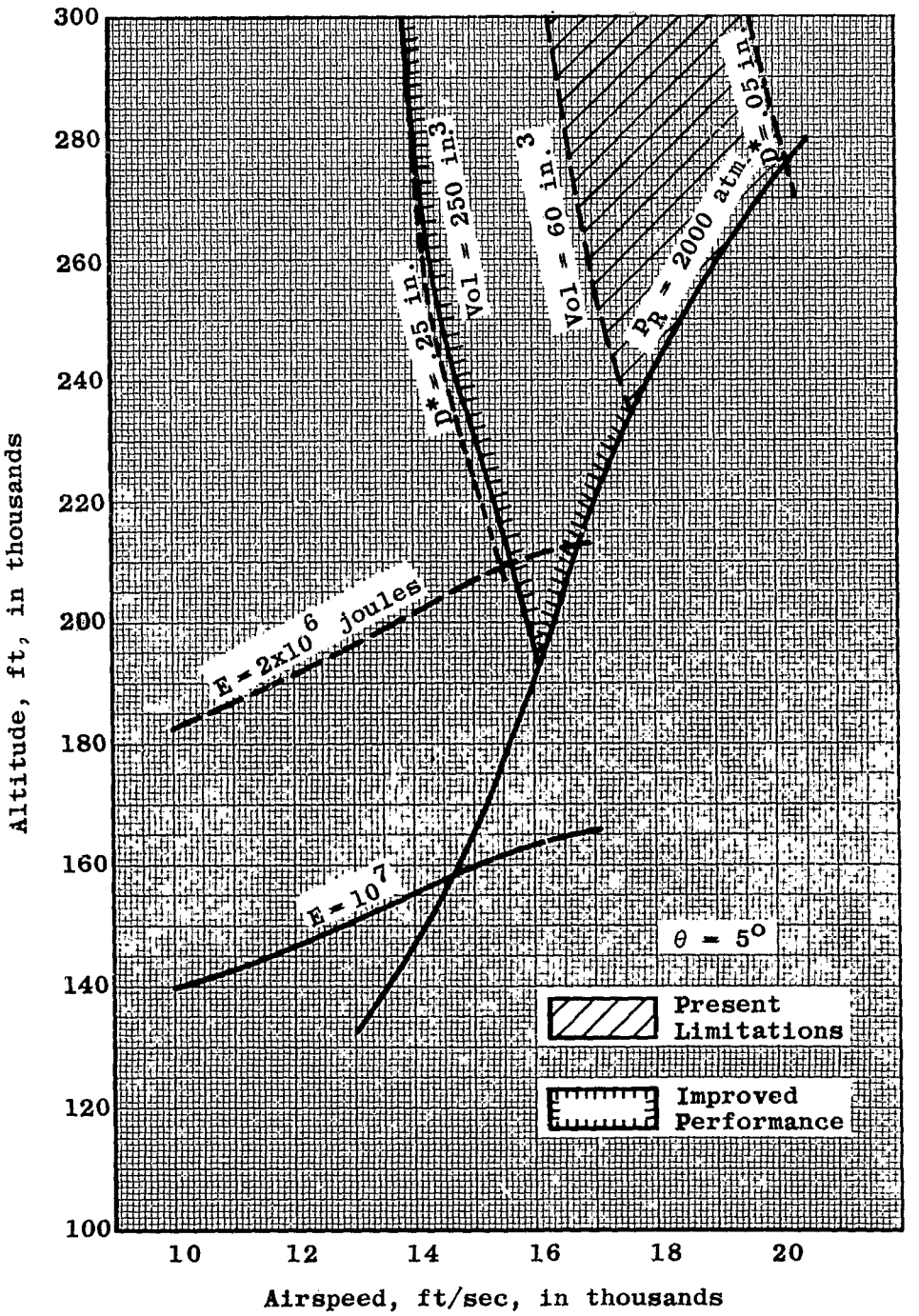

Fig.37 Mechanical and electrical performance limitations for flight duplication
(b) Effective test section diameter 50 in.

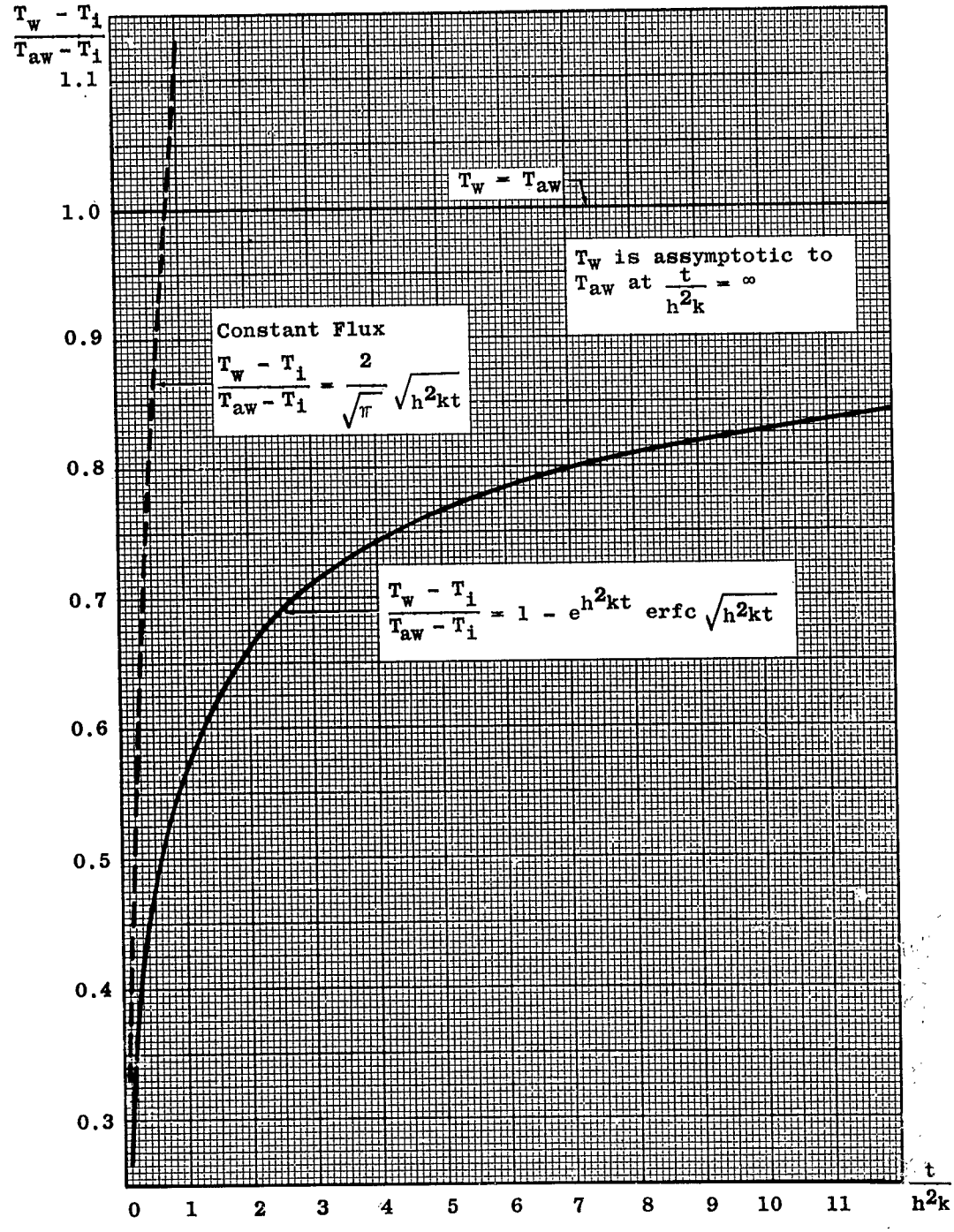

Fig.38 Wall temperature rise

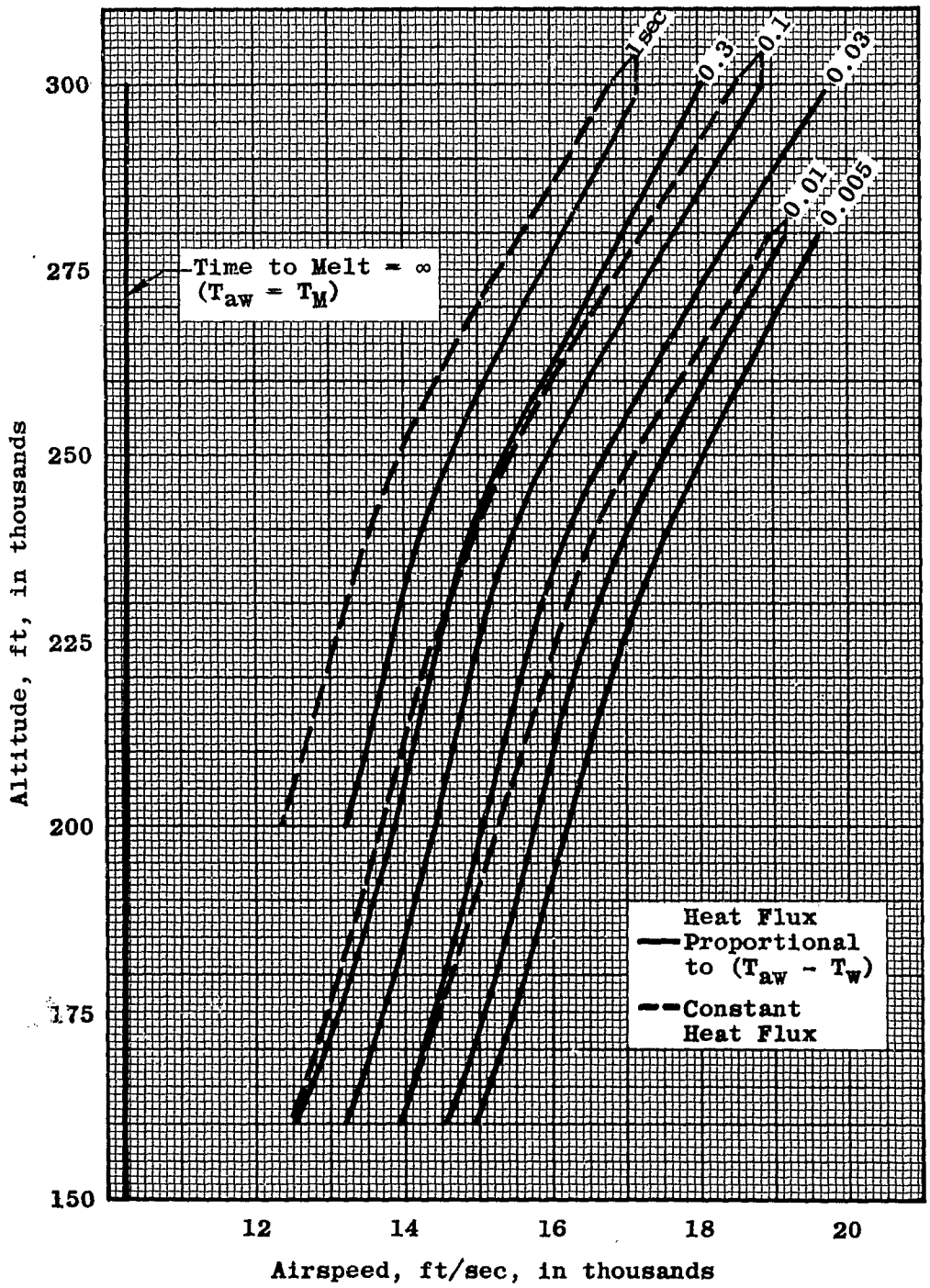

Fig.39 Time to melt a tungsten throat for flight-simulating tunnel

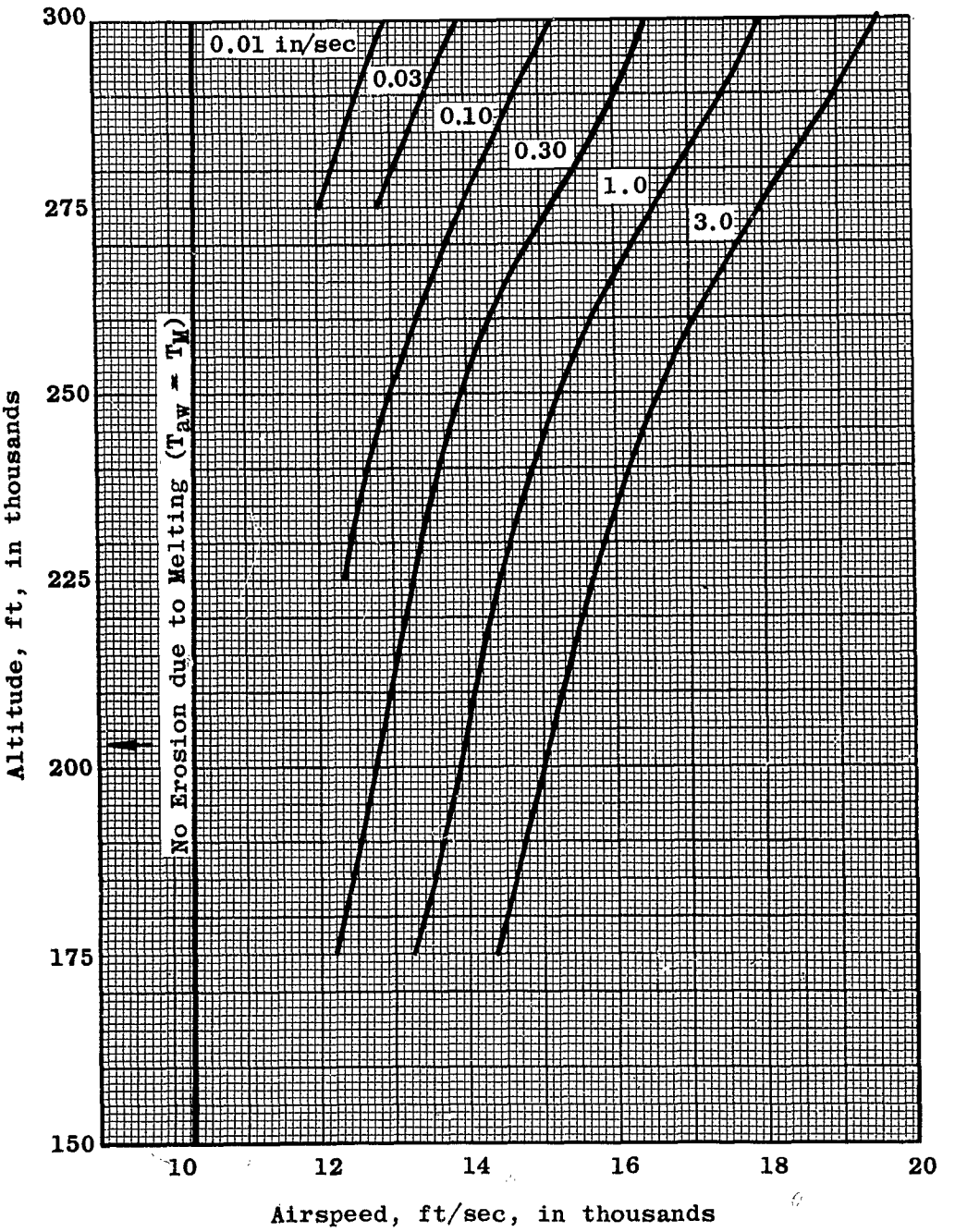

Fig. 40 Rate of erosion of a tungsten throat due to melting only

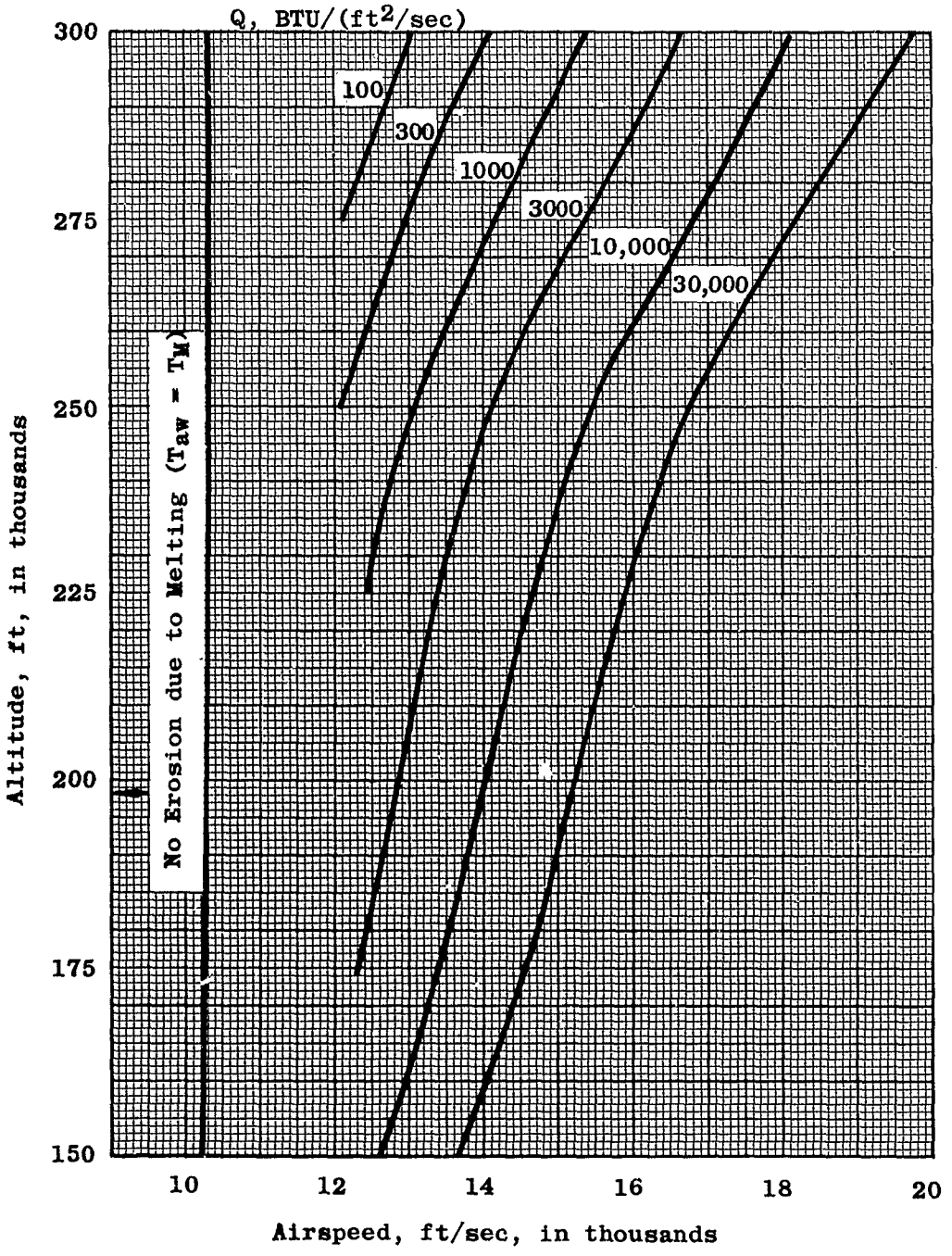

Fig.41 Heat transfer to a melting tungsten throat

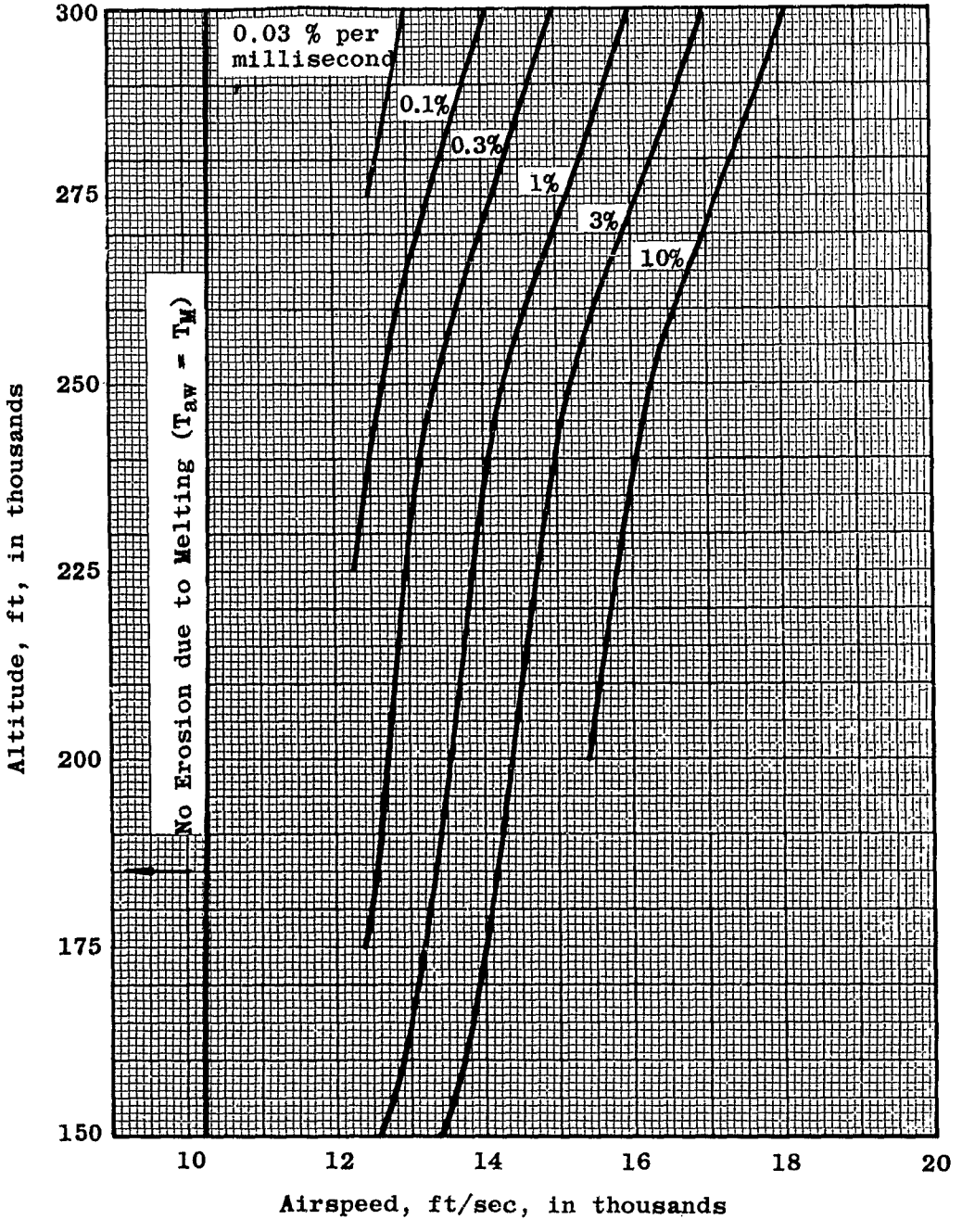

Fig. 42 Rate of decrease of area ratio due to melting only
(a) Effective test section diameter 16 in.

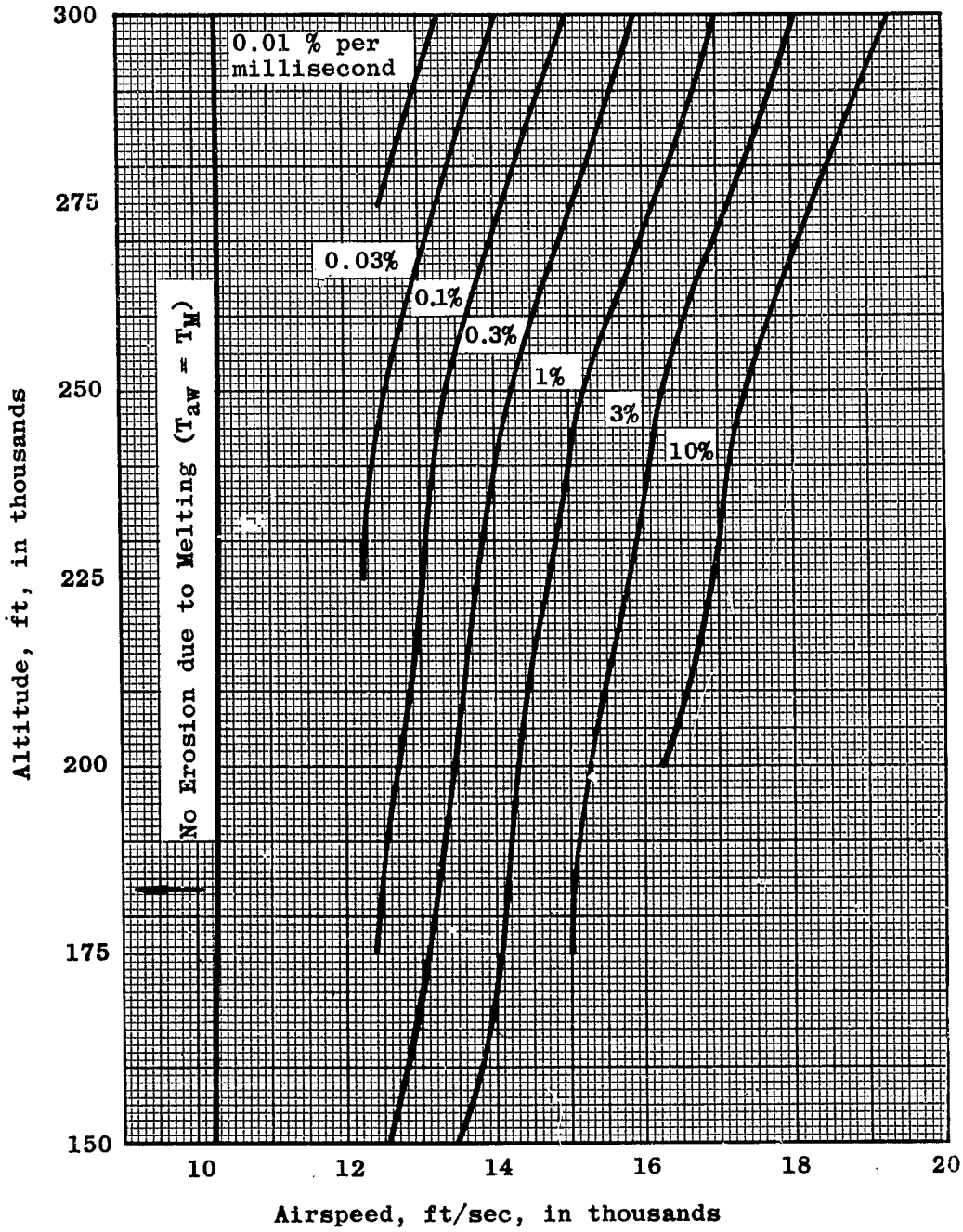

Fig. 42 Rate of decrease of area ratio due to melting only
(b) Effective test section diameter 50 in.

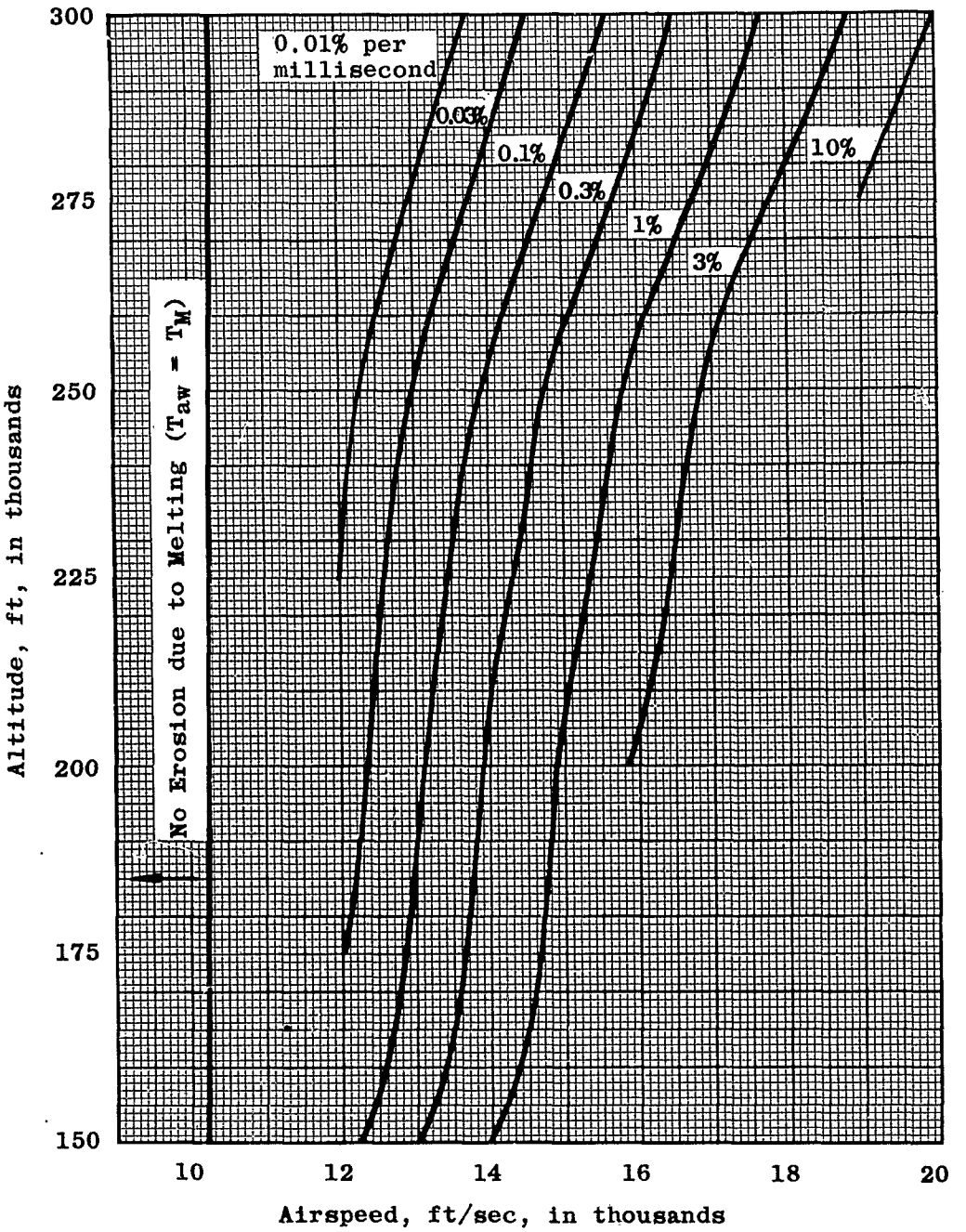

Fig. 42 Rate of decrease of area ratio due to melting only
(c) Effective test section diameter 100 in.

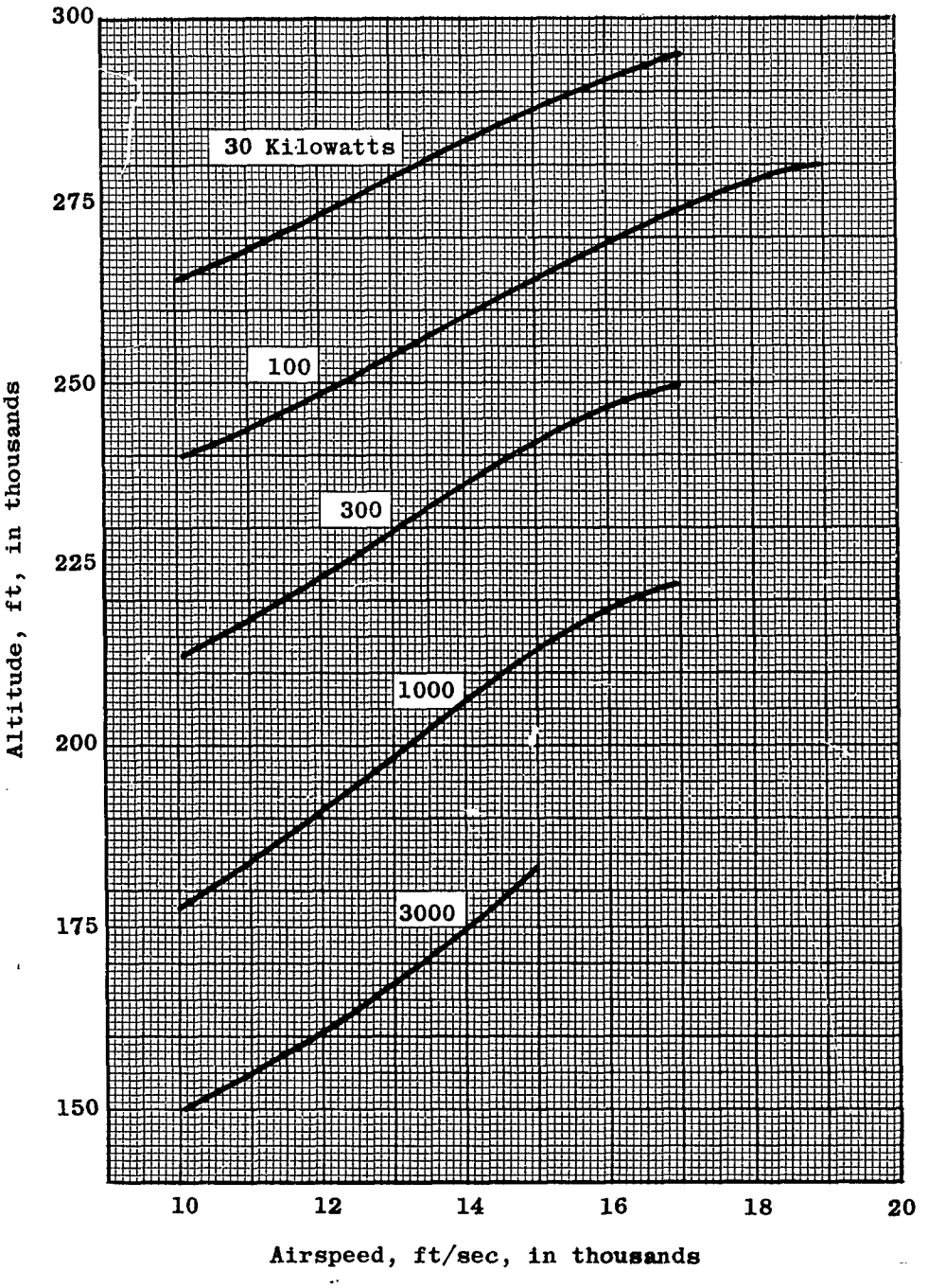

Fig.43 Power required for flight duplication in a continuous tunnel

(a) Effective test section diameter 16 in.

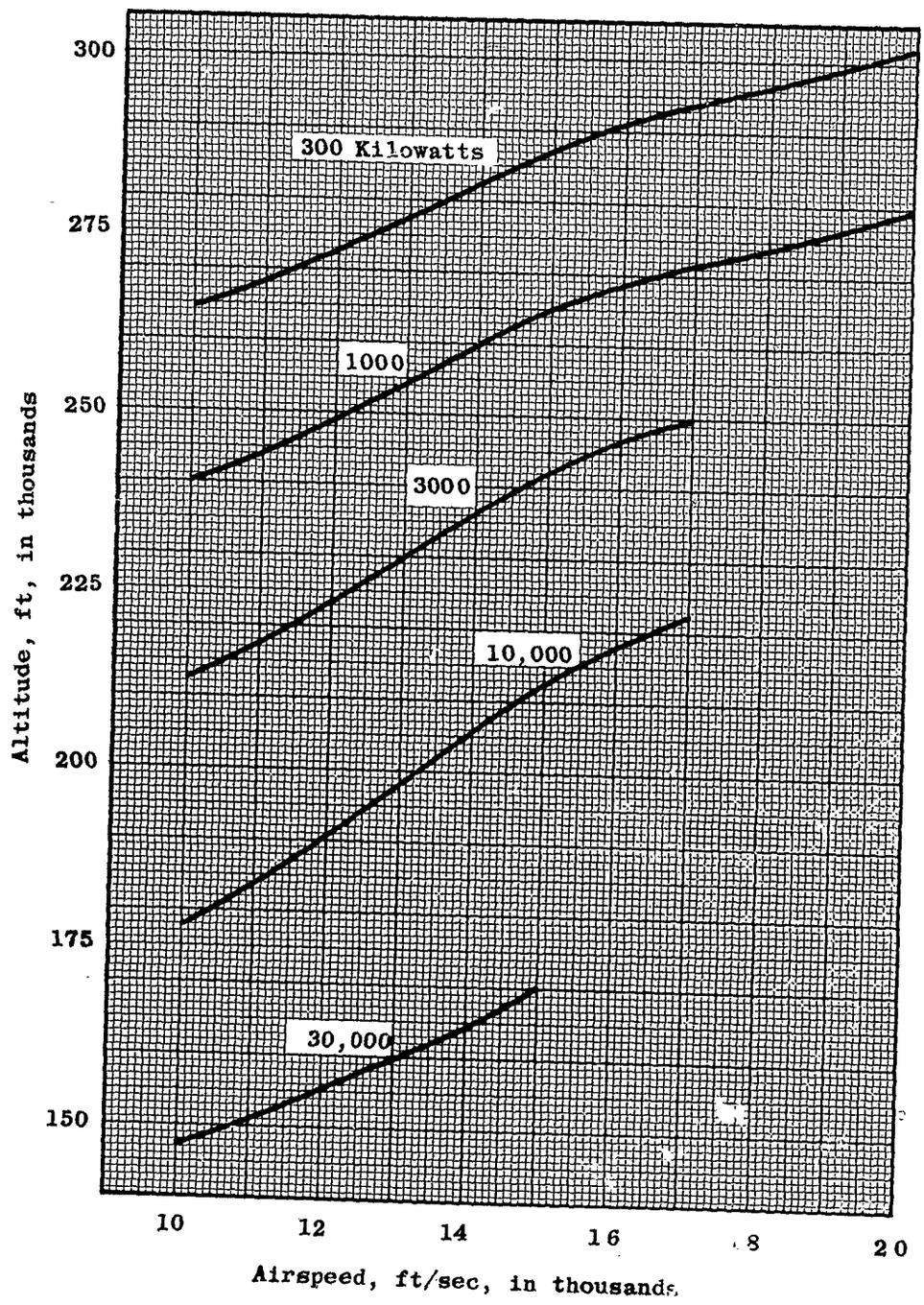

Fig.43 Power required for flight duplication in a continuous tunnel

(b) Effective test section diameter 50 in.

DISTRIBUTION

Copies of AGARD publications may be obtained in the various countries at the addresses given below.

On peut se procurer des exemplaires des publications de l'AGARD aux adresses suivantes.

BELGIUM BELGIQUE	Centre National d'Etudes et de Recherches Aéronautiques 11, rue d'Egmont Bruxelles.
CANADA	Director of Scientific Information Services, Defence Research Board Department of National Defence 'A' Building Ottawa, Ontario.
DENMARK DANEMARK	Military Research Board Defence Staff Kastellet Copenhagen Ø.
FRANCE	O.N.E.R.A. (Direction) 25, avenue de la Division-Leclerc Châtillon-sous-Bagneux (Seine)
GERMANY ALLEMAGNE	Wissenschaftliche Gesellschaft für Luftfahrt Zentralstelle der Luftfahrtdokumentation Munchen 64, Flughafen Attn: Dr. H.J. Rautenberg
GREECE GRECE	Greek Nat. Def. Gen. Staff B. MEO Athens.
ICELAND ISLANDE	Director of Aviation C/o Flugrad Reykjavik Iceland
ITALY ITALIE	Centro Consultivo Studi e Ricerche Ministero Difesa - Aeronautica Rome.

LUXEMBURG LUXEMBOURG	Luxemburg Delegation to NATO Palais de Chaillot Paris 16.
NETHERLANDS PAYS BAS	Netherlands Delegation to AGARD 10 Kanaalstraat Delft, Holland.
NORWAY NORVEGE	Chief Engineering Division Royal Norwegian Air Force Deputy Chief of Staff/Material Myntgaten 2 Oslo, Norway Attn: Lt. Col. S. Heglund
PORTUGAL	Subsecretariado da Estado da Aeronautica Av. da Liberdade 252 Lisbon. Attn: Lt. Col. Jose Pereira do Nascimento
TURKEY TURQUIE	M. M. Vekaleti Erkaniharbiyei Umumiye Riyaseti Ilmi Istisare Kurulu Mudurlugu Ankara, Turkey Attn: Brigadier General Fuat Ulug
UNITED KINGDOM ROYAUME UNI	Ministry of Supply TIL, Room 009A First Avenue House High Holborn London, W.C.1.
UNITED STATES ETATS UNIS	National Aeronautics and Space Administration 1512 H Street, N.W. Washington 25, D.C.

Printed by Technical Editing and Reproduction Ltd
95 Great Portland St. London, W.1.